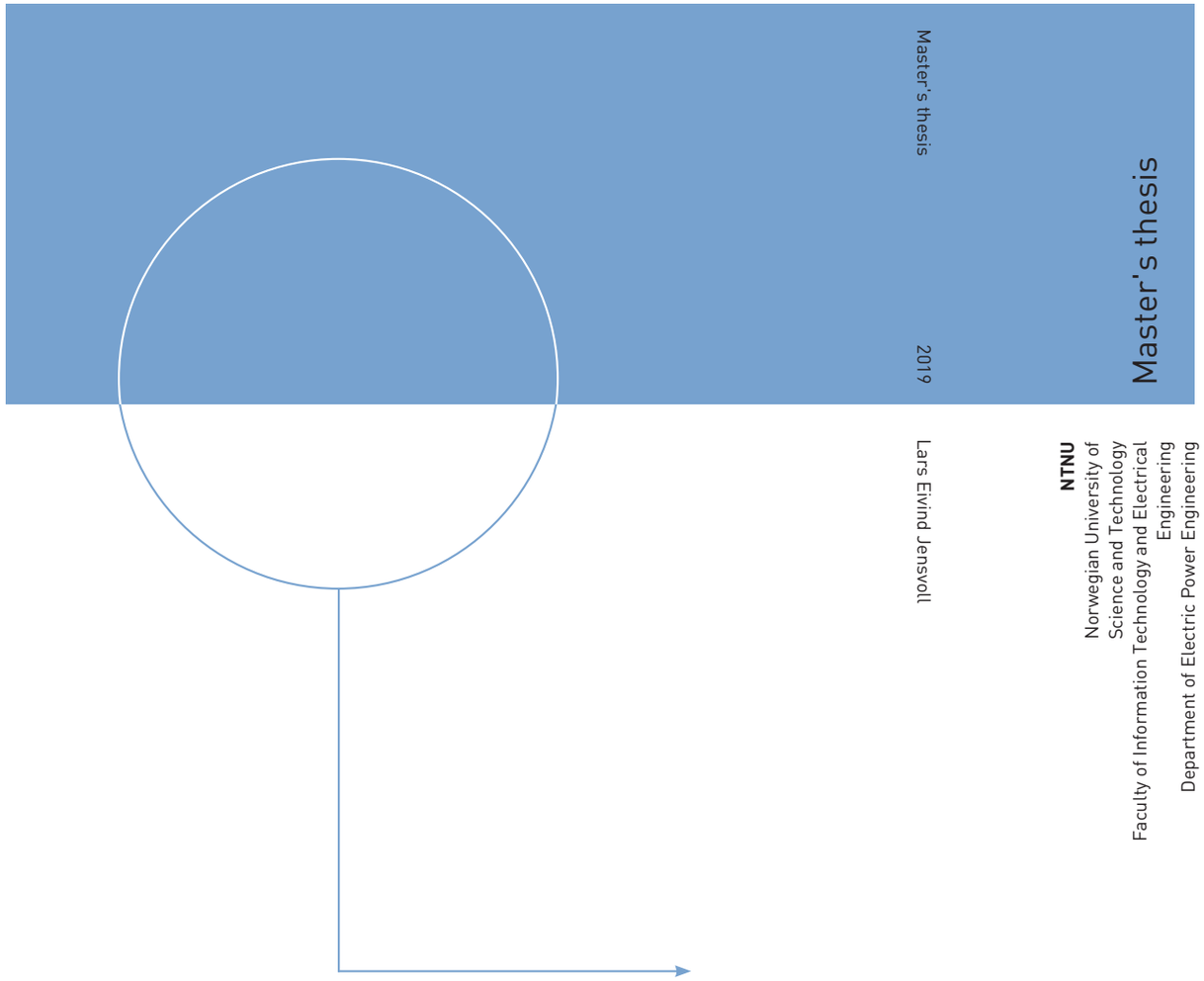

Master's thesis

2019

Lars Eivind Jensvoll

**NTNU**
Norwegian University of
Science and Technology
Faculty of Information Technology and Electrical
Engineering
Department of Electric Power Engineering

Lars Eivind Jensvoll

# Transients During Energization of Unloaded Generator Step-Up Transformers

June 2019

NTNU
Norwegian University of
Science and Technology

NTNU
Norwegian University of
Science and Technology

NTNU

Norwegian University of
Science and Technology

# Transients During Energization of Unloaded Generator Step-Up Transformers

Lars Eivind Jensvoll

Energy and Environmental Engineering
Submission date: June 2019
Supervisor: Hans Kristian Høidalen, ELKRAFT
Co-supervisor: Ronny Goin, Statkraft

Norwegian University of Science and Technology
Department of Electric Power Engineering

# Abstract

A typical hydropower station found in the Norwegian power system is composed of a generator and its step-up transformer installed in constructed caverns in a mountain hill. The step-up transformer is connected to an outdoors high voltage switchyard via cables having typical length of several hundred meters. The switchyard constitutes the connection to the rest of transmission grid. Hydropower stations are connected and disconnected from the power grid based on price variations in the electricity market. As connection occurs by the circuit breakers at the switchyard, the generator step-up transformer experiences a voltage change from zero voltage to system voltage in an instant. Because the generator is disconnected from the transformer at the time connection, the transformer is energized under no load conditions.

Generator step-up transformers are of the most important and costly equipment found in the transmission system, and they are expected to have a high level of availability. Energizing the transformers from their high voltage side may cause overvoltages and high inrush currents which are transient in nature. The transient inrush current is rich on harmonics and can have an amplitude in the same order of magnitude as the transformer short circuit current. It can therefore cause both severe dynamic stress on the transformer wingdings and cause protection systems to disconnect the transformer. The high overvoltages occurring at the transformer terminals are an important cause of insulation degradation, thus damaging the transformer over time.

This thesis report first presents the theory behind transformer inrush currents caused by energization from the switchyard. Then, overvoltages caused by interaction between the cable and the transformer are described. Several transformer energizing events are simulated using an Electromagnetic Transient Program (EMTP), where energizing times, energizing strategies, power grid configurations and feeding cable lengths are varied in order to analyze their impact on then transient inrush currents and terminal overvoltages. One of the main findings of this thesis, is that the energizing times resulting in low inrush currents tends to give high terminal voltages, and vice versa. Additionally, the high inrush currents and energizing voltages can be reduced by using point-on wave switching, most effective when residual flux of the generator step-up transformer core is known.

# Sammendrag

En standard vannkraftstasjon i det norske kraftsystemet består av generator og transformator installert i fjellanlegg. Fra transformatoren går det kabler til et utendørs koblingsanlegg med effektbryter, samleskinne og linjeavganger. Kablene har en typisk lengde som kan variere fra noen få hundre meter til over en kilometer. I dagens kraftmarked er inn- og utkobling av vannkraftstasjonene avhengig av prisvariasjoner i markedet. Innkobling kan skje ved å lukke effektbryteren i koblingsanlegget, noe som gjør at transformatorterminalene spenningssettes fra nettet, som i denne oppgaven er 420 kV. Generatoren er ikke innkoblet på dette tidspunktet, noe som gjør at transformatoren står i tomgang.

En generatorstegtransformator er blant det viktigste og mest kostbare utstyret installert i et kraftsystem. Fet stilles derfor høye krav til transformatorens pålitelighet. Å spenningssette en generatortransformator fra strømnettet kan resultere i transiente overspenninger og strømmer, som begge kan være skadelige for transformatoren. Innkoblingsstrømmen inneholder flere harmoniske komponenter og kan i tillegg være av samme størrelsesorden som en kortslutningsstrøm. Høye spenninger i transformatoren bidrar til raskere nedbrytning av isolasjonsmaterialet, noe som øker sannsynligheten for kortslutning ved overslag.

Denne masteroppgaven forklarer først utfordringene ved å spenningssette en generatortransformator fra høyspenningssiden, med hovedfokus på de innkoblingsstrømmene og overspenningene som oppstår. Deretter gjøres det beregninger ved hjelp av et programvareverktøy utviklet for å beregne elektromagnetiske transienter. Det undersøkes hvordan ulike parametere som innkoblingstidspunkt, kortslutningsytelse i nettet og kabellengde påvirker de strømmene og spenningene som oppstår. Av de viktigste funnene i denne oppgaven er at de innkoblingstidspunktene som resulterer i lave innkoblingsstrømmer har en tendens til å gi høye innkoblingsspenninger, og omvendt. Likevel kan både strømmene og spenningene reduseres ved bruk av fasestyrt innkobling.

# *Acknowledgements*

Throughout the writing of this thesis I have received great support and assistance from people possessing immense knowledge. Therefore, I would first like to thank my supervisor Prof. Hans Kristian Høidalen at NTNU, for his support and assistance. His expertise, especially in ATPDraw, has been invaluable for completing this thesis. His consistent support guided me in the right direction to ensure this thesis was completed to a high standard, yet allowed this paper to be a work of my own.

I would also like to acknowledge my co-supervisor Ronny Goin at Statkraft, for his untiring effort in sharing his knowledge and providing me with the insight necessary to carry out this work. I hope our paths cross again.

Besides my supervisors, my sincere thanks also goes to Bjørn Gustavsen at Sintef Energy Research, and László Prikler at Budapest University of Technology and Economics. I am gratefully indebted to them for their very valuable comments on the EMTP model in this thesis.

Finally, I must express my very profound gratitude to my family and to my friends for providing me with unfailing support and continuous encouragement throughout my years of study, and through the process of writing this thesis. This accomplishment would not have been possible without them. Thank you.

Trondheim, June 2019

# Table of Contents

# List of Figures

# List of Tables

# Chapter 1

# Introduction

## 1.1 Background

Hydropower has been the main source of energy in Norway's electric system for more than 100 years. Today, Norway has more than 1500 hydropower plants with a total installed capacity over 32000 MW [1]. A typical outline of a Norwegian hydropower station is seen in Figure 1.1. The station can have one or more generators, and each generator with its appurtenant step-up transformer are located inside a rock cavity in a mountain hill [2]. The generator step-up transformer is connected to an outdoor switchyard through a feeder cable whose typical length ranges from a few hundred meters to above one kilometer. The switchyard is connected to the main grid via overhead lines. The generic layout in Figure 1.1 shows only the main components. Station transformers, current limiting series reactors, surge arresters and measurement equipment are omitted for the sake of simplicity.

The process of connecting a hydro power plant to the grid can be done in two distinct ways. The generator can be used to slowly energize the step-up transformer and the feeder cable, before the circuit breakers in the switchyard connects the station to the grid. By this method the voltage is equal on each side of the switchyard before the circuit breaker is closed. The second procedure is to energize the step-up transformer from the high voltage grid via the feeder cable. The transformer's low voltage side is left open by means of open generator circuit breakers. The generator circuit breakers remains open until the transformer voltage at the low voltage side has stabilized and is synchronized with the generator voltage. The first method of energizing is preferred as it causes less stress on the transformer. By that reason the second procedure takes all the focus in this thesis.

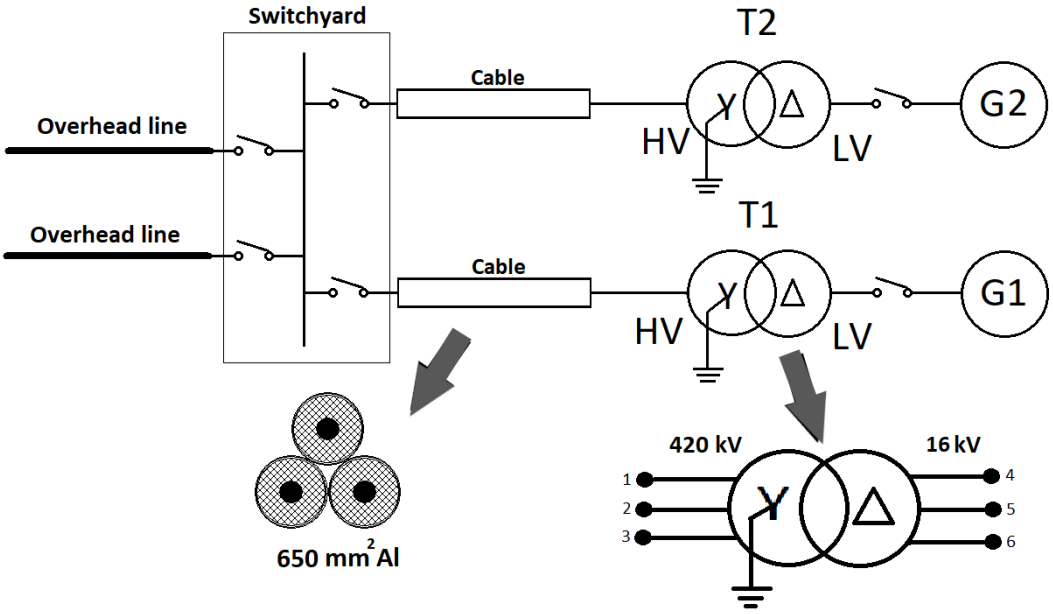


Figure 1.1: Generic layout of a typical hydro power station.
Figure based on fig.1 in [2].

Energizing the generator step-up transformer from the high voltage side represents an abrupt change in the circuit conditions. The transformer terminals experiences a voltage change from zero voltage to system voltage in an instant. High and harmonic rich inrush current are associated with uncontrolled energization of unloaded generator step-up transformers [3]. The first current peak can be in the same order of magnitude as the transformer short circuit current, thus result undesirable events such as severe dynamical stress in the transformer windings, false operation of protective relays, and voltage dips that can influence the electrical grid's power quality [4, 5]. Furthermore, energizing unloaded transformers via a feeding cable may create high voltages on transformer terminals [6]. This can occur if resonance frequency of the cable and transformer match, or if one of the harmonics of the inrush current is close to the resonant frequencies [7, 8].

Simulating the events of transformer energizing may reveal the undesirable outcomes not unveiled by on site measurements. Transformer energizing transients, especially the inrush currents, are heavily dependent on the initial conditions of the transformer [9, 10]. These initial conditions can be troublesome to measure and record due to either operational restrictions, system operating configurations or system contingencies. As a result, in order to obtain as much information as possible about the transient events occurring after a transformer energization, it is desirable to perform several simulation studies [11].

## 1.2 Problem Description and Limitations

The focus of this report is to study both the transient inrush currents and the overvoltages that occur on the high voltage side of the generator step-up transformer, when the transformer is being energized from the upstream network via a feeder cable. The voltages occurring at the low voltage side are therefore out of scope for this project. Key parameters are altered to observe and analyze their influence on the transient inrush current and voltage. Data used in this thesis is mainly based on Statkraft's hydropower plant *Nedre Røssåga* and its connection to the main grid. This thesis work is limited to use a system consisting of only one feeder cable and its associated step-up transformer. Cables, station transformers and compensation reactors, all located at the low voltage side are omitted from the model. The simulation model is tested for different energizing events and finally compared to measurements performed at *Nedre Røssåga*.

In order to study the phenomena related to transformer energizing transients, a large number of simulations are performed using an Electromagnetic Transient Program (EMTP) [12]. The royalty-free software called Alternative Transients Program (ATP) is used to run the simulations. The ATP file is created using ATPDraw, a graphical pre-processor to the ATP version of EMTP [13].

## 1.3 Aim of Thesis

The following list precisely defines the aim and expected outcome for this thesis, and what this report endeavour contributing to.

- Explain the phenomena of inrush current and resonant overvoltages that can occur when energizing an unloaded generator step-up transformers from the high voltage side.

- Perform transformer energizing simulations of inrush current and terminal overvoltages for varying energizing times, energizing strategies, power grid configurations and feeder cable lengths. Validate the simulation model by comparing site measurements from Nedre Røssåga with simulation results.

- Give general recommendations on transformer energization based on the results from simulations, and provide proposals for further work in this field.

## 1.4 Structure of Report

The rest of this thesis is structured as follows.

Chapter 2 introduces the theory necessary for understanding the potential problems related to energizing generator step-up transformers from their high voltage side. Special emphasis is placed on transformer inrush current and overvoltages due to resonance caused by interaction of transformer and feeder cable. A brief summary of the most important theory is offered at the end of the chapter.

Chapter 3 describes how the simulation model used for transient studies is established using ATPDraw. Modelling techniques are presented together with the information used to determine the parameters of each of the main components. The last section of this chapter unveil in its entirety the completed model.

Chapter 4 presents the simulations performed using the model of Chapter 3. The first half of the chapter presents the results from general energizing simulations where energizing is done for varying energizing times, energizing strategies, power grid configurations and feeding cable lengths. The second half presents special energizing simulations which are compared to measurements on from Nedre Røssåga.

In Chapter 5 the most important results of Chapter 4 are analyzed and discussed by using the theory presented in Chapter 2. Simulations are compared to the measurements, and the deviation between simulations and measurements are explained. The final section evaluates the strengths and weaknesses of the model of chapter 3.

Chapter 6 concludes the work of this report. The questions from section 1.3 is answered and general advise based on the obtained results are given. This chapter ends with a section proposing a handful recommendations for further work.

# Chapter 2

# General Theory on Switching Transients in Transformers and Cables

This chapter introduce the fundamental behaviour of electrical transients as a result of switching operations. The theory is aimed at explaining potential problems related to energizing generator step-up transformers through a feeder cable at the high voltage side. Starting with introducing switching transients in general, this chapter will then explain transformer inrush currents and the commonly used mitigation techniques. The feeder cable is introduced in the third section of this chapter, and the focus shifts from inrush currents to resonant overvoltages. At the end, a short section in dedicated to the practical aspects of switching operations, before the chapter ends with a brief summary of the most important objectives form each section.

## 2.1 Introducing Electrical Switching Transients

Electrical transients are temporarily responses to sudden changes in the circuit conditions. The changes can be anything from controlled switching operations to severe short circuit faults. Even though the transient period is usually very short compared to the time spent at steady state conditions, it is during the transient period that the circuit equipment experiences the highest stresses from overvoltages and high currents. When dealing with transient currents, it should be remembered that the forces are proportional to the square

of the current. In other words, a doubling in current results in force being fourfold. High inrush currents may therefore challenge both the mechanical and the thermal rating of electrical equipment, such as transformers or electrical motors. Transient overvoltages can exceed the electrical withstand capacity of insulators and protective devices, thus lead to flash-overs and short circuits. Knowledge about electrical transients are therefore of great importance.

An electrical transient is the reaction that occurs when an electrical system passes from one steady state condition to another steady state condition. Energy has to be exchanged between different parts of the electrical network in order to reach a new steady state. The energy exchange has a certain inertia, meaning the redistribution of energy takes a finite amount of time. Redistribution of energy is subject to the principle of energy conservation, meaning the total amount of energy in the isolated system is constant. The three parameters Resistance, Inductance, and Capacitance are the fundamental units that constitute any electrical circuit. While resistances dissipate energy through heat, inductors and capacitors has the ability to store energy in magnetic fields and electric fields respectively. Under steady state conditions the energy stored in inductors and capacitors are interchanged cyclically with the frequency of the alternating current. During the transient period the energy is redistributed at a different pace before a new steady state is reached. Greenwood [14] accentuate three simple, yet crucial, facts to remember when trying to comprehend electrical transients:

1. Current through an inductor cannot change instantly
2. Voltage across a capacitor cannot suddenly change
3. Energy conversion must be preserved at all times

How the inductive and capacitive effects imprints on the transient currents and voltages when closing a switching is explained by two examples. This is the fundamental knowledge later used to analyze the energization of a generator step-up transformer through a long feeding cable. The following examples are very simple and are based on *ideal* switching operations. Because of their simplicity, the circuits analytically without much difficulties.

**Energizing an Inductive Circuit**

Figure 2.1 shows an RL-circuit represented by a series combination of resistance and inductance. The source impedance is negligible compared with the load, which has a steady state power factory given by Equation (2.1).

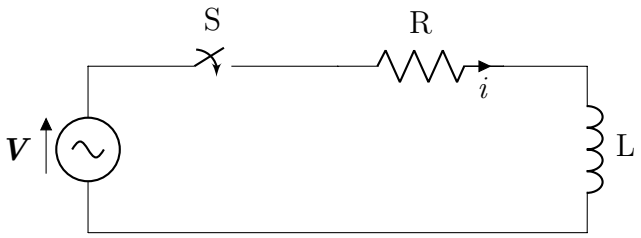


Figure 2.1: A simple RL circuit with a sine wave drive.

$$cos(\phi) = \frac{R}{|Z|} = \frac{R}{(R^2 + \omega^2 L^2)^{1/2}} \tag{2.1}$$

When the switch S is closed the current flowing in the circuit is expressed using Kirchhoff's law of voltage. By including the arbitrary phase angle $\theta$, the switch can be closed at any instant on the voltage cycle. The result is the first order differential equation

$$Ri + L\frac{di}{dt} = \boldsymbol{V} = V_m sin(\omega t + \theta) \tag{2.2}$$

Which has the well known solution

$$i(t) = \frac{V_m}{\sqrt{R^2 + (\omega^2 L^2)}} \cdot \Big[ sin(\omega t + \theta - \phi) - e^{-\alpha t} \cdot sin(\theta - \phi) \Big] \tag{2.3}$$

Where,

$V_m$ = the amplitude of the applied voltage

$\alpha$ = the time constant given by the relationship $R/L$

$\theta$ = the initial angle of the voltage

Equation 2.3 is divided in two distinct parts, where the first term being the particular solution showing that the current is sinusoidal in steady state. The second term is the complementary solution expressing the transient period. Because of the exponential term, the transient part will eventually decay to zero. Different initial conditions, based on when on the voltage cycle the switch is closed, will result in different outcome. Some initial conditions will give high transient currents that should be avoided.

Utilizing the fact that the current through an inductor cannot change instantly when evaluating Equation (2.3), it is seen that the current will start at zero regardless of the

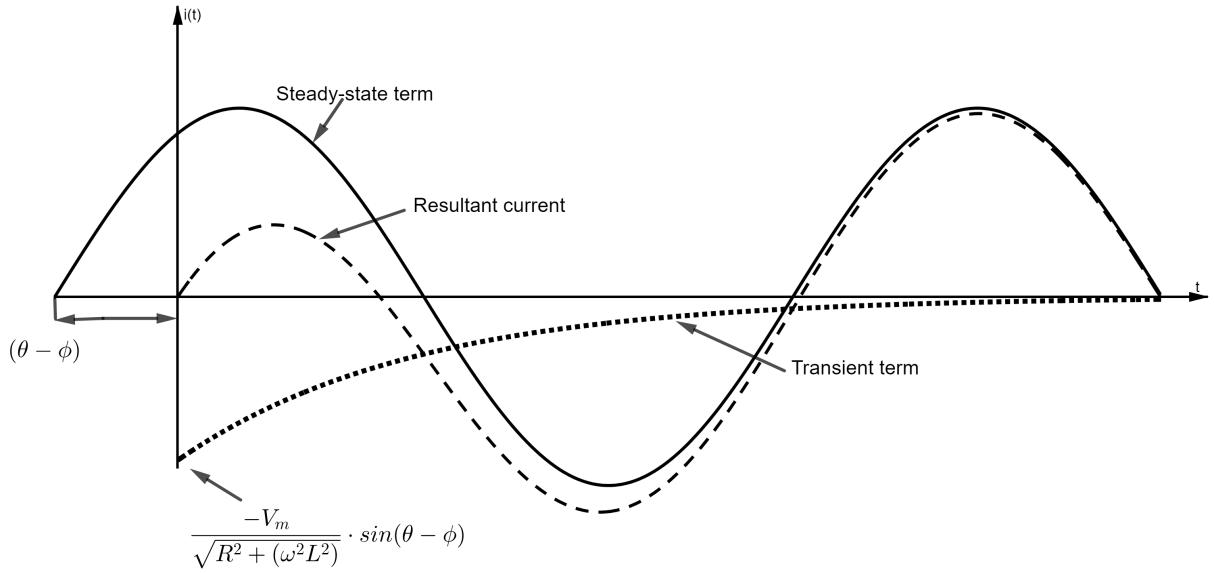


Figure 2.2: The transient response of the RL-circuit.

switching instant. This is also seen from the plot of the current response in Figure 2.2. In the figure, an arbitrary angle $\theta$ is used when closing the switch, resulting in a negative transient. The transient term is expressed by the complementary solution of Equation (2.3), while the resultant current is the combination of both the particular solution and the complementary solution, in other words the whole expression of Equation (2.3).

Further evaluation of Equation (2.3) reveals that the best instant to close the circuit is at voltage zero, that is when $\theta = \phi$. At this instant the transient offset will be zero, thus the current flowing in the circuit will be symmetrical from the start. On the contrary, closing the switch at the instant when $\theta - \phi = \pm\pi/2$, the transient term attains its maximum value. This will give the current maximum offset, and the first peak of the resultant current will be almost twice the amplitude of steady state component.

**Energizing a Capacitive Circuit**

In contrast to the previous example with an RL-circuit, current in the series LC-circuit shown in Figure 2.3 can be described by a second order differential equation. Since energy is exchanged between the inductor and the capacitor, the circuit will oscillate with the natural frequency given in Equation (2.4), no matter how the circuit is energized. The circuit in Figure 2.3 has no time constant and will therefore continue to oscillate. In a practical circuit there will be some resistance and thus the oscillations will gradually be damped out.

$$\omega_0 = \frac{1}{\sqrt{LC}} \tag{2.4}$$

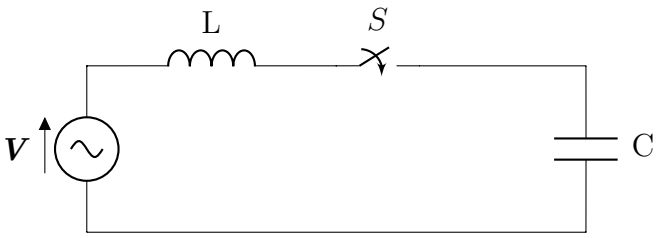


Figure 2.3: The oscillatory LC circuit.

It is important to remember that the circuits in these two examples are very simplified. The parameters have been lumped together, the source impedance has been neglected, and the switches has been regarded as ideal switches. For such simplified circuits, the solution can easily be obtained analytically. This is not the case for more complex networks of three phases, consisting of long cables, saturable transformers, generators and other equipment. However, it is still true that the three parameters Resistance, Inductance, and Capacitance are the fundamental units that constitute the components in the network. In the following section, the fundamentals of transients will be expanded into transformer inrush currents caused by actuation of the switches on the transformer high voltage side.

## 2.2 Transient Currents Caused by Transformer Energization

Transformer energization is one of the most commonly performed operation in the power grid, but it is also an action that under right circumstances can cause abnormal switching transients. The transients due to transformer energization is a special case of energizing an inductive circuit, as done in section 2.1 This section focus on the transient currents occurring when energizing a generator step-up transformers by actuating circuit breakers on the power grid side of the transformer, with the generator side left open.

Figure 2.4 shows a simplified model of the on-line transformer energizing when the generator side is left open. It is clear that such on-line transformer switching constitutes a sudden change in the circuit conditions, thus producing electrical transients. These transients are generally safely damped within reasonable time and cause no further problems

for the electrical equipment. However, potential problems related to this method of energizing may cause very large inrush currents with significant harmonic content. Because the inrush current contains both even and odd harmonics, resonant overvoltages can occur when the transformer is energized together with a line or a cable. After the transient inrush period has ceased, a transformer usually draws just a small magnetizing current of between 0.5 and 2% of its rated current [14]. The phenomena of inrush current will be treated first, while resonant overvoltages are treated in section 2.3.

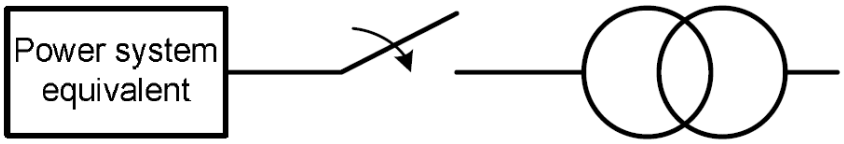


Figure 2.4: Diagram of the transformer energizing process [11].

### 2.2.1 Inrush Current in Single Phase Transformers

A transformer's magnetizing current is the current required to magnetize the iron core. Because of the nonlinear properties of the ferromagnetic core material, the magnetizing current is not sinusoidal. Instead, the magnetizing current will follow a hysteresis loop as the one seen in Figure 2.5. Hence, during steady state the current will oscillate between $\pm I_m$ while the flux varies sinusoidally as a function of the applied voltage.

When a transformer is energized under no-load conditions, the magnetizing current drawn by the transformer sets up the flux necessary to induce a voltage so that it is equal to the voltage applied at the transformer terminals. If the transformer core is fully de-magnetized before voltage is applied, the flux density $B$ will follow the initial magnetization curve, starting at point 1 in Figure 2.5. Then, as the field intensity $H$ increases the curve flattens out and saturation is eventually reached, point 2 of the figure. When the field intensity decreases and eventually reaches zero, the flux density has a non-zero value called *residual flux density* or *remanence flux*. This means that as the transformer is switched off from the power system and the current in the winding is zero, the transformer core still has a flux flowing in the core, denoted $B_r$ at point 3.

The inrush current phenomenon is caused by the nonlinear relationship between the core flux and the winding current, as displayed in Figure 2.5. As the curve starts to flatten out after the knee point, a marginal increase in flux will cause the current to in-

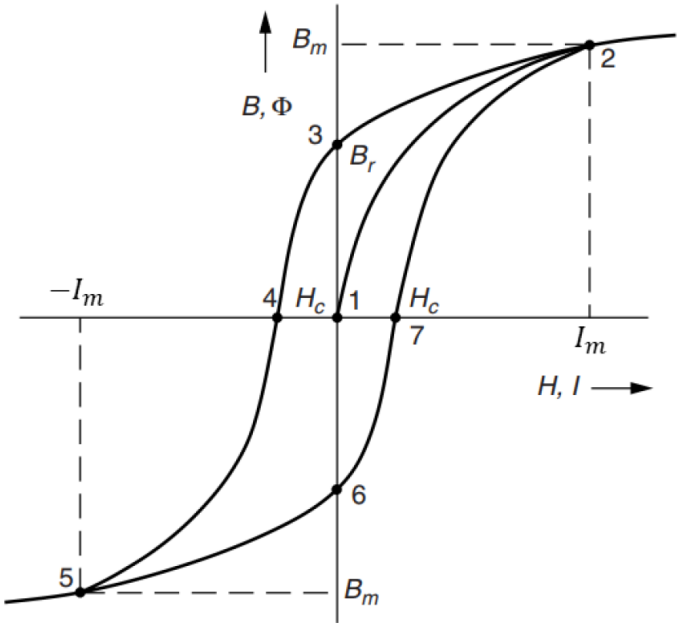


Figure 2.5: Magnetizing curve and hysteresis loop of a transformer core [15].

crease drastically and the transformer is said to be saturated. When a sinusoidal voltage $u(t) = U_0 \cos(\omega t)$ is applied at a transformer's windings at an instant $t_0$, a flux $\phi(t)$ is established in the transformer core. The relationship between voltage and flux is given by Equation (2.5), where $\phi_0 = U_0/(N\omega)$ is the nominal flux and $N$ is the number of windings.

$$\phi(t) = \phi_r + \frac{1}{N}\int_{t_0}^{t} u(\tau)d\tau = \phi_r - \phi_0 \sin(\omega t_0) + \phi_0 \sin(\omega t) \tag{2.5}$$

In the above equation, $\phi_r$ denotes the residual flux in the transformer core. The equation reveals that the flux is in quadrature with the applied voltage and the flux magnitude can be altered by changing the time of energization. With the residual flux being zero, the minimal amplitude of the flux is $\phi_0$ and its maximum amplitude is $2\phi_0$. By including the residual flux in Equation (2.5), the theoretical maximum value is $3\phi_0$. This is obtained by energizing at zero voltage such that the generated flux has the same polarity as the residual flux. Because transformers are designed to operate at rated voltage with flux just below the knee-point, the core will go into deep saturation and thus draw a very high magnetizing current. This is illustrated in Figure 2.6. From the right hand side of the figure it is seen that the flatter the saturation curve is, the larger the inrush current

magnitude will be.

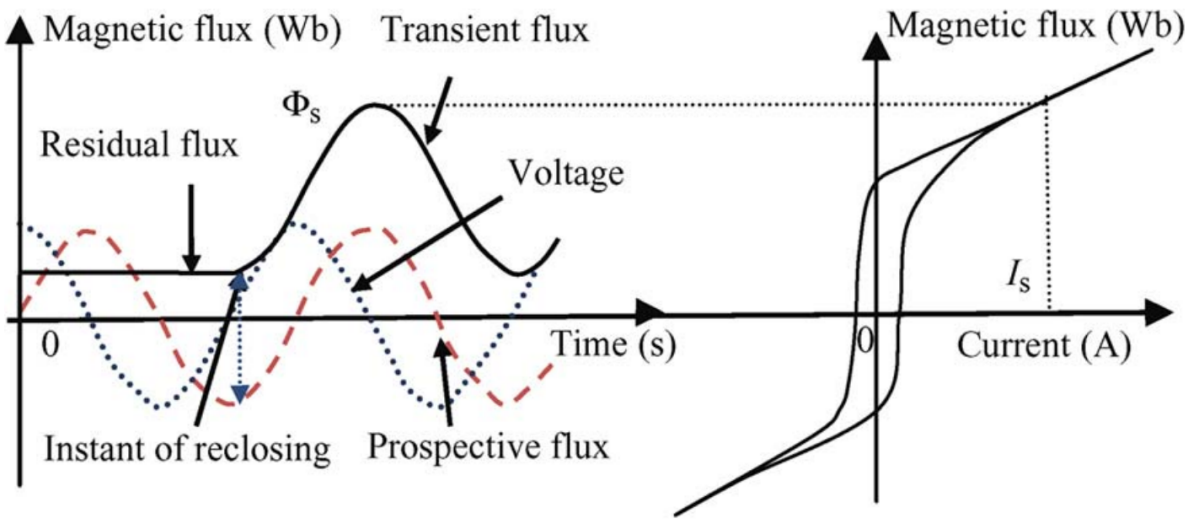


Figure 2.6: Inrush current created by flux asymmetry [16].

Magnetizing inrush current occurs in a transformer whenever the time of energization is such that the polarity and magnitude of the residual flux *do not* agree with the polarity and magnitude of the instantaneous value of the steady state flux which would normally be required for the particular point on the voltage wave at which the circuit breaker is closed [17]. In Figure 2.6 the required flux is labelled *prospective flux*, and it has its maximum value at opposite polarity of the residual flux at the time of energization. This results in a maximum inrush current given that the residual flux is at its maximum value.

The time of energization is often referred to as the *switching angle*, as it is the point on the voltage wave that dictate the magnitude of the resulting flux. In contrast to the situation displayed in Figure 2.6, the inrush current can be eliminated if the prospective flux is equal in magnitude and polarity to the residual flux at time of energization. This is done by choosing the time of energization such that $\phi_r = \phi_o \sin(\omega t_0)$ in Equation (2.5). The flux will then, from the instant of energization, follow the remaining sinusoidal term with amplitude $\phi_0$. Figure 2.7 displays how the instant of energization influence the magnitude of the flux. Remembering that modern transformers usually operates just below the saturation knee point at nominal flux $\phi_0$, this instant of energization will result in no inrush current.

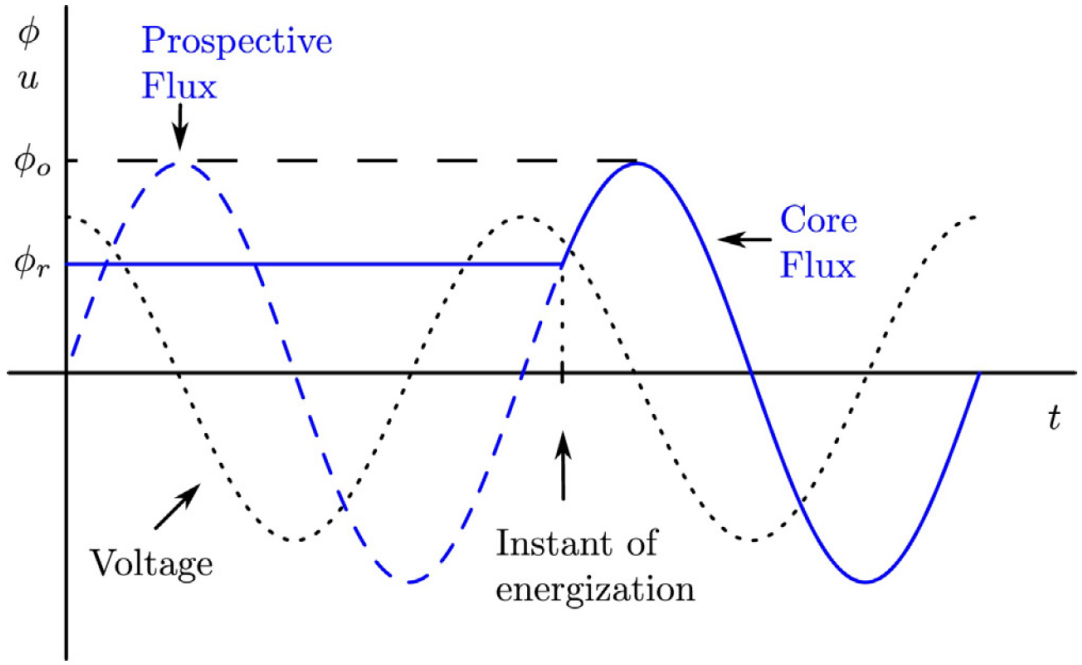


Figure 2.7: Optimal instant of energization to eliminate inrush currents [18].

### 2.2.2 Inrush Current in Three Phase Transformers

The foregoing theory regarding inrush current in single phase transformers is now extended into including three phase transformers. The inrush currents in three phase transformers are more complicated than for single phase transformers because of electric connection and magnetic coupling of the three phases. This section will focus on core form transformers consisting of three and five limbs, as the ones displayed in Figure 2.8 and 2.9 respectively. Three phase transformers with separated cores and grounded windings can be considered as three single phase transformers and are therefore not treated in this section.

#### 2.2.2.1 Three Legged Transformer Core

Figure 2.8 shows the physical structure of a three legged stacked transformer core. With this transformer core, energizing only one phase will induce a dynamic flux in the two remaining phases. The flux in the two remaining phases will no longer be the static residual flux, but instead be a dynamic flux dictated by the energized phase. Because of the core topology, the residual flux in a three legged transformer inherently sums to zero when the transformer has been operated with balanced terminal voltages. In addition, the residual flux typically forms a pattern where the flux in one leg is close to zero and

the flux in the two other legs have a finite magnitude with polarity opposite of each other. This pattern is often denoted $[0, -r, +r]$, $r$ being the static residual flux. Knowledge about the residual flux is of great importance when energizing transformers in order to reduce the inrush currents.

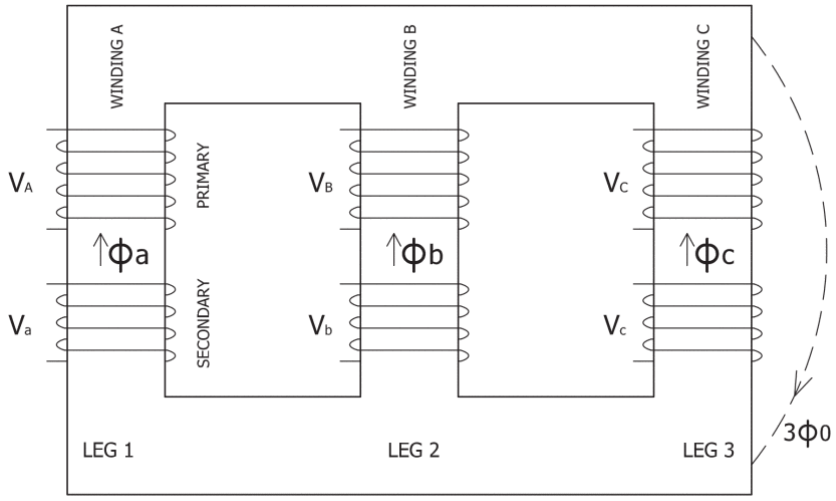


Figure 2.8: Three legged stacked transformer core [19].

Contrary, if the transformer is operated with unbalanced terminal voltages, the sum of the three phase fluxes will not sum to zero [20]. At such a situation, the flux in the three legs may have the same direction or the limbs may have been saturated. The return path for the flux is therefore no longer inside the iron core but instead through the air gap between the yokes. More precisely, the zero sequence flux will flow outside of the core legs, and through the air and transformer tank. This is the zero sequence flux path which has a much higher reluctance than the flux path in the core legs. Three legged core transformers are therefore classified as high reluctance transformers, and the inductance at saturation is referred to as the air core inductance. In Figure 2.8 the zero sequence flux path is denoted $3\phi_0$.

#### 2.2.2.2 Five Legged Transformer Core

Unlike the three-legged transformer core, a five-legged core provides a low reluctance path for the zero sequence flux. In addition to the three main legs, a five legged transformer has two outer legs without windings, as seen from Figure 2.9. In the figure, the zero sequence flux $\phi_0$ is distributed evenly in the two outer legs. Because of them, the top and bottom yoke does not have to carry the full complement of flux from each phase.

The top and bottom yokes can therefore be made with reduced cross sectional area [21]. This is a commonly used feature for generator step up transformers, because the reduced cross sectional area results in a reduced transformer height, which is a cherished feature in typical mountain installed hydro power plants.

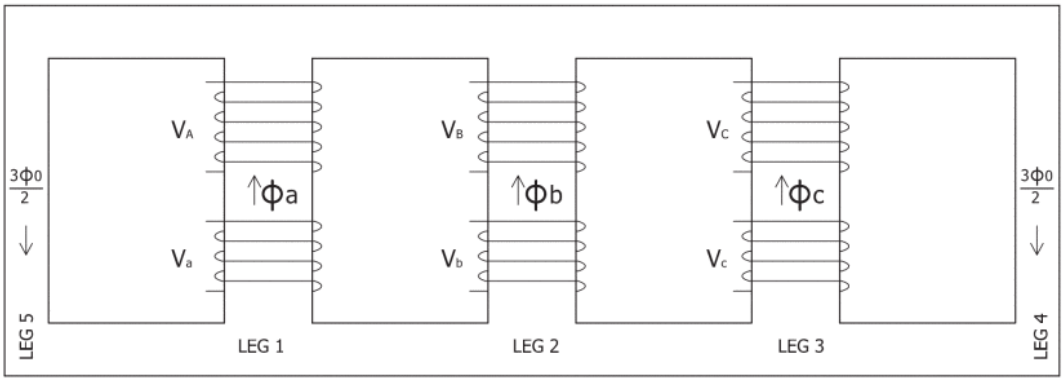


Figure 2.9: Five legged stacked transformer core [19].

Under normal balanced operation of a five legged transformer, the dynamic core flux will sum to zero in the entire core [22]. However, as both the voltage and current are balanced three phase systems, the flux in the three main legs will also have a vector sum of zero at the yoke. Still, a portion of the flux will flow in the outer legs and when the transformer is de-energized, the residual flux has no typical pattern such a three legged transformer core. If the five legged transformer has at least one delta winding, the flux in the three main legs will sum to zero and only the the zero sequence flux will flow in the outer legs [22]. However, if the outer legs gets saturated, the five legged core will act as a three legged core having its zero sequence flux path through the air and transformer tank [23].

### 2.2.3 Controlled Switching for Reduction of Inrush Currents

It was seen in section 2.2.1 how the inrush current depends on the switching angle and the residual flux. Then it was seen that the inrush current can be avoided if the residual flux is accounted for when energizing a transformer. As the previous section revealed, the inrush current in three phase transformers with multi-legged cores are more complicated than the inrush current in single phase transformers. In order to achieve low inrush currents during energization of large power transformers, controlled switching strategies, also called point-on-wave switching, is a powerful and commonly used method [24]. Theoretically, the inrush current in three and five limb transformers with a delta winding can be completely

eliminated by using controlled switching strategies. By having independent pole operated circuit breakers and measurements of the residual flux, the first phase can be energized at the instant when the residual flux equals the prospective flux. The last two phases can then be energized when their induced dynamic flux match the prospective flux for the respective phases.

The residual flux in the three main legs of a transformer is seldom zero. If the transformer has been magnetized before, the residual flux can have values up to 85% of nominal flux, although values in the range of 20% to 70% are more typical [25]. Because the prospective flux and the core flux must sum to zero for an unsaturated delta connected transformer, the induced dynamic core flux in the two un-energized phases must be equal to their respective prospective fluxes two times per cycle [22]. Furthermore, the residual flux often forms a pattern with approximately zero residual flux in one leg and a finite flux of opposite polarity in the other two main legs. Based on this, the three switching strategies *Rapid Closing Strategy, Delayed Closing Strategy*, and *Simultaneous Closing Strategy* has shown to be very effective in reducing the inrush currents in Yn-$\Delta$ transformers [26].

#### 2.2.3.1 Rapid Closing Strategy

By this strategy, one phase is energized first and the remaining two phases are energized together within a quarter cycle. Each phase is energized at its optimal instant, defined by the intersection between the prospective flux and the residual flux. After the first phase is energized, a dynamic flux is induced in the last two phases. The induced dynamic flux will then intersect with the residual flux within a quarter cycle, as seen in Figure 2.10. Usually two instants of optimal energizing occurs, named A and B in Figure 2.10. Because the slopes of the induced dynamic flux coincide with the slope of the prospective flux at instant A, this instant is preferred over instant B.

The rapid closing strategy is the hardest strategy to implement as it requires knowledge about the residual flux in all three phases and an independent pole operated circuit breaker [27]. The division of core flux is non-linear at the time period between the first and the two last phases are energized. Knowledge about the transient core flux characteristics are therefore required in order to perform a desirable switching [22].

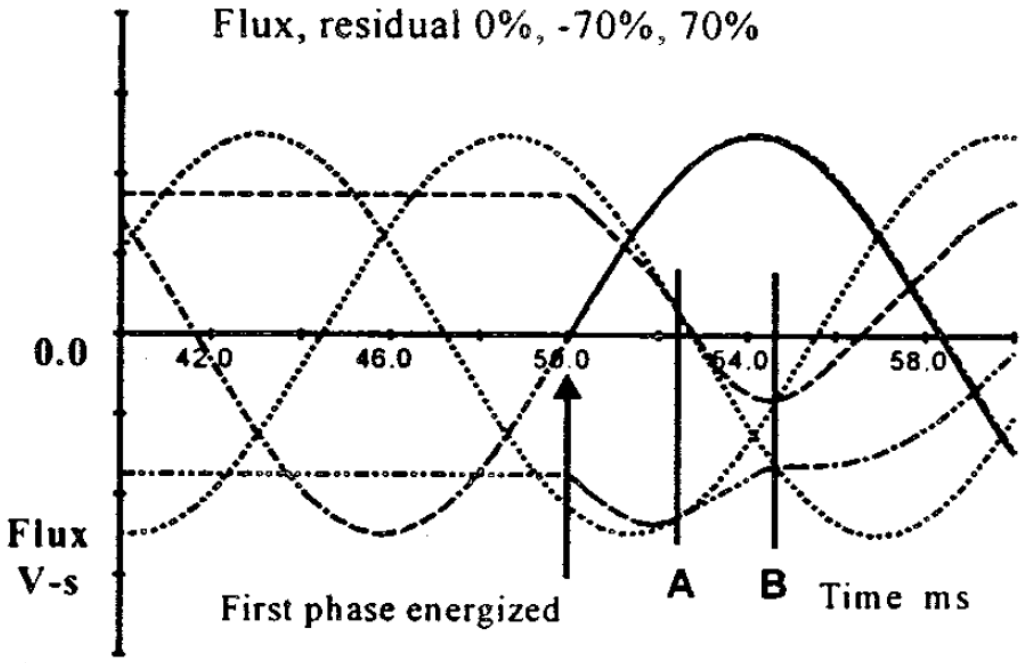


Figure 2.10: Prospective and induced dynamic flux [26].

#### 2.2.3.2 Delayed Closing Strategy

The delayed closing strategy is easier to implement because it requires only an independent pole operated circuit breaker and residual flux measurement of just one of the phases [24]. The phase with residual flux measurement is closed when its prospective and residual flux are equal, whereas the two remaining phases are closed after a few cycles. The residual flux in the two un-energized phases will after a short time be dissipated and replaced with a proportion of the dynamic flux from the energized phase. This occurrence is called core flux equalization and is demonstrated in Figure 2.11 for a three legged core transformer [18]. Because of core flux equalization, knowledge about the transient core flux characteristics is not needed.

From the figure it is seen that phase A is energized at the instant $t_0$ where the prospective and residual fluxes are equal. Phase B and C are energized simultaneously at instant $t_1$. Furthermore, it is highly advantageous to let the phase with the highest residual flux be energized first [27]. Firstly, energizing at high prospective flux means energizing at low voltage, thus reducing the imposed stress level on the transformer. Secondly, when energizing at a high prospective flux one has the possibility to close the circuit breaker on the rising absolute voltage, hence reduce the impact of mechanical closing deviation.

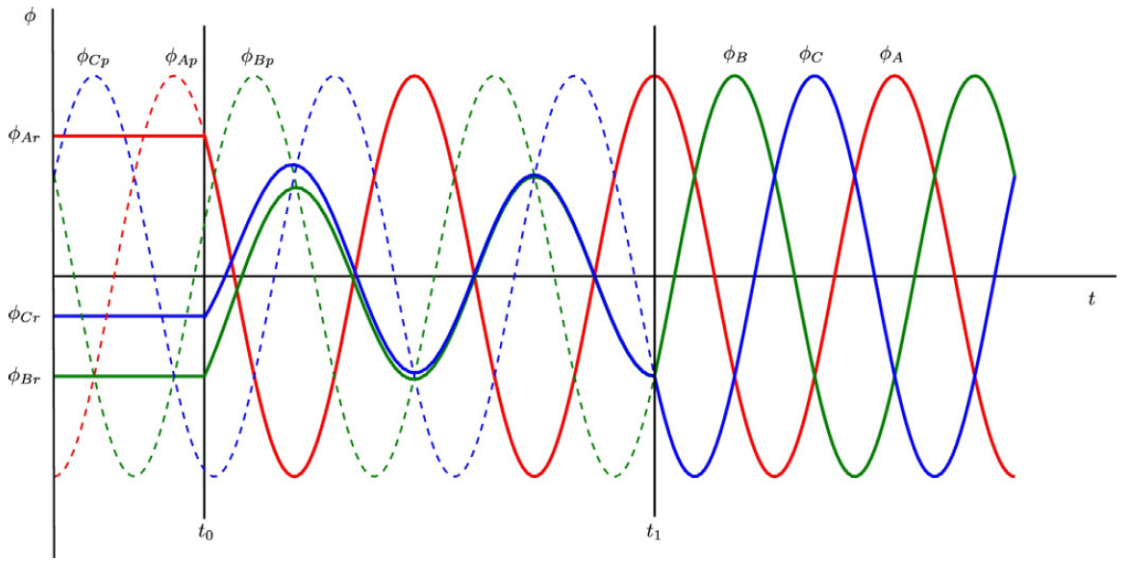


Figure 2.11: Actual flux (solid lines) and prospective flux (dashed lines) when using delayed switching [18].

Mechanical closing deviation and other aspects of real circuit breakers will be further examined in section 2.4.

#### 2.2.3.3 Simultaneous Closing Strategy

Simultaneous closing is a strategy where the circuit breakers for all thee phases are mechanically closed at the same time [26]. An independent pole operated circuit breaker is not required, but in order to eliminate the inrush current one must have knowledge about the residual flux in all three phases. In addition, the residual flux must follow the pattern of $0, -r, +r$ for the strategy to be effective [28]. This can be obtained using controlled de-energization, where the circuit breakers are opened at one phase's voltage peak so that its residual flux will be close to zero [18]. Energization of the transformer happens at the instant when the residual and prospective flux match for the phase with lowest residual flux. In other words, if residual flux is zero in one phase, energization will take place at voltage peak. The two phases with residual flux levels $+r$ and $-r$ will not have peak voltage at the instant of mechanical closing. Pre-strike will therefore occur slightly later resulting in a near optimal energization [26]. Further explanation of pre-strike is left for section 2.4.

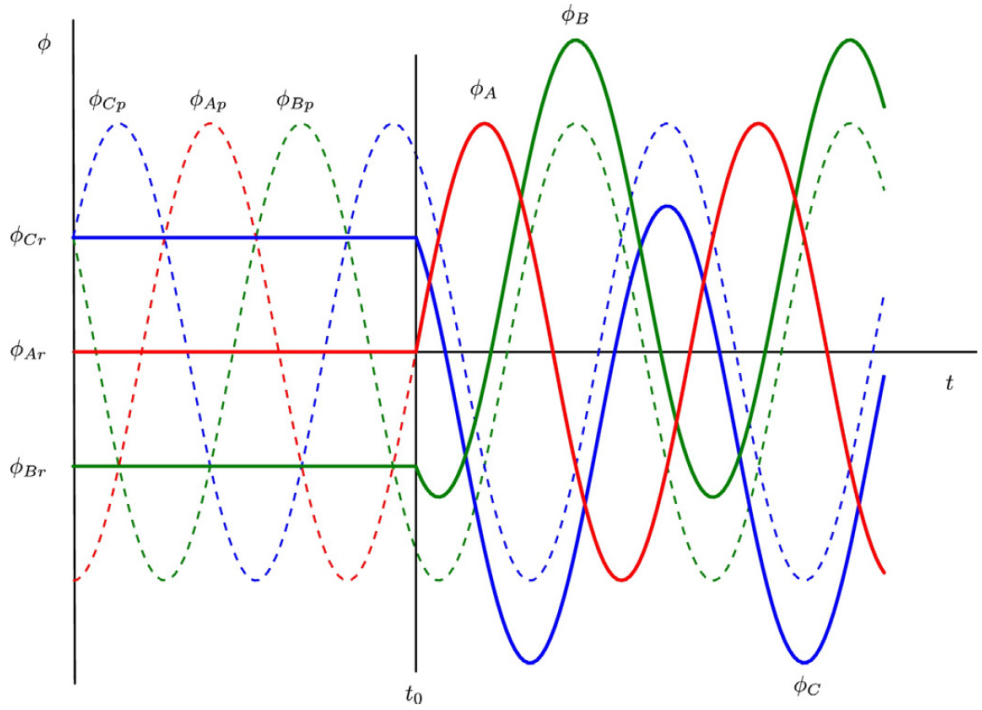


Figure 2.12: Actual and prospective flux when using simultaneous switching [18].

Figure 2.12 illustrates the simultaneous closing strategy where phase A has zero residual flux and phase B and C has $-\frac{1}{2}\phi_0$ and $+\frac{1}{2}\phi_0$ flux respectively. It is seen that the flux peak in phase B and C will be slightly higher than nominal flux, thus the inrush current is not completely eliminated by the use of simultaneous closing strategy.

## 2.3 Transient Voltages in Cables and Transformers

Nn this section the transients occurring in the feeder cable connecting the generator step-up transformer to the main grid is treated. First, the travelling wave equation is used to mathematically describe how electromagnetic waves propagate through a line or a cable. Finally, the interaction between transformers and cables and how resonant overvoltages may occur when energizing an unloaded transformer is explained. The main focus is understanding overvoltages caused by resonance caused by the feeder cable, as it is crucial when energizing generator step-up transformers.

### 2.3.1 Travelling Waves in Lines and Cables

In the previous examples of section 2.1, the parameters R, L and C were treated as concentrated constants. These constants are in reality distributed parameters, and when studying some parts of the power system, the approximation of lumpiness does no longer hold. For instance, when performing transient studies on transmission lines and cables it is necessary to have models capable of supporting travelling waves of voltage and current. A model with distributed parameters meets this requirements, and it is usually used when the length of the circuit reaches the same order of magnitude as the wave length of the electromagnetic wave applied at the circuit. The adoption of distributed parameters challenge some notions commonly used when analyzing lumped circuits. The current in the circuit is no longer uni-valued at *all* points of the line, meaning that the current in a specific line can have different values at different positions at the same time. In addition, the voltage can be discontinuous in a model using distributed parameters.

Figure 2.13 shows a short segment of a single phase line or cable, represented with distributed parameters. From the figure, it is seen that the line model is split up in infinitesimal segments in order to represent the voltage and current as a function of both time and position. The short line segment, $dx$, includes resistance and inductance per unit length, capacitance to ground, and leakage conductance. Figure 2.13 is used as reference when deriving the equations describing the wave propagation, done for steady state conditions for a single phase line in Appendix A.

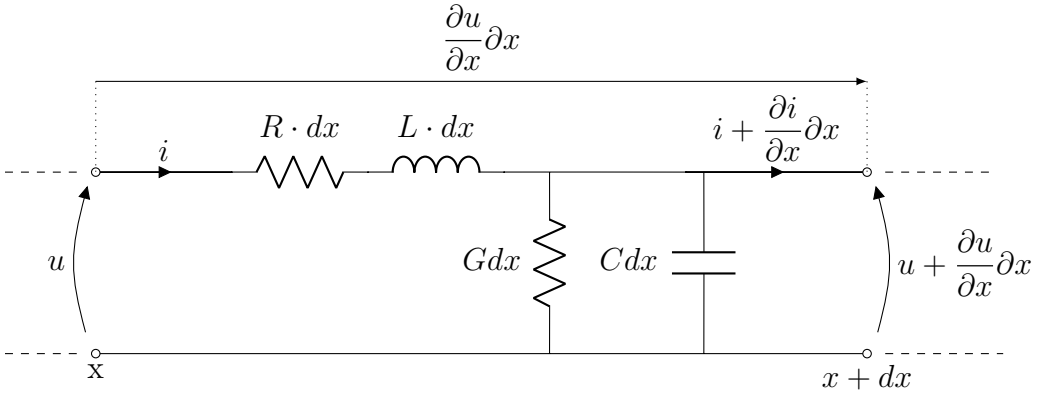


Figure 2.13: Single phase circuit of a length $dx$ of an overhead line.

Equation (2.6) is the second order differential equation describing how voltage propagates through the line in Figure 2.13. The equation is called the Telegrapher's equation for voltage and is valid for all frequencies. Partial derivatives are used because the voltage is a function of both time and position. This is the full voltage equation where losses are

included.

$$\frac{\partial^2 u}{\partial x^2} - LC \cdot \frac{\partial^2 u}{\partial t^2} - (LG + CR) \cdot \frac{\partial u}{\partial t} - RG \cdot u = 0 \tag{2.6}$$

The general solution to the wave equation is the sum of a forward travelling wave and a backward travelling wave. This is elaborated for a loss less line in Equation (A.8), in Appendix A. When the two waves of opposite direction meet they add algebraically which can result in either a doubling or cancelling of the wave amplitude. The wave velocity is given by the parameters of the line and is limited by the speed of light $c$, as seen in Equation (2.7). In the equation, $\mu_0$ is the vacuum permeability, $\varepsilon_0$ and $\varepsilon_r$ is the absolute and relative permittivity of the medium in which the magnetic and electric field travels.

$$v = \frac{1}{\sqrt{LC}} = \frac{1}{\sqrt{\mu_o \varepsilon_0 \varepsilon_r}} = \frac{c}{\sqrt{\varepsilon_r}} \tag{2.7}$$

As mentioned, a consequence of the distributed parameters is that the current is no longer uni-valued, and the voltage can be discontinuous. This is because the propagation velocity in the line or cable is determined by the properties of the line, and limited by the speed of light. For instance, if a current is applied to a 300 meter long overhead line, the current will not be registered at the far end until at least one microsecond has passed, the speed of light being 300 meters per microsecond. As the velocity is dependent upon in which medium the electromagnetic wave travels, the voltage and current waves will propagate at a slower speed in cables than in overhead lines. For instance, an XLPE cable has a relative permeability of about 2.25 which will reduce the propagation speed with approximately 33%.

One important parameter when dealing with line theory is the relation between voltage and current waves. The relationship is constant and commonly known as the characteristic impedance or the *surge impedance*. For a line or cable where the losses are included, the impedance is given by Equation (2.8). The surge impedance is a strict proportionality between voltage waves and current waves on a line, and it has the unit of *ohms*. The surge impedance is independent of the length because all quantities are in per unit length. additionally, as seen from Equation (2.8), if the losses are neglected the surge impedance is reduced to $\sqrt{L/C}$.

$$Z_o = \sqrt{\frac{R + j\omega L}{G + j\omega C}} \tag{2.8}$$

It is important to remember that the equations presented in this section are based on single phase systems while most power systems today have three phases. One must therefore include mutual effects of multiple wires for a more accurate description of travelling waves in an actual power system. Nevertheless, the *fundamentals* of traveling waves in lines and cables are the same for three phase and single phase networks.

### 2.3.2 Reflection and Refraction of Travelling Waves

As mentioned, the surge impedance $Z_0$ is the proportionality factor relating current and voltage. In cables, the electromagnetic fields are confined between the conductor and the screen, thus the wave speeds are dependent on the insulation material. When the travelling current and voltage waves arrives at a discontinuity in the cable, from either a junction of cables, or transition to overhead lines, the surge impedance will most probably change. Therefore, some adjustments has to be done to the travelling waves in order not to violate the constant proportionality between the voltage and the current [14].

Figure 2.14 illustrates how the voltage and current waves are refracted and reflected when they arrive at a junction in a cable. The characteristic impedance changes from $Z_A$ to $Z_B$ over the junction, resulting in two new wave pairs being initiated. The reflected wave pair travels in opposite direction of its initial wave pair, and is superimposed on the initial wave. The refracted wave pair will continue in the same direction as its initiating wave, along impedance $Z_B$, with a reduced amplitude. Seen from the right hand side of Figure 2.14, the two new wave pairs are balanced and continuous, and the energy conservation is consequently satisfied.

The amplitudes of the new waveforms are found using the characteristic impedances and the fact that the voltage and the current is continuous at the point of junction. By utilizing Kirchhoff's current law at the junction, the reflection coefficient $a$ and the refraction coefficient $b$ can be expressed as in Equation (2.9) and (2.10). As seen from the equations, the incident wave can be either doubled or become zero when arriving at a junction. If the junction divides into more than one line, the same methodology is used to find different reflection and refraction coefficients.

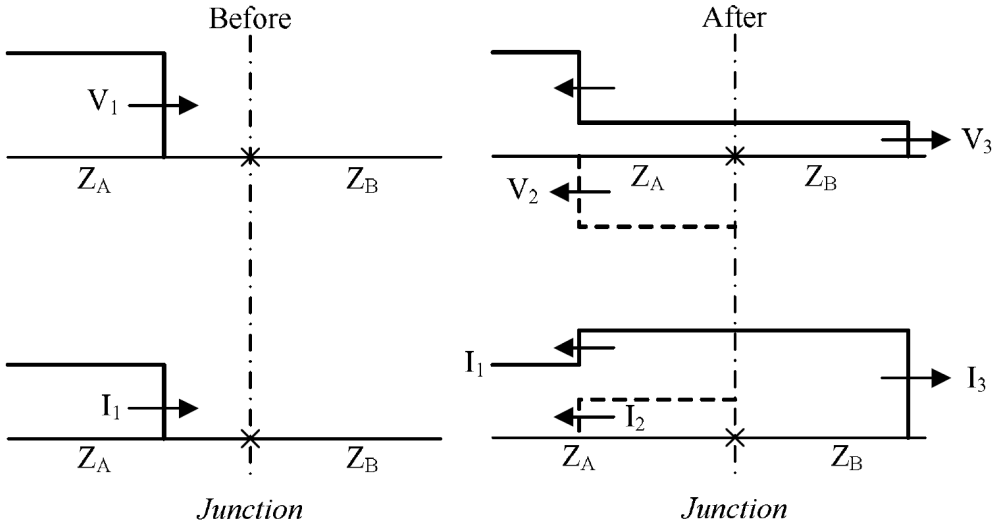


Figure 2.14: Voltage and current waves at a cable junction [29].

$$V_2 = \left(\frac{Z_B - Z_A}{Z_A + Z_B}\right) \cdot V_1 = a \cdot V_1, \qquad \text{where } [-1 \leq a \leq 1] \tag{2.9}$$

$$V_3 = \left(\frac{2Z_B}{Z_A + Z_B}\right) \cdot V_1 = b \cdot V_1, \qquad \text{where } [0 \leq b \leq 2] \tag{2.10}$$

Seen from Equation (2.10), if $Z_B$ is greater than $Z_A$ the refracted wave will be greater than its initial wave. This is because voltage is defined by the amount of charge on the line, and the line's capacitance to ground. If the capacitance decrease, the voltage has to increase in order to preserve the amount of charge on the line [30]. Situations where the refracted wave is greater than its initial wave often occurs when a travelling wave arrives at an overhead line or a transformer with high surge impedance, coming from a cable having low surge impedance. As for transformers, the surge impedance is frequency dependent, thus it can be challenging to predict the reflection and refraction coefficients [31].

### 2.3.3 Travelling Waves at Line Terminations

Termination of a line (or a cable) is treated as a special case of a line with a junction. The extreme cases of a line termination are short circuit termination and open circuit termination. Between these two extremes are several possible terminations, where the line is terminated in some type of equipment. The possible terminations can be capacitive, resistive, inductive, or a combination of all three. In this section, the two extremes will

be used to further explain the behaviour of travelling waves at line terminations.

#### 2.3.3.1 Short Circuit Termination

The main distinctive of a short circuit is that it is impossible to develop voltage across it. Thus, the two nodes at each side of a short circuit are forced to have the same voltage level. Therefore, when a travelling wave of voltage arrives at a short circuit, the reflected voltage will precisely cancel out the initial voltage wave. This results in the refracted voltage being zero. This can also be seen by setting the impedance $Z_B$ equal to zero in Equation (2.9) and (2.10).

The current wave reaching the short circuit will be reflected back in the initial wave resulting in a doubling of the current flowing in the line. When the reflected voltage wave forces the line voltage to be zero, the electric energy cannot be dissipated and therefore has to be transformed. The electric energy stored in the electric field is consequently converted into magnetic energy, which is sustained by doubling the current [30]. As it was mentioned in section 2.1, doubling of the current results in the magnetic forces being fourfold.

Figure 2.15 illustrates the behaviour of current and voltage when a short circuit occurs on a transmission line fed by a constant voltage source having zero internal impedance. First the initial voltage is cancelled out by a voltage wave travelling towards the source. The current has doubled in size on its way to the source, where it will be reflected again thus increasing the current flowing in the line. The short circuit current continue to rise step-wise at intervals of $2\tau$, where $\tau$ is the travelling time of the waves from the source to the short circuit and vice versa. If the voltage source is time-varying, the wave sent out of the line will also vary with time, thus change in voltage occur also before the reflected wave reaches the source.

#### 2.3.3.2 Open Circuit Termination

A line terminated in an open circuit can be understood as the opposite of a short circuit termination. The open circuit at the end of a transmission line results in the current at that point being zero at all times. Thus, when a current wave arrives at the line termination a negative current wave is reflected, cancelling out the current on the line. As energy must be conserved when the current is zero, the voltage is doubled. In contrast

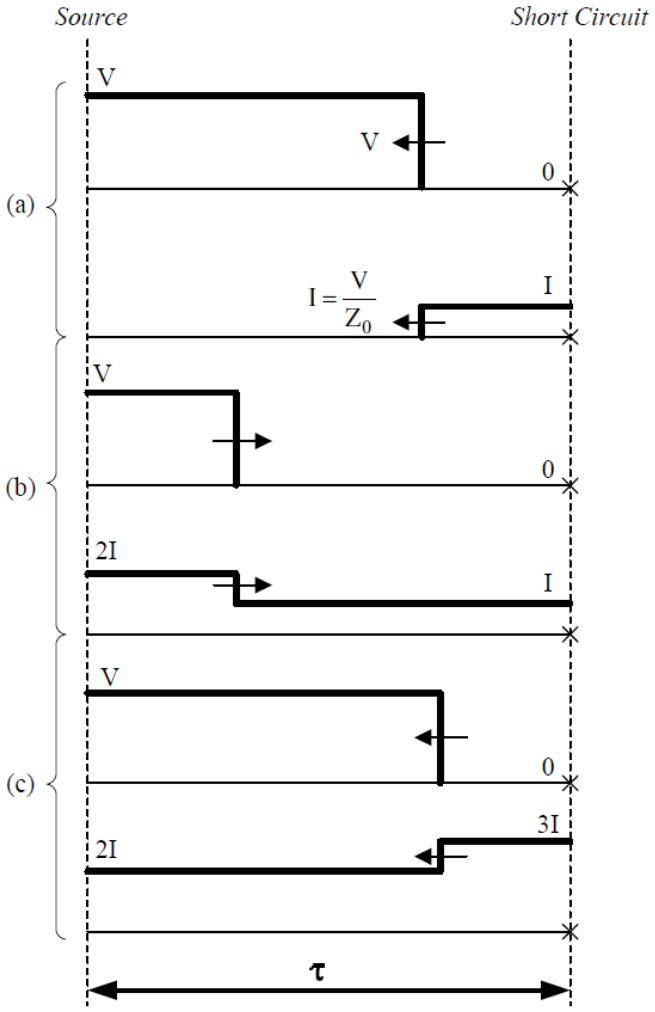


Figure 2.15: Behaviour of travelling waves when a short circuit occurs on a transmission line [29].

to the short circuit termination, energy is now converted from the magnetic field to the electric field, which is sustained by doubling the voltage.

The travelling wave behavior at an open circuit termination of a transmission line fed by a constant voltage source is displayed in Figure 2.16. As the current reflected from the open circuit cancels out the line current, the reflected voltage results in a doubling of line voltage. This voltage doubling effect created by open circuits can be very harmful for the system equipment and insulation when lies and cables are energized. As a consequence lines and cables are usually energized at zero voltage, by the use of independent pole operated circuit breakers [32].

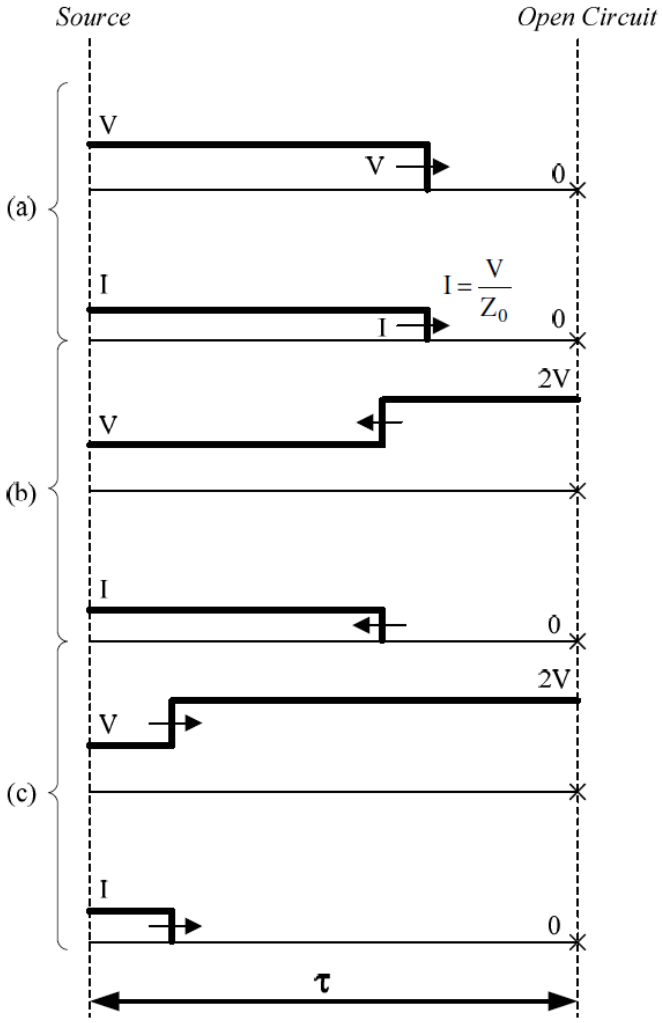


Figure 2.16: Behaviour of travelling waves when energizing at an open circuited transmission line [29].

#### 2.3.3.3 Cable Resonance Frequency

As it was explained in section 2.3.1, the speed of which a travelling wave propagates through a cable is dependent on the insulation material of the cable. The travelling time of the electromagnetic waves is dependent on the travelling velocity and the cable length. In the previous examples of wave reflections the travelling time was denoted $\tau$. As the travelling wave is reflected, the frequency of reflection is equal to the inverse of four times the travelling time [7]. This is expressed mathematically in Equation (2.11). It was seen in Equation (2.7) of section 2.3.1 that the propagation velocity $v$ is limited by the speed of light and the relative permittivity of the cable insulation $\varepsilon_r$.

$$f_{\lambda/4} = \frac{1}{4\tau} = \frac{v}{4L} = \frac{c}{4L \cdot \sqrt{\varepsilon_r}} \tag{2.11}$$

The frequency $f_{\lambda/4}$ in Equation (2.11) is called the quarter wave resonance frequency of a cable [33]. Resonance occurs if the cable is excited at this frequency. When energizing generator step-up transformers through a relatively long feeding cable, resonance will occur if the cable resonance frequency coincide with the resonance frequency of the transformer. In real cable-transformer systems, the dominant oscillation frequency is less than the quarter wave resonance frequency due to the transformer capacitance. The difference in quarter wave frequency and dominant oscillation frequency will decrease with increasing cable length and reduced transformer capacitance [33]. This will be further explained in the following sections.

### 2.3.4 Overvoltages Caused by Cable - Transformer Interaction

When energizing a transformer via a feeder cable as seen in Figure 2.17, it is not only the inrush currents that may cause problems. As the cable has a shunt capacitance to ground, the capacitance can be seen in parallel with both the network inductance and the transformer inductance. The parallel resonance frequency is inversely proportional to the square root of the capacitance of the cable and the series inductance, as stated in Equation (2.12). In section 2.1, this frequency was mentioned as the natural frequency of an LC-circuit. At the resonance frequency the impedance becomes very large, and excitation by a current of equal frequency may results in high voltages.

$$f_r = \frac{1}{2\pi\sqrt{LC}} \tag{2.12}$$

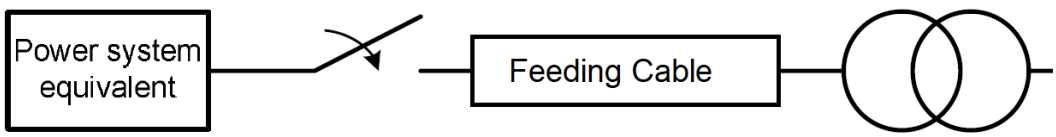


Figure 2.17: Diagram of transformer energization via feeder cable.

The transformer inrush currents are known for having high magnitudes and significant harmonic content. When a generator step-up transformer is energized through a feeding

cable, the harmonic current may interact with the resonant frequencies of the system. If the resonances get excited, damaging overvoltages can be produced. If the damping is low, the overvoltages may have a long duration. This is a critical situation as the surge arresters installed to protect transformers from damage due to high voltages only have a limited capacity to absorb energy. As the surge arrester continuous operating voltages usually are well above system voltage, the surge arresters become ineffective for temporary overvoltages [33]. As a consequence, temporary overvoltages may be sustained for several seconds [34].

In practical systems it is not only the parallel resonance that is of interest. Because complex networks usually contains mixed parallel and series combinations of capacitors and inductors forming series-parallel circuit, several resonance frequencies may occur [35]. The number of resonance frequencies is dependent the number of capacitive and inductive elements in the circuit. The problem with resonances becomes even more complex when non-linear saturable inductances are a part of the circuit. This is the case for iron core transformers, where the non-liner inductance of the transformer interact with the capacitances of cables and other equipment. This is referred to as *ferroresonance*, briefly explained in the following section.

#### 2.3.4.1 Ferroresonance

The resonance phenomenon in nonlinear circuits, known as ferroresonance, is a special case of the LC-resonance introduced in section 2.1. As electrical resonance occurs in a circuit when the capacitive reactance equals the inductive reactance, this point can occur at several frequencies when the inductance is non-linear. Even though ferroresonance is rare, it may occur when only one or two phases of a transformer is energized. Figure 2.18 shows three examples of ferroresonance occurring when energizing a transformer. Ferroresonance is possible for all transformer core configuration, but is most likely to occur in five-limb transformers [36].

When energizing transformers as seen in Figure 2.18, ideally no current should flow until all three switches are closed. Still, current can be seen flowing in the phases where the switches are not closed due to the capacitances in the circuit. Because of multi-legged transformer cores, voltages are induced in the open phases. Voltage will then *backfeed* the cable back to the open switches [37].

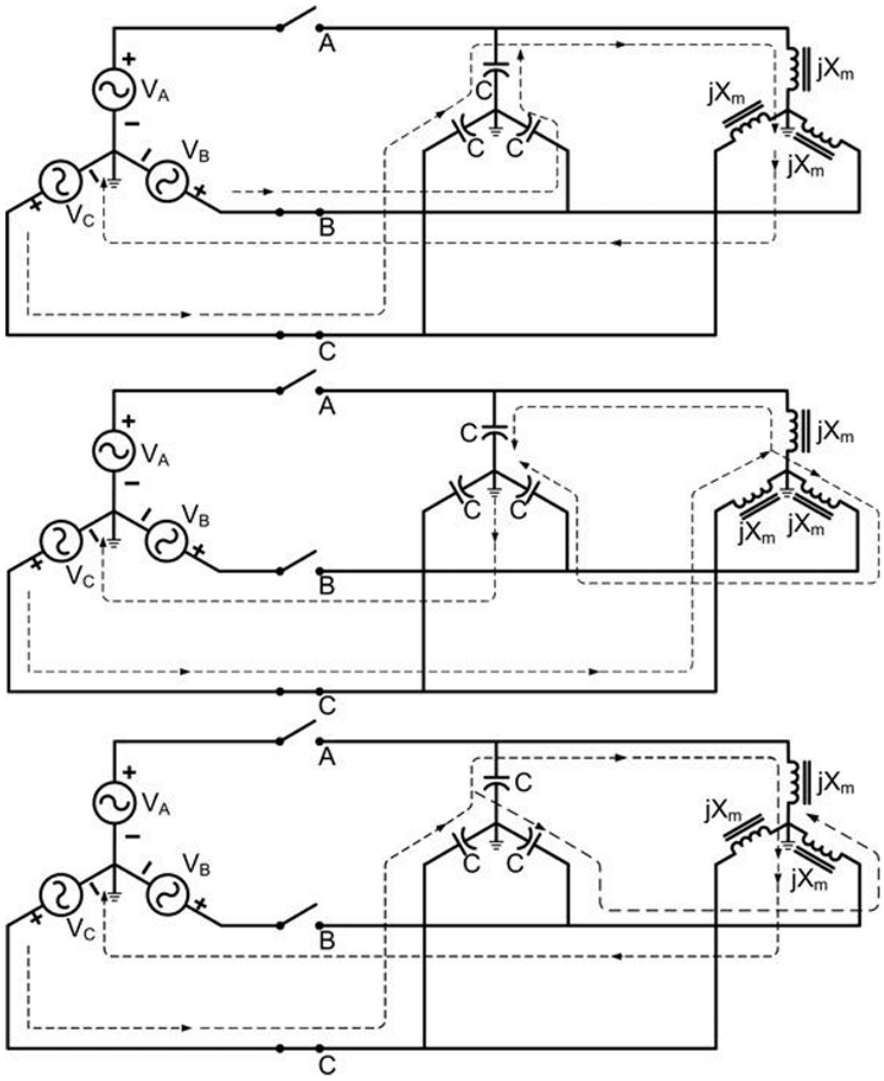


Figure 2.18: Examples of ferroresonance in three phase systems [37].

## 2.4 Practical Aspects of Circuit Breakers

In this section, the practical considerations regarding circuit breakers when performing a regular switching operation is explained. As for the preceding sections, the switches and their operations have been regarded as ideal, meaning that the switch can change instantly between being in open and closed position. In practice, a switching operation consists of several factors which influence the outcome of the switching. This section is limited to dealing with circuit breakers having mechanically moving contacts, as they are most common in high voltage systems and for the energization of transformers.

Figure 2.19 illustrates the five operating stages for a mechanical switching device. In stage 1 and 5, the switch is in open position having no galvanic connection between the

two sides. The switch acts as a perfect insulator regardless of the voltage level across its terminals. In stage 2, the switch is about to close, but as the contacts are approaching each other an electrical breakdown occurs over the gap. When the voltage across the gap exceeds the dielectric strength of the insulating material an electrical arc is created. In practice, electrical connection occurs before mechanical contact is established, as it is in stage 3. When the switch is closed, it is essential that he switch has a low resistance in order to keep the ohmic losses down, thus avoiding a high temperature increase.

Stage 4 shows how the contacts are mechanically separated when the switch is being opened. The electric arc can continue to burn across the gap if the energy dissipation is not controlled, or if the arc is not interrupted. For instance, a one kilo-ampere electric arc over a two metre long air gap will not be extinguished by itself [38]. Circuit breakers used to interrupt maximum current are therefore designed to decrease the arc's conductivity by cooling. After the arch is extinguished, the switch is in open position acting as a perfect insulator again.

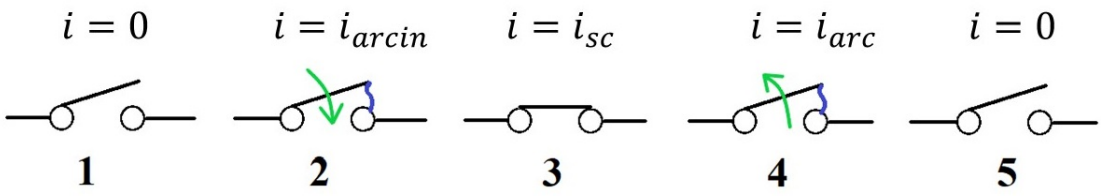


Figure 2.19: Operating stages of an electrical switch.

#### 2.4.0.1 Electrical Pre-arching

As mentioned, when closing a circuit breaker, electrical connection occurs before the poles have mechanical contact. As the gap between the poles is reduced, dielectric breakdown will occur when the voltage exceed the dielectric strength. This phenomena is often referred to as *pre-strike* or *pre-arch*, and is illustrated in Figure 2.20. For high voltage circuit breakers, the closing time refers to mechanical contact of the poles. The time interval between the circuit breaker being in the open position and until current starts to flow is called *make time* [39].

The voltage withstand capacity is a function of contact gap distance. During the closing operation, the dielectric strength becomes a function of time and it decays from its maximum value to zero at a rate called *Rate of Decrease of Dielectric Strength* (RDDS) [39].

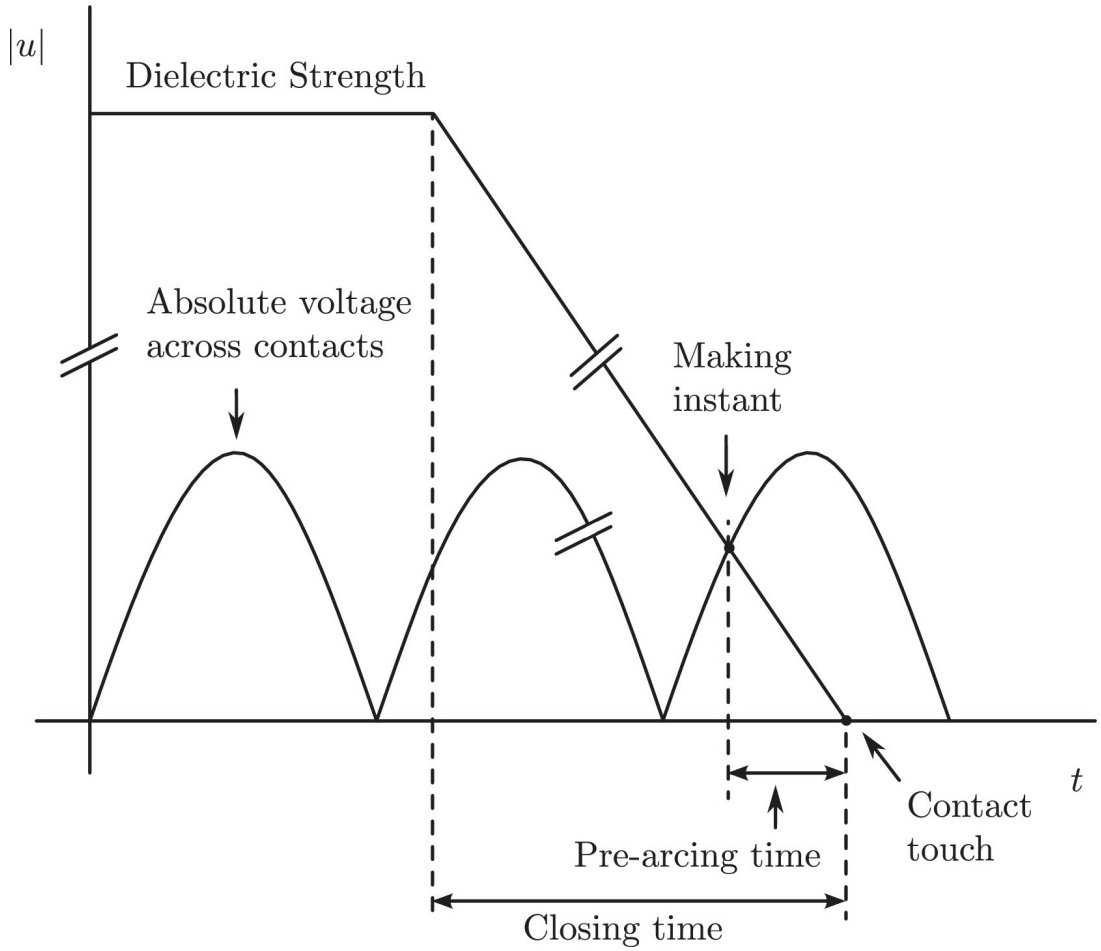


Figure 2.20: Pre-arching characteristics of a HVAC circuit breaker [18].

The RDDS is determined by the travel curve of the moving contact, the contact geometry, and the insulating medium between contact points. It is one of the most important characteristics for circuit breakers used in controlled switching procedures [40]. As the contacts cannot move with infinite speed, the RDDS has a finite value greater than zero, and pre-arching will therefore occur. Field tests have shown that the closing time can be shorten with as much as 1.2 ms due to pre-arching if the making instant was intended to occur at the voltage peak [28]. The effect of pre-strike must therefore be compensated for when implementing controlled switching techniques, like those explained in section 2.2.3.

#### 2.4.0.2 Mechanical Timing Deviation

A mechanical driven circuit breaker will have some operating time deviation because of changes is the system characteristics. Some of these characteristics, such as ambient temperature, battery voltage, and operating pressure can be compensated for by knowing

the correlation between them and the operating time. Although these features may cause a high closing time variation they can still be compensated for by adjusting the time for when the closing signal is sent. This will not affect the accuracy requirement needed when performing a controlled switching operation.

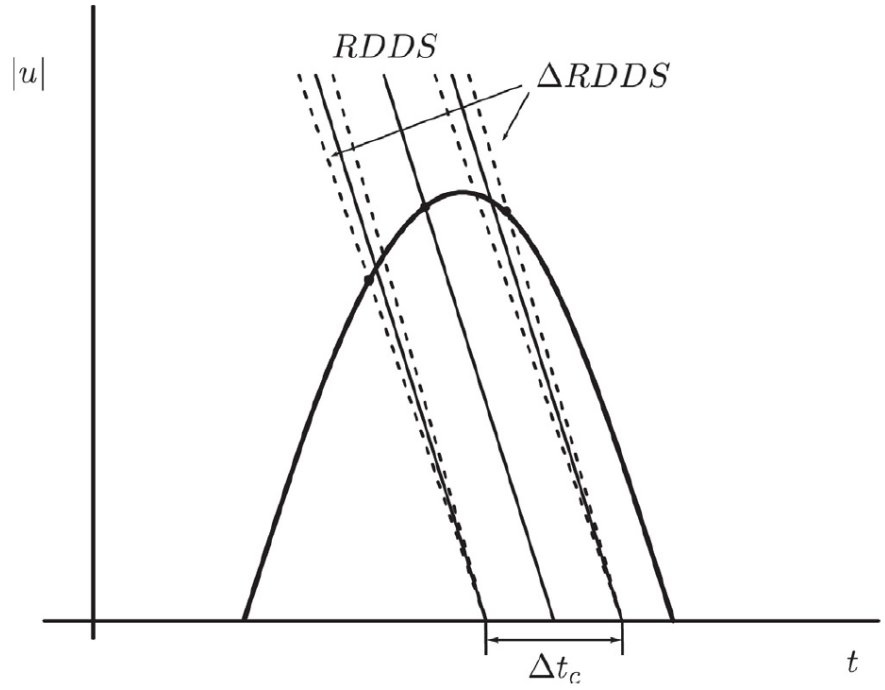


Figure 2.21: Making instant deviation caused by scattering of the CB's characteristics [18].

Still, a mechanical driven circuit breaker will in addition have some random statistical variation of the operating time that excludes the influence from external variables already mentioned [39]. By this definition, external variables refers to all variables which might have a systematic influence on the operating time. The scatter of mechanical operation time is known as *jitter*, and it will influence the making time. The mechanical time scatter recommendation is limited to ± 1 ms [39]. Figure 2.21 shows how the making instant deviation is caused by the combined effects of closing time deviation and variation in RDDS. The figure also reveals that because of mechanical time scatter, closing the circuit breakers on a rising voltage wave will reduce the inaccuracy of the making time compared to when closing at a falling voltage [26].

It has been seen that practical circuit breakers differs from ideal circuit breakers mainly by including the effects of pre-arching and closing time deviation. By doing so, the realistic switch cannot change instantly between being open and being closed, which adds complexity to the switching operation. Still, controlled switching strategies are the most

commonly used strategies to reduce inrush currents and severe overvoltages [41–43].

## 2.5 Summary of Preceding Theory

The theory of this chapter has covered the general challenges associated with energizing generator step-up transformers through a feeding cable. The concept of electrical transients was first explained before it was extended to include cables and transformers. The main objectives from each section of the preceding chapter are summarized as follows.

- An electrical transient is the temporally response to a sudden change in the network conditions. Energy is exchanged between the different parts of the circuits before a new steady state is reached. The transients analyzed in this chapter are caused mainly by switching operations.

- The amplitude of the inrush currents occurring when energizing a three phase transformer from its high voltage side is dependent on several factors. Having the greatest influence on the inrush current is the residual flux of the core legs, the closing strategy used, and the transformer core's knee point.

- Traveling waves of voltage and current is a phenomenon emerging when circuits constants are treated as distributed parameters instead of concentrated parameters. The current is no longer uni-valued at all points of a line, and the voltage can be discontinuous.

- Overvoltages in cable-transformer systems can occur when the resonances in the network are being excited by either the harmonics of the inrush currents, or the cable resonance frequency of travelling waves. Ferroresonance may occur when the non-linear inductance of a transformer core is interacting with the shunt capacitance of the feeder cable.

- Closing a circuit breaker on a rising voltage wave will reduce the inaccuracy of the making time compared to when closing at a falling voltage. This is crucial when implementing closing strategies used to mitigate inrush currents.

# Chapter 3

# EMTP Model for Energizing Studies

In this chapter the components constituting the simulation model are presented and explained in detail. Statkraft's hydro power plant Nedre Røssåga is used as reference when the simulation model is created in ATPDraw. The purpose of the present chapter is to describe the modelling methodologies used to obtain the complete representation of the network under study. Because transient phenomena happen at a range of frequencies, the model is divided into a study zone and an external zone. The elements of interest, that is the components where transient occur as well as the equipment interacting and influencing the transients, are all a part of the study zone. Since it can be difficult to determine which components that will be influencing the transients and not, drawing a solid line between the study zone and the external zone can be arduous.

## 3.1 Representation of the Main Components

Given that the frequencies of transients are different from the power system frequency, it is not possible to focus on a single fixed frequency when modelling the components of the study zone [44]. For instance, when simulating transients related to re-striking phenomena, the frequency spectrum ranges from below 1 kHz and up to tens of MHz [45]. When studying the energization of generator step-up transformers where the inrush currents are of interest, the typical frequencies of interest are composed of low order harmonics up to 1 kHz [46]. With the presence of a feeding cable between the circuit breaker and the transformer, the frequencies are dependent on the wave reflections as described in section 2.3.2.

Figure 3.1 presents the model and its components that will be modelled throughout this chapter. As seen from the figure, transformer energization by switching includes not only the transformer but also the circuit breaker, the upstream network, and the cable between them. The following sections demonstrates how the different parts are modelled in ATPDraw, based on obtainable background data and the components available in ATPDraw.

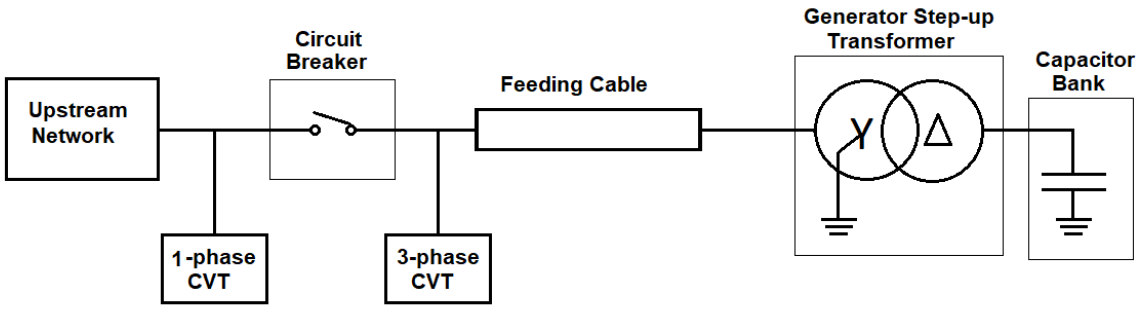


Figure 3.1: Schematic view of the generator step-up transformer energizing outline.

### 3.1.1 The Generator Step-up Transformer

The transformer being energized has to be modelled with sufficient details to represent the phenomena of interest. When studying transformer energization and voltage resonances, the transformer has to be modelled in such a way that it has a correct response in the frequency range of interest. For said situations, Cigré Working Group C4.307 highlights the following aspects, in order of importance, that needs to be represented in the model [11]:

- Leakage impedance and winding resistance
- Nonlinear saturation and core losses
- Air-core inductance
- Magnetic phase coupling
- Residual flux
- Frequency dependent winding losses
- Zero sequence impedance
- Hysteresis and frequency dependent iron losses
- Capacitance

The generator step-up transformer is modelled by using the hybrid transformer model implemented in ATPDraw under the name XFMR. The model includes an inverse inductance matrix for leakage inductance, optionally frequency dependent winding resistances, capacitive coupling, and a topologically correct core model with individual losses in legs and yokes [47]. It is a three phase model supporting 2 to 4 windings, suitable for frequencies up to 5 kHz [48]. The transformer can have either a three-limb, five-limb, shell-form, or triplex core construction. In addition, the parameter data for resistance, inductance, capacitance and core can be selected independently from three different sources; typical values, test report, and typical data. Parameter data based on test reports requires only standard open- and short-circuit tests, optionally supplemented with capacitive measurements. It is by the use of test report data the generator step-up transformer is modelled.

Figure 3.2 shows the electrical circuit of the hybrid transformer model having three phases, two windings and a three legged core. The four distinct parts, leakage inductance (blue), topologically correct core (green), winding resistance (orange), and capacitive effects (red) are all included in the figure. When a five legged core is modelled, $L_0$ is changed to a saturable core section like $Z_y$ and $Z_l$, representing the outer leg. It is by the principle of duality that the magnetic core is modelled as an electric circuit using only standard EMTP components [47]. In addition, by having knowledge about the relative core dimensions of the legs and yoke, the core losses can be split between legs and yokes, and the limbs can be saturated individually.

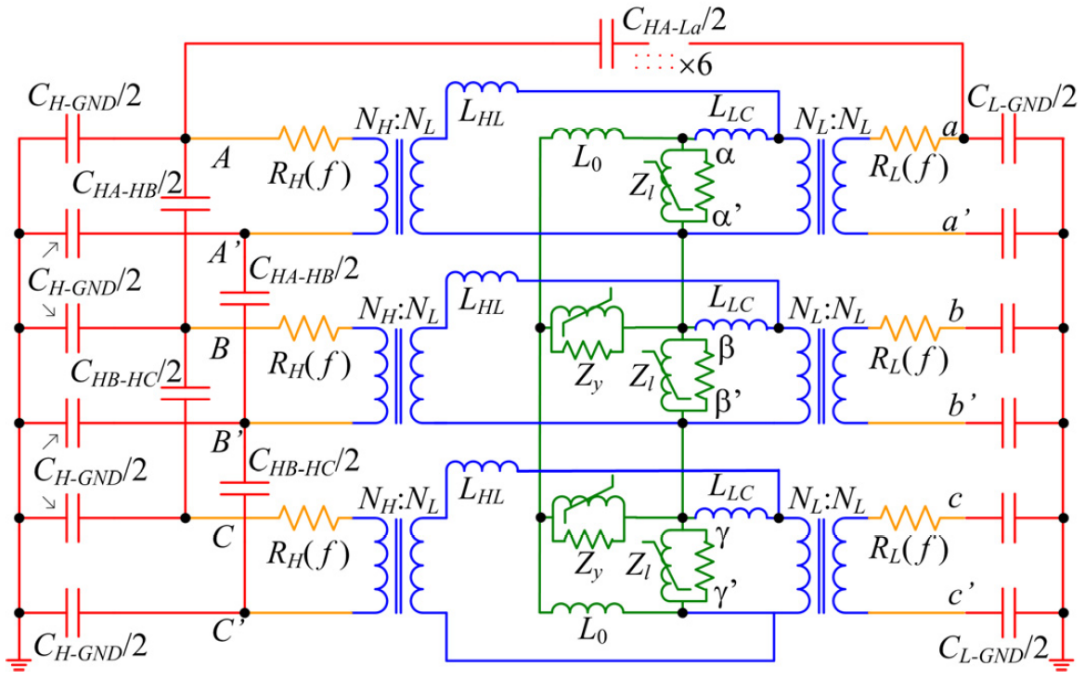


Figure 3.2: Electric circuit of XFMR having 2 windings, 3 phases and a 3-legged core [49].

In this thesis, the transformer model is based on test report data from Nedre Røssåga. The 260 MVA 420/16 kV transformer has a 5-legged stacked core with YNd11 coupling. Data from the open- and short-circuit tests are summarized and presented in Table 3.1. Data for the capacitances between phases where not available, thus set to zero. The capacitance between windings, that is primary to ground, secondary to ground and primary to secondary, are presented in Table 3.2.

| **Main data** | [kV] | [MVA] | [kA] | Coupling |
|---|---|---|---|---|
| HS | 420 | 260 | 0.357 | YN |
| LS | 16 | 260 | 9.382 | d11 |
| **Open-circuit** | $E_0$ [%] | [MVA] | $I_0$ [%] | $P_0$[kW] |
| LS | 90 | 260 | 0.035 | 76.70 |
| | 100 | 260 | 0.044 | 99.77 |
| | 110 | 260 | 0.096 | 110.0 |
| **Short-circuit** | [kV] | [MVA] | $ek$ [%] | $P_k$ [kW] |
| HS/LS | 420/16 | 260 | 12.2 | 460.55 |

Table 3.1: Test report data for the generator step-up transformer.

| **Capacitance** | Primary | Secondary | Primary-Secondary |
|---|---|---|---|
| C [nF] | 2.139 | 6.595 | 2.218 |

Table 3.2: Capacitance between windings in per phase values.

Because the core dimensions of the generator step-up transformer at Nedre Røssåga are not available, relative core dimensions of a 290 MVA five-legged stacked core transformer used in [47], are used as substitute. The yoke and outer leg areas are 0.54 times the main leg cross-sectional area. For the yoke and outer legs, the lengths are respectively 1.5 and 2.5 times the main leg length. The core dimensions are used by ATPDraw to split the core into resistive and inductive elements for the yoke and legs.

The flux linkage as a function of current is assumed to follow Frolich equation with three parameters[1]. In his master's thesis, Dr. Chiesa expanded the equation to include a final segment accounting for the air core inductance [51]. This resulted in the transformer model to more accurately reproduce the inrush currents occurring under deep saturation of the transformer core [51]. For the generator step-up transformer at Nedre Røssåga, the

[1]For more information about Frolich equation, refer to [47] and [50].

value of the air core inductance is not specified in the data-sheet, but is by ATP estimated to be 4.79616 mH.

For the transformer model to accurately reproduce the inrush currents occurring when the core is saturated, the model has to be able account for both residual flux and hysteresis losses. This is ensured by modelling the core non-linearities as Type-96 inductors, a standard component of ATP [52]. In Figure 3.2 seen as a current dependent inductance in the core. As it is regarded as out for scope for this thesis to explain how the XFMR routine builds the transformer model in ATP, it is referred to [53] and [54] for more information.

The transformer zero sequence impedance is 82 Ω, as stated in the data sheet, and it is assumed to be purely inductive. With that in place, every aspect proposed by CIGRE Working Group C4.307 is represented in the transformer model.

### 3.1.2 The Feeding Cable

The feeding cable is the the component connected to the terminals of the generator step-up transformer. Because the cable is closest to the nodes of interest, it must be modelled with a great level of detail in order to reproduce the voltages occurring at the transformer terminals. Since the cable is able it interact with the energized transformer, and possibly create resonance overvoltages at the terminals, the cable model has to support travelling waves.

The Bergeron cable model [52] is used to model the feeding cable. It is a constant frequency model based on travelling wave theory, as explained in section 2.3.2. Lossless line segments are combined with lumped series resistances, as seen in Figure 3.3, to represent travelling waves but still include losses. The cable resistance is split into three lumped portions placed at the the ends and at the middle of the cable. As long as the total cable resistance is much smaller than the characteristic impedance, that is $R \cdot l \ll Z_0$, the errors from lumping the resistance are acceptable [55].

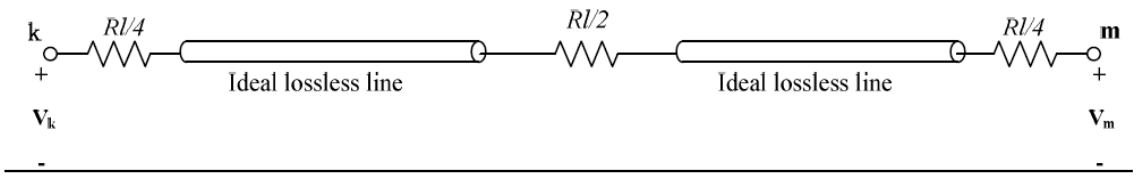


Figure 3.3: Structure of Bergeron cable model [56].

The parameters of the model are said to be constant, but the model is still frequency dependent. This means that the parameters resistance, capacitance and inductance $(R, C, L)$ are constant, but the shunt admittance and series impedance are frequency dependent, givens as:

$$Y = j\omega C \qquad \text{and} \qquad Z = R + j\omega L \tag{3.1}$$

The cable connecting the the generator step-up transformer and the grid is in reality three single core aluminum cables in trefoil formation. The cable data sheet used to obtain geometric data is found in Appendix B, and the extracted data used in ATPDraw are presented in Table 3.3. The rightmost two columns of the table contains the relative permittivity and permeability of the insulation.

| **Data** | $R_{in}$ [mm] | $R_{out}$ [mm] | Rho $[\Omega \cdot m]$ | $\mu_r$ | $\varepsilon_r$(ins) | $\mu_r$(ins) |
|---|---|---|---|---|---|---|
| Core | 5.66 | 15.25 | 2.826E-8 | 1.0 | 2.25 | 1.0 |
| Sheath | 46.15 | 47.865 | 2.826E-8 | 1.0 | 2.25 | 1.0 |

Table 3.3: Data used to obtain the cable model.

As the cable has a 630 mm$^2$ conductor with an outer diameter of 30.5 mm, it has to be modelled with an inner radius of 5.66 mm in order to preserve both the cross-sectional area and the outer diameter. In ATPDraw, the cable section template was created by calculating the line parameters at 50 Hz for a cable length of 1000 meters. The three cables are modelled as trefoil formation located one meter above the ground surface, as if mounted on a cable tray. Figure 3.4 depicts the trefoil formation of the cables.

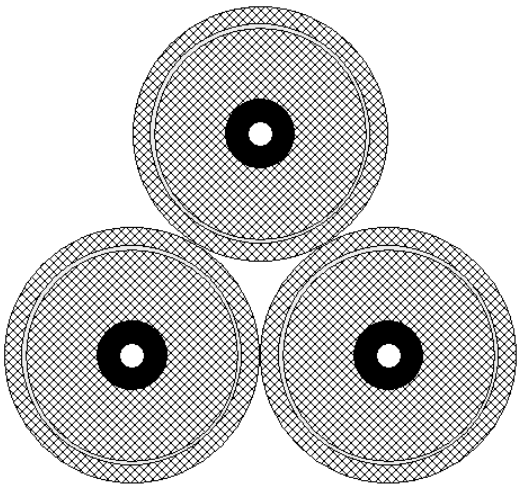

Figure 3.4: The trefoil formation of the feeder cables.

#### 3.1.2.1 Cable Modelling Discussion - A Side Note

A distributed parameter model at constant frequency, in other words the Bergeron model, is only recommended when the studies involve only a single frequency of interest. The Bergeron model yields a good approximation for low order harmonics and power frequency analysis, but transients studies over a greater frequency range will contain errors. This is due to the fact that the Bergeron model is a constant parameter model, meaning that the cable parameters such as $L$, $C$ and $Z_0$ are calculated at a specified frequency. As a consequence, the user is left with a trade of for at which frequencies the model should be most accurate.

ATPDraw offers some frequency-dependent models in its standard components assortment, and both single phase and multi phase models are available. JMarti is a line/cable model which represents the frequency dependence of all parameters, not just for one frequency as the Bergeron model. The JMarti model can be fitted for a wide frequency range, but it assumes a constant transformer matrix during modal calculations. Neglecting the frequency dependency of the transformation matrix is acceptable for overhead lines, but not for cables [52]. This has been tested in [57], where it was seen that the JMarti model for cables has significant weaknesses, especially for calculation of induced voltages. The JMarti line was tested for the feeder cable in this thesis, but with little success. As a final note it is stressed that the JMarti model still is very suitable for overhead line modelling.

### 3.1.3 Upstream Network Representation

The hydro power station is connected to the main grid via a feeding cable and circuit breakers. In general, the upstream network consists of several substations and generators interconnected via high voltage overhead lines. Because of the degree of extension and complexity of the power grid, a detailed representation of the whole upstream network is simply not possible. Simplified equivalent networks are therefore commonly used. By simplifying the overlying supply grid both the time to build the model and the computational burden is reduced. For the model to maintain its accuracy it is important that the network equivalent reproduce the frequency response of the actual network. This is especially important when simulating transformer inrush current and resonant overvoltages, or other electromagnetic transients occurring over a wide frequency range [58].

When energizing a generator step-up transformer via a feeding cable, the upstream network behind the busbar connecting the power grid and the circuit breaker is outside of the study zone. Still, the simplified network representation has to represent the most important natural frequencies from almost DC and up to around one kHz. In this study, the upstream network (lines and substation equipment) are represented up to the closest substation in the grid. From there, the rest of the network is represented by its power frequency network equivalent. This method is commonly used because it reduces the computational burden and the time needed to build the model [11]. The power frequency network equivalent is composed of the network's Thevenin impedance, found from short circuit calculations based on steady state power flow analysis.

As seen from Figure 3.5, two feeders depart from the outdoor switchyard at Nedre Røssåga. For simplicity they are in this thesis named feeder 1 and 2, where feeder 1 is a 40 kilometer long FeAl 380 duplex overhead line. It is modelled as a JMarti overhead line segment in ATPDraw, based on characteristics of steel reinforced aluminum conductors used in Norway [59]. The second feeder departing from Nedre Røssåga is connected via a 420/300 kV 1000 MVA autotransformer. Because only limited data is available for this transformer, the hybrid transformer XFMR based on typical values, is used to build the model. Table 3.4 sums up the data used to generate the line and autotransformer.

| **Overhead Line** | $R_{in}$ [mm] | $R_{out}$ [mm] | Resistance [$\Omega/km$] | Bundle |
|---|---|---|---|---|
| Conductor | 5.70 | 17.0 | 0.0477 | 2 |
| **Transformer** | [kV] | [MVA] | $ek$ [%] | Core |
| HS/LS | 420/300 | 1000 | 4.4 | 3-legged |

Table 3.4: Data used to generate the overhead line and the autotransformer.

As the distance from the transformer of interest increases, the rest of the system can be represented by its power frequency equivalent and a voltage source [11]. Thevenin equivalents based on short circuit data are used to represent the connected system as shown in Figure 3.5. The damping angle is set to 82.6°, given by the X/R ratio from network studies performed in 2017. The Thevenin impedances for feeder 1 and 2 are found from short circuit calculations based on steady state power flow analysis. In Table 3.5, the underlying short circuit data used to obtain the thevenin impedances applied in the power frequency model are presented. It is pointed out that the power grid data is limited by the transmission system operator, and the data used in this thesis is therefore of semi fictional character.

| **Main data** | $S_{sc}$ [MVA] | $I_{sc}$ [kA] | X/R | **Thevenin impedance** R +jX [Ω] |
|---|---|---|---|---|
| Feeder 1 | 4200 | 5.77 | 7.7 | 5.40 + j41.65 |
| Feeder 2 | 3100 | 5.97 | 7.7 | 3.74 + j28.76 |

Table 3.5: Data used to obtain the Thevenin equivalent impedances for line 1 and 2.

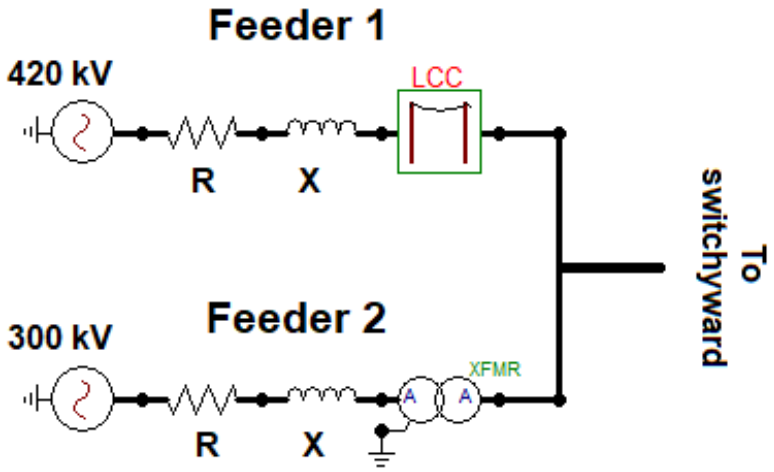


Figure 3.5: The upstream network representation showing the two feeders departing from Nedre Røssåga.

## 3.2 Modelling of Auxiliary Components

A hydro power station includes more than just the generator-step-up transformer, its feeding cable, and the supplying network. Auxiliary components at site can be important factors when performing a transient analysis. Treated in this thesis are the capacitive voltage transformers (CVT), used for performing measurements at the site, and the circuit breaker constituting the link between the supply network and the feeding cable. In addition, surge arresters are placed on each end of the feeding cable.

### 3.2.1 Capacitive Voltage Transformer

The simulation model of Nedre Røssåga contains two capacitive voltage transformers. A single phase CVT is connected at phase B of the upstream network busbar, and 3 CVTs are connected between each phase and ground, located between the feeding cable and the circuit breaker. Each of the capacitive voltage transformers are modelled as seen in Figure 3.6, consisting of two capacitances in series, a compensating reactor, a step-down transformer, and a damping impedance.

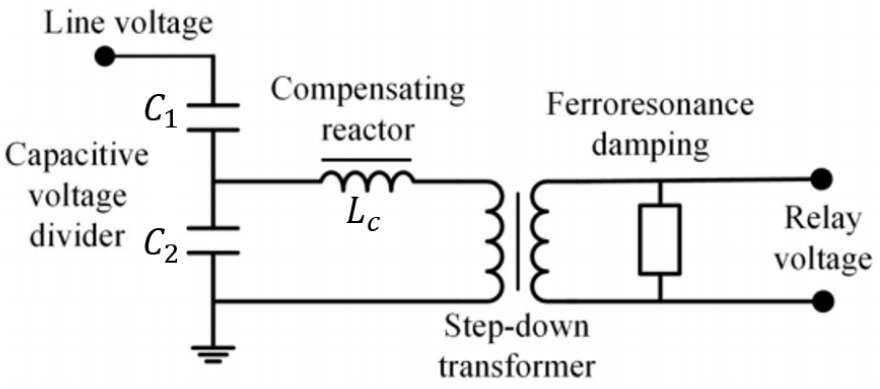


Figure 3.6: Simplified circuit diagram of a capacitive voltage transformer [60].

The data used to construct the capacitive voltage transformer in ATPDraw are presented in Table 3.6. Because only limited data are available from the CVT data sheet, the compensating reactor and the ferroresonance damping component have to be estimated based on general design data. The burden, which in the model is a merger of both the ferroresonance damping and the relay impedance, is assumed to be purely resistive.

| **Parameter** | $C_1\ [\mu F]$ | $C_2\ [\mu F]$ | $L_c\ [mH]$ | Turns ratio | Burden [Ω] |
|---|---|---|---|---|---|
| Data | 0.0050 | 0.1064 | 90950* | 172:1 | 1000* |

* Estimated values, not from data sheet.

Table 3.6: Data used to construct the capacitive voltage transformer.

The primary function of the capacitances $C_1$ and $C_2$ is to step down the line voltage to an intermediate level, usually around 5 kV to 20 kV [61]. In order to prevent any phase shifts from the capacitors, the compensating reactor is designed to cancel out the capacitor reactance at system frequency, according to NEK IEC 61869-5 [62]. The value of the compensating reactor $L_c$ can accordingly be obtained by the usage of Equation (3.2),

from [62]. The equation states how $L_c$ is determined based on the capacitances $C_1$ and $C_2$ for the power system frequency $f_R$. Inserting $f_r = 50$ Hz and the values of $C_1$ and $C_2$ from Table 3.6 yields an inductor of 90950 mH.

$$L_c = \frac{1}{(2\pi f_R)^2 \cdot (C_1 + C_2)} \tag{3.2}$$

### 3.2.2 Independent Pole Operated Circuit Breaker

A three phase independent pole operated circuit breaker is used to connect Nedre Røssåga and the electrical grid. CIGRE Study Committee 33 proposed a guideline for how to represent circuit breakers when studying transient phenomena for different frequency ranges [63]. The guidelines are summarized and presented in Table 3.7. It can be seen that when simulating closing operations for low frequency and slow-front transients, mechanical pole spread is the most important part to consider. From the table it is seen that pre-strikes are negligible for low frequency transients but important for slow-front transients

<table>
<tr><th colspan="2" rowspan="2">Operation</th><th>Low frequency transients</th><th>Slow-front transients</th><th>Fast-front transients</th><th>Very fast-front transient</th></tr>
<tr><th>(0.1 Hz - 3 kHz)</th><th>(50 Hz - 20 kHz)</th><th>(10 kHz - 3 MHz)</th><th>(100 kHz - 50 MHz)</th></tr>
<tr><td rowspan="2">Closing</td><td>Mechanical pole spread</td><td>Important</td><td>Very important</td><td>Negligible</td><td>Negligible</td></tr>
<tr><td>Prestrikes</td><td>Negligible</td><td>Important</td><td>Important</td><td>Very important</td></tr>
<tr><td rowspan="4">Opening</td><td>High current interruption</td><td colspan="2">Important only for interruption capability studies</td><td>Negligible</td><td>Negligible</td></tr>
<tr><td>Current chopping</td><td>Negligible</td><td colspan="2">Important only for interruption of small inductive currents</td><td>Negligible</td></tr>
<tr><td>Restrike characteristics</td><td>Negligible</td><td rowspan="2">Important only for interruption of small inductive currents</td><td>Very important</td><td>Very important</td></tr>
<tr><td>High frequency current interruption</td><td>Negligible</td><td>Very important</td><td>Important</td></tr>
</table>

Table 3.7: Modelling guidelines for circuit breakers in transient studies [63].

The circuit breaker used in this thesis is modelled as a three phase ideal time controlled switch with independently operated poles. This method of representing circuit breakers is commonly used when simulating transients related to transformer energization [28,64–66].

As explained in section 2.4, ideal switches can change instantly between open and closed position. For opening operations, the ideal time operated switch in ATPDraw opens at the first current zero crossing after the specified opening time. Alternatively, a current margin can be included such that opening happens at the first instant the current is less than the margin, after the specified opening time. To clarify, by including a current margin, the switch will open at $t > T_{open}$ if $|I| < I_{margin}$. This feature can be added to approximate current chopping, as needed when modelling slow- and fast-front transients. For simulations in this thesis, the current margin is hence set to zero.

## 3.3 The Complete Model in ATPDraw

The complete EMTP model is constructed by connecting the components introduced in the preceding sections of this chapter. Figure 3.7 shows the ATPDraw circuit and how the components are linked together. The generator step-up transformer is located on the right hand side of the figure, having a three phase 130 nF capacitor bank connected to its low voltage side. At the high voltage terminals of the same transformer, core flux measurements are created by integrating the phase voltage for each phase. The same method is used to obtain the prospective flux measurements, but here the upstream grid voltage is integrated instead. Max/min models are included to monitor the maximum amplitudes of both voltage and current.

Two surge arresters, located at each cable end, are modeled as exponential current-dependent resistors. It is a built in component in ATPDraw, and is used to protect the transformer from overvoltages due to lightning or switching operations in the network.

When running simulations in a model using travelling wave components, the simulation time step is limited by the propagation time in the shortest line/cable. For the Bergeron cable model the simulation time step is limited to a maximum of half of the propagation time of the shortest line modelled [11]. If the cable is very short, the simulation time step will have to be even smaller and thus increase the total simulation time. The energization process will be simulated by closing the circuit breaker separating the supply network from the generator step-up transformer. All simulation results are presented in the next chapter.

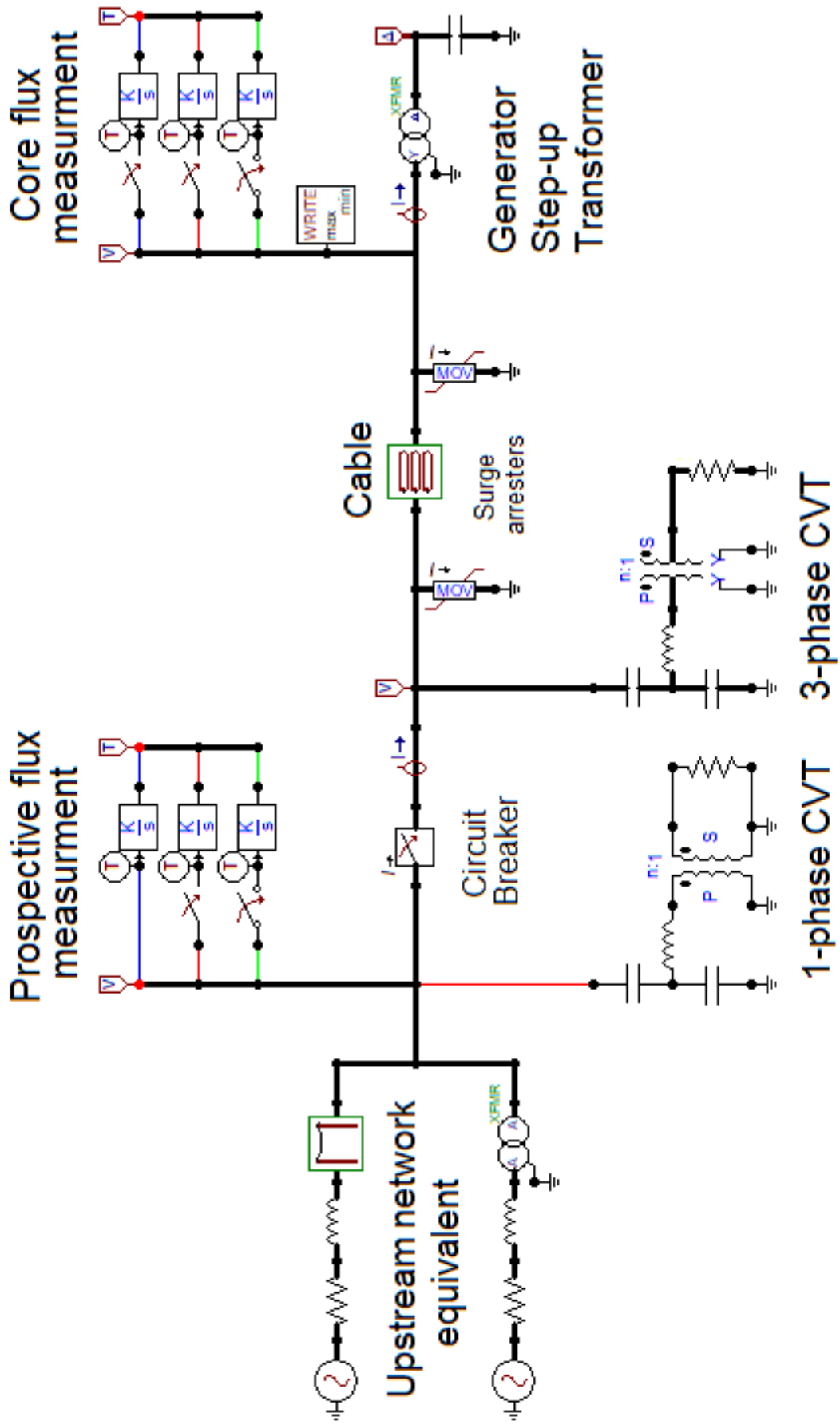


Figure 3.7: Insert mad picture caption here picture of complete model.

# Chapter 4

# EMTP Simulation Results

This chapter presents the results obtained by performing energizing simulations on the model from the previous chapter. In the first section, transformer inrush currents and the HV-terminal overvoltages are simulated for various energizing times, energizing strategies, power grid configurations and feeding cable lengths. In the second section, simulations are compared to measurements from Nedre Røssåga, for two events of energization. Analysis of results and further discussion of the simulations are left for chapter 5.

## 4.1 General Transformer Energizing Simulations

In the following results, simulation measurements of current and voltage are performed at the high voltage terminals of the generator step-up transformer. Unless stated otherwise, simulation are performed using the upstream network from section 3.1.3, and without residual flux in the transformer core. When the instantaneous voltage and current waveforms are displayed in graphs, the peak value of the nominal voltage or current is considered as 1 pu. In other words, the base values are the rms values multiplied by $\sqrt{2}$, and the transformer rating at the high voltage terminals are taken as reference. The base values are given in Table 4.1.

| Per unit | Formula | Base Value |
|---|---|---|
| Voltage | $V_{base} = \sqrt{2} \cdot \frac{420 \text{ kV}}{\sqrt{3}}$ | 342930 [V] |
| Current | $I_{base} = \sqrt{2} \cdot \frac{260 \text{ MVA}}{\sqrt{3} \cdot 420 \text{ kV}}$ | 505.45 [A] |

Table 4.1: Base values for voltage and current.

### 4.1.1 Effect of Closing Times

Figure 4.2 to 4.7 shows the effect on maximum voltage and current based on changes in closing times for phase A, B, and C. In the figures mentioned, phase A is energized at time $T_a$, and phase B and C are energized simultaneously at time $T_a + Delay$. A delay time of 0 ms will therefore represents simultaneous closing strategy, as explained in section 2.2.3.3. The time $T_a$ is relative to the negative voltage peak of phase A, meaning that at $T_a = 0$, phase A has its negative peak, seen from Figure 4.1. Both $T_a$ and $Delay$ goes from 0 ms to 10 ms with steps of 0.5 ms, and measurements are made for all phases.

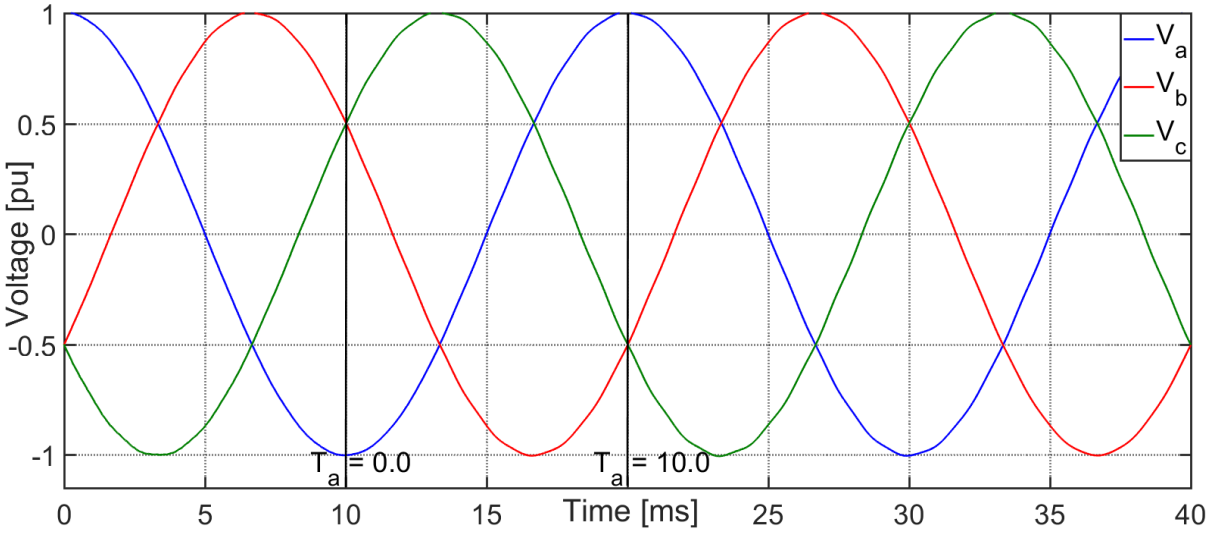


Figure 4.1: Reference time $T_a$ and the voltage in phase A, B, and C.

The overall maximum values of voltage and current from Figure 4.2 to 4.7 are presented in Table 4.2. Highest current peak occurs in phase C and the highest voltage peak occurs in phase B. Detailed data from Figure 4.2 to 4.7 are presented in Table C.1 to C.6, where the maximum values for current and voltage are written in bold text.

| | Phase | Value [pu] | $T_a$ [ms] | Delay [ms] | Figure | Table |
|---|---|---|---|---|---|---|
| Current | C | 1.4348 | 5.5 | 4.5 | 4.6 | C.5 |
| Voltage | B | 1.5710 | 9.0 | 7.0 | 4.5 | C.4 |

Table 4.2: Overall absolute maximum current and voltage peaks.

#### 4.1.1.1 Phase A

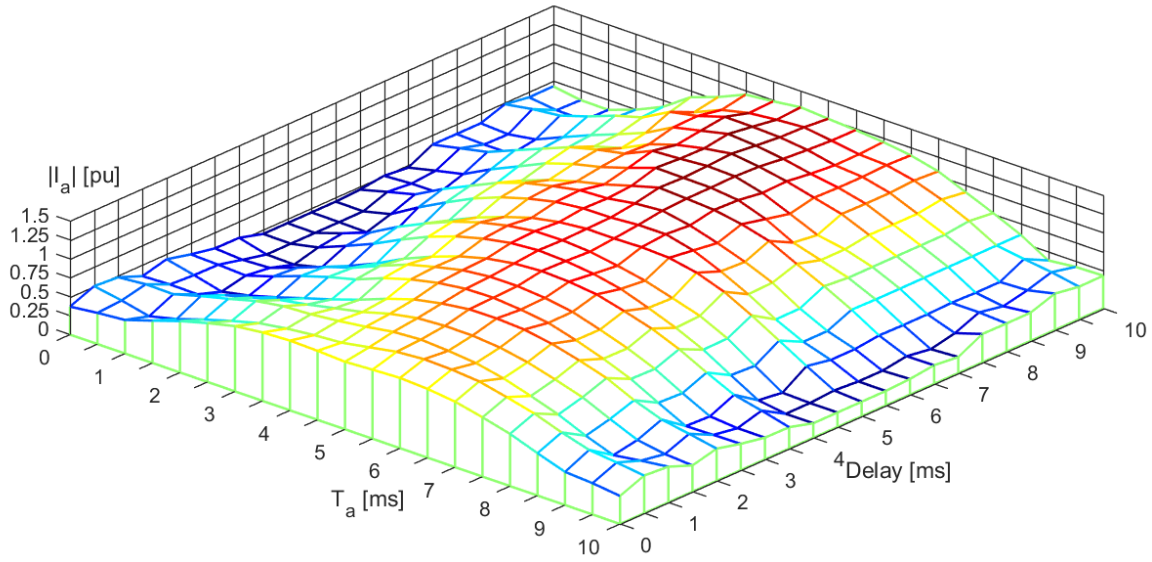


Figure 4.2: Maximum current peak at phase A as a function of $T_a$ and *Delay*.

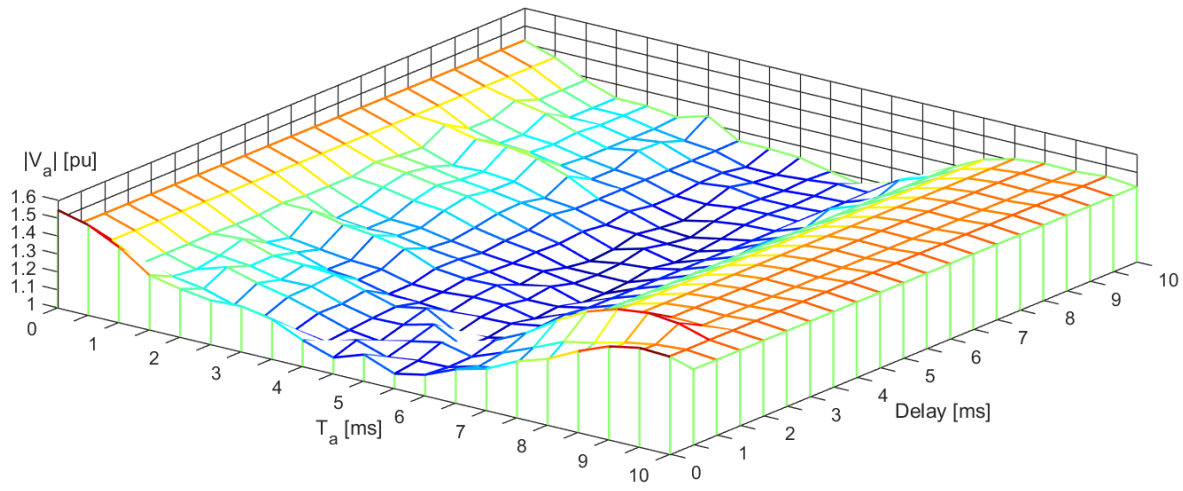


Figure 4.3: Maximum voltage peak at phase A as a function of $T_a$ and *Delay*.

#### 4.1.1.2 Phase B

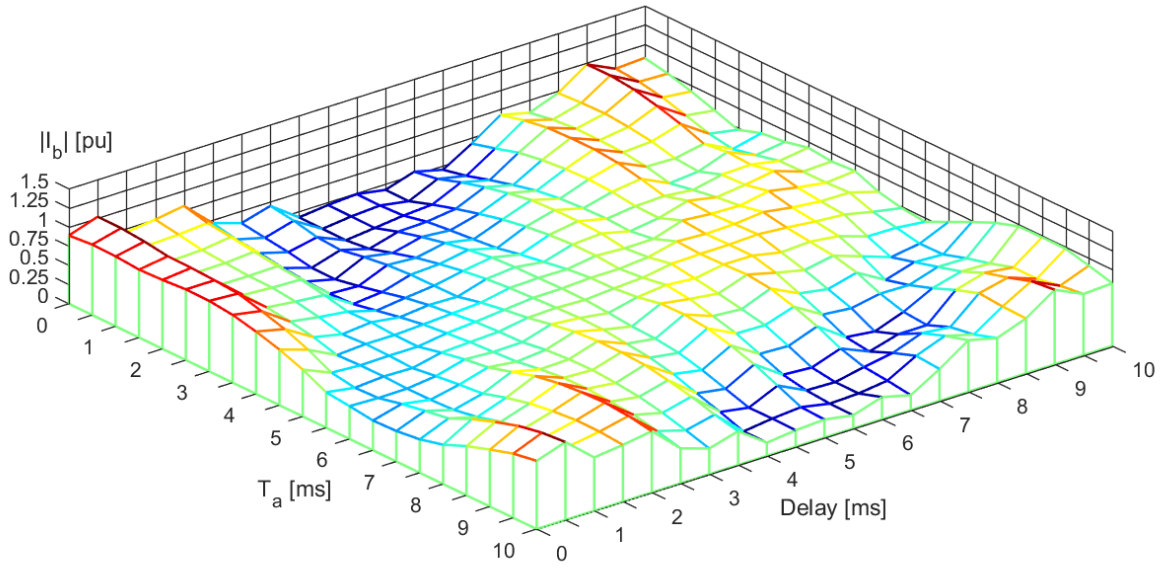


Figure 4.4: Maximum current peak at phase B as a function of $T_a$ and *Delay*.

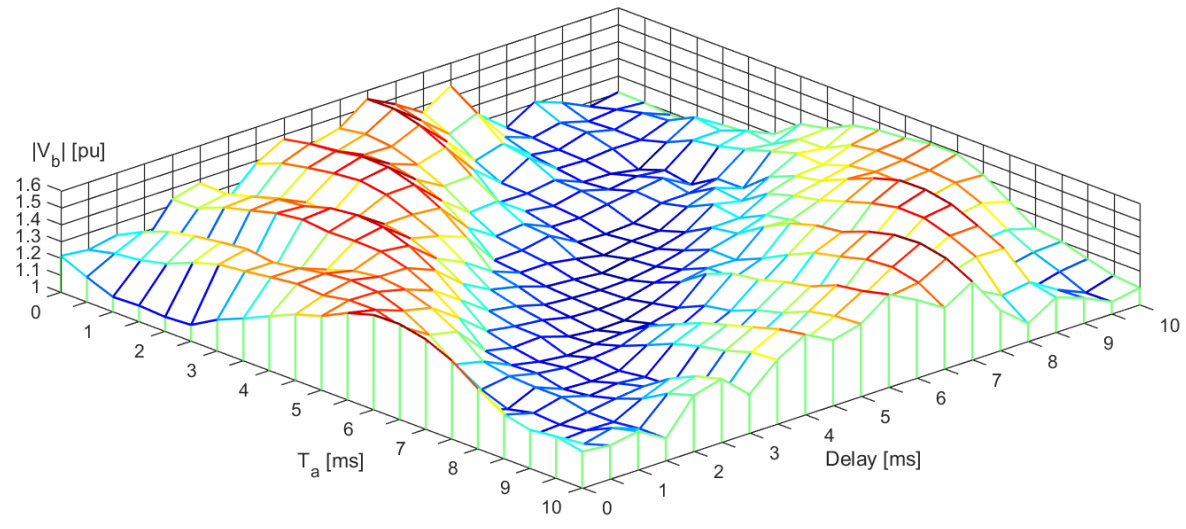


Figure 4.5: Maximum voltage peak at phase B as a function of $T_a$ and *Delay*.

#### 4.1.1.3 Phase C

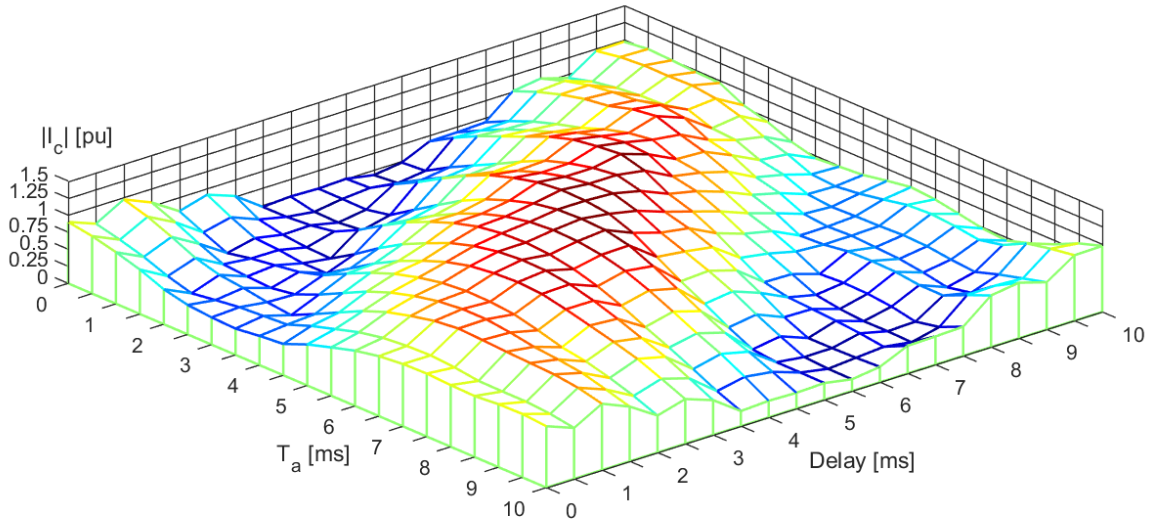


Figure 4.6: Maximum current peak at phase C as a function $T_a$ and *Delay*.

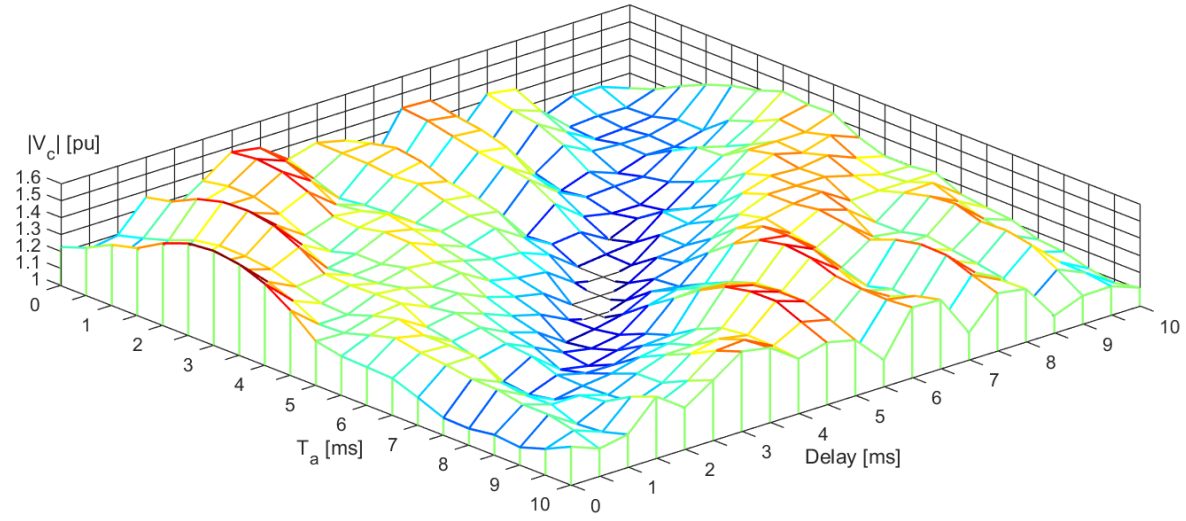


Figure 4.7: Maximum voltage peak at phase C as a function of $T_a$ and *Delay*.

#### 4.1.1.4 Time Plots of Maximum Current and Voltage

Time plot for the two situations accentuated in Table 4.2 are shown in Figure 4.8 and 4.9. Figure 4.8 shows the current for a switching time $T_a = 5.5$ and $Delay = 4.5$, which gives an overall maximum current peak in phase C. Figure 4.9 shows the voltage for a switching time $T_a = 9.0$ and $Delay = 7.0$, which gives an overall maximum voltage peak in phase B.

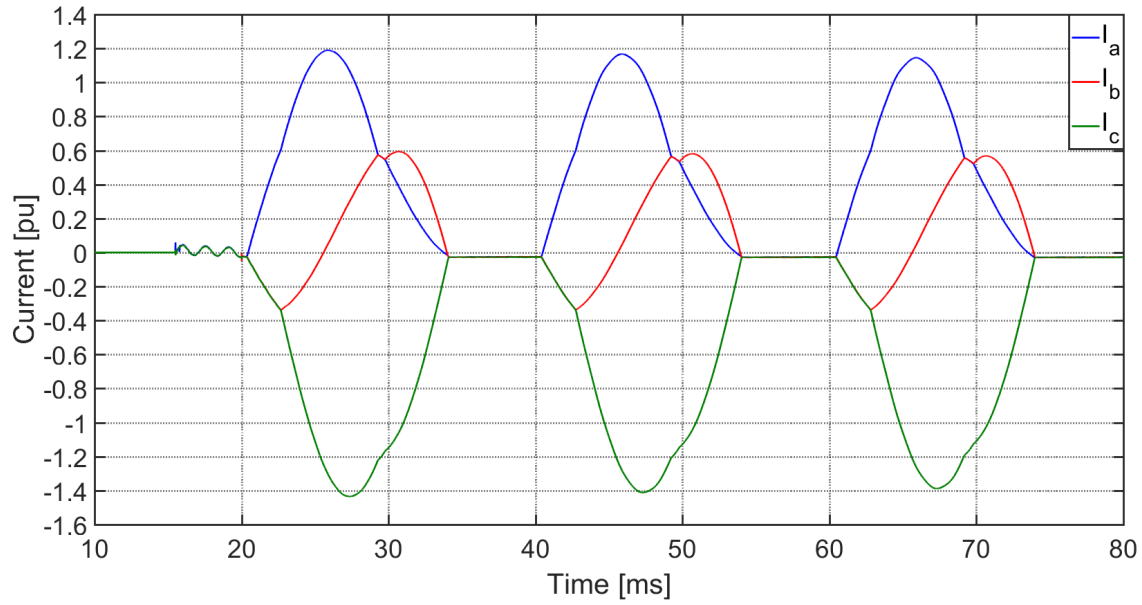


Figure 4.8: Current in phase A, B and C for $T_a = 5.5$ and $Delay = 4.5$.

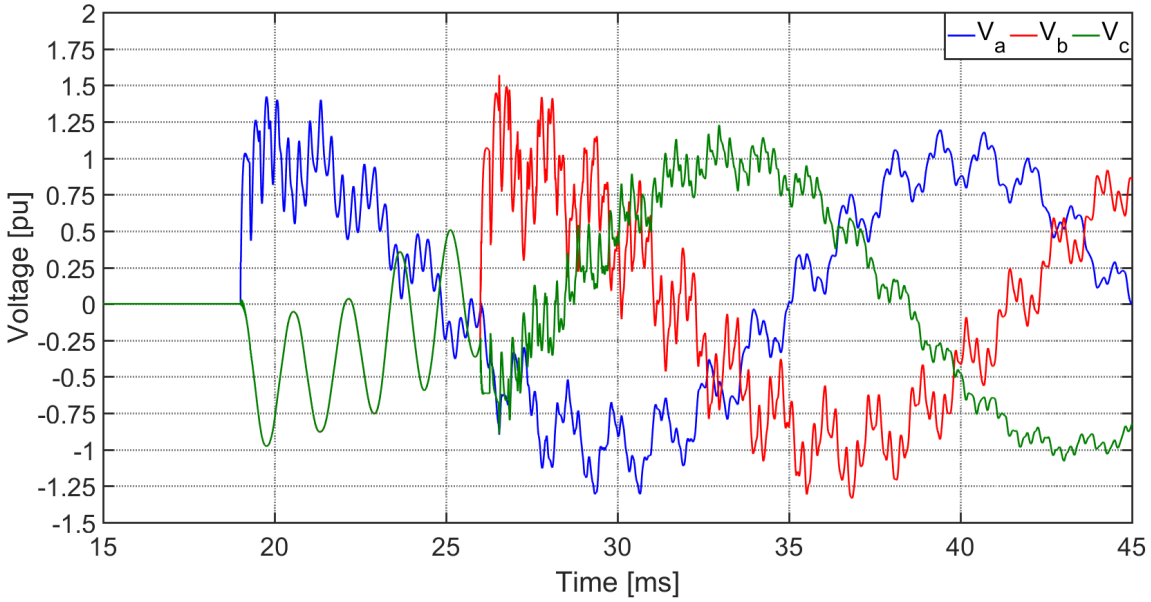


Figure 4.9: Voltage in phase A, B and C for $T_a = 9.0$ and $Delay = 7.0$.

#### 4.1.1.5 Time Plots of Minimum Current and Voltage

Each combination of $T_a$ and *Delay* gives a maximum current and voltage peak in each phase, seen from Figure 4.2 to Figure 4.7. The minimum current and voltage are found by comparing the maximum amplitudes across all three phases, and then select the minimum. Figure 4.10 shows time plot for lowest current, obtained by energizing times $T_a = 0.5$ ms and $Delay = 4.0$ ms. Figure 4.11 shows time plots for minimum voltage, where the energizing times $T_a = 4.5$ ms and $Delay = 5.5$ ms are used.

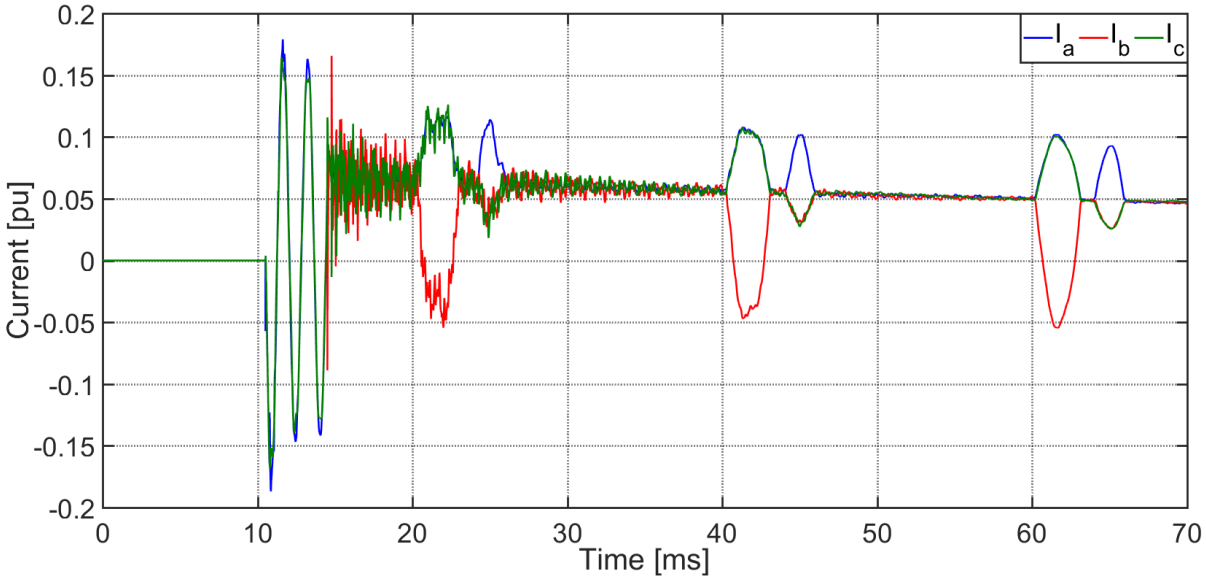


Figure 4.10: Current in phase A, B and C for $T_a = 0.5$ ms and $Delay = 4.0$ ms.

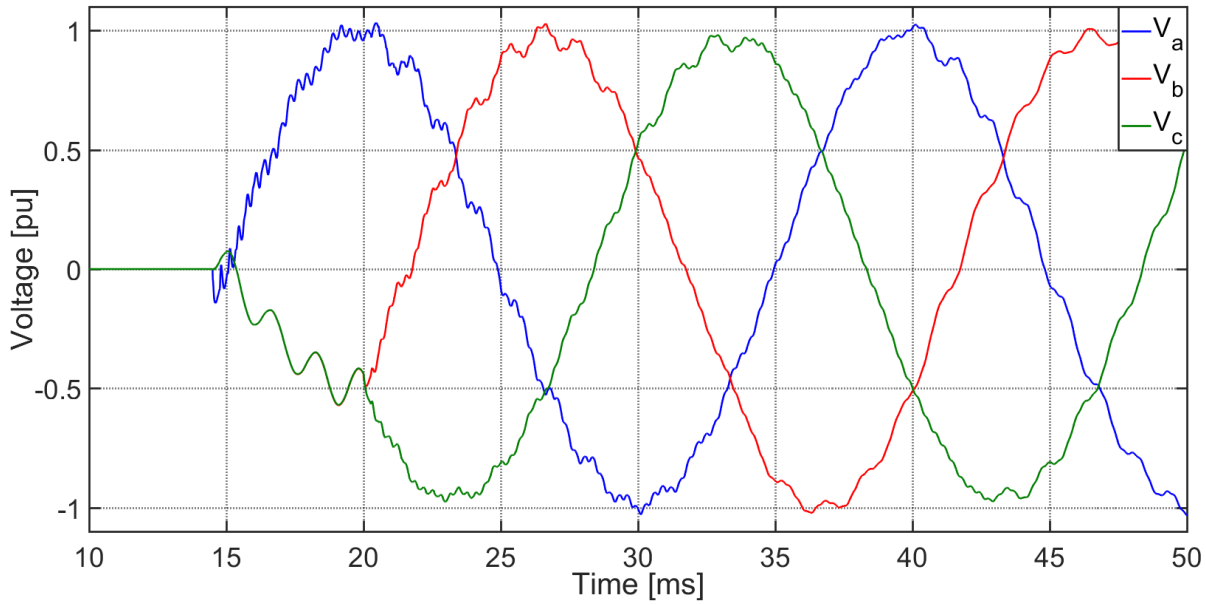


Figure 4.11: Voltage in phase A, B and C for $T_a = 4.5$ ms and $Delay = 5.5$ ms.

#### 4.1.1.6 Time Plots of Maximum Current and Voltage for a Weak Grid

A weak grid is created by disconnecting feeder 1 and feeder 2 of the supply network from Figure 3.5. In Figure 4.12 and 4.13 subscript 1 and 2 represents the network without feeder 1 and 2 respectively. The energizing times are the same as in the previous plots.

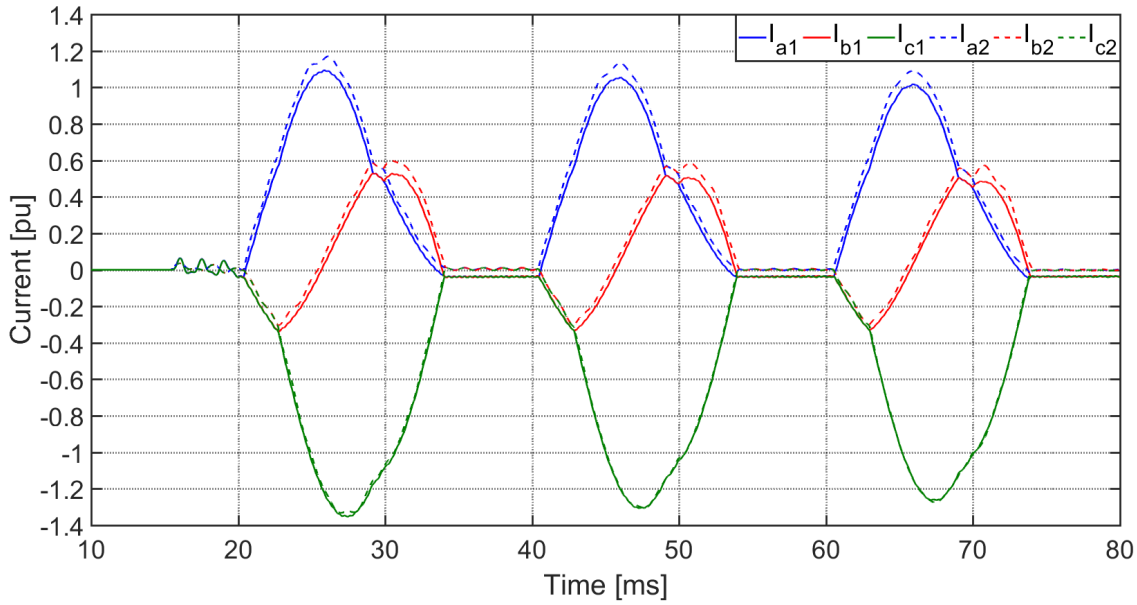


Figure 4.12: Current in phase A, B and C for $T_a = 5.5$ and $Delay = 4.5$, without feeder 1 (solid lines) and without feeder 2 (dashed lines).

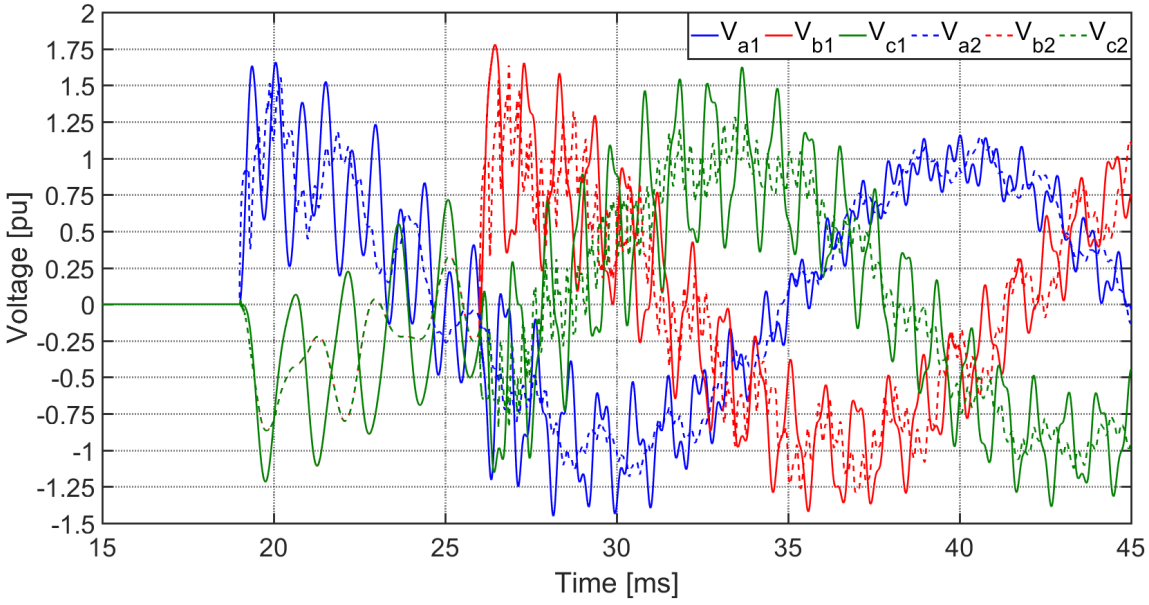


Figure 4.13: Voltage in phase A, B and C for $T_a = 9.0$ and $Delay = 7.0$, without feeder 1 (solid lines) and without feeder 2 (dashed lines).

### 4.1.2 The Effect of Cable Length

The effect of cable length is tested with the full grid, and for the energizing times found to give maximum current ($T_a = 5.5$ and $Delay = 4.5$) and maximum voltage ($T_a = 9.0$ and $Delay = 7.0$). The cable length is varied by steps of 50 meters.

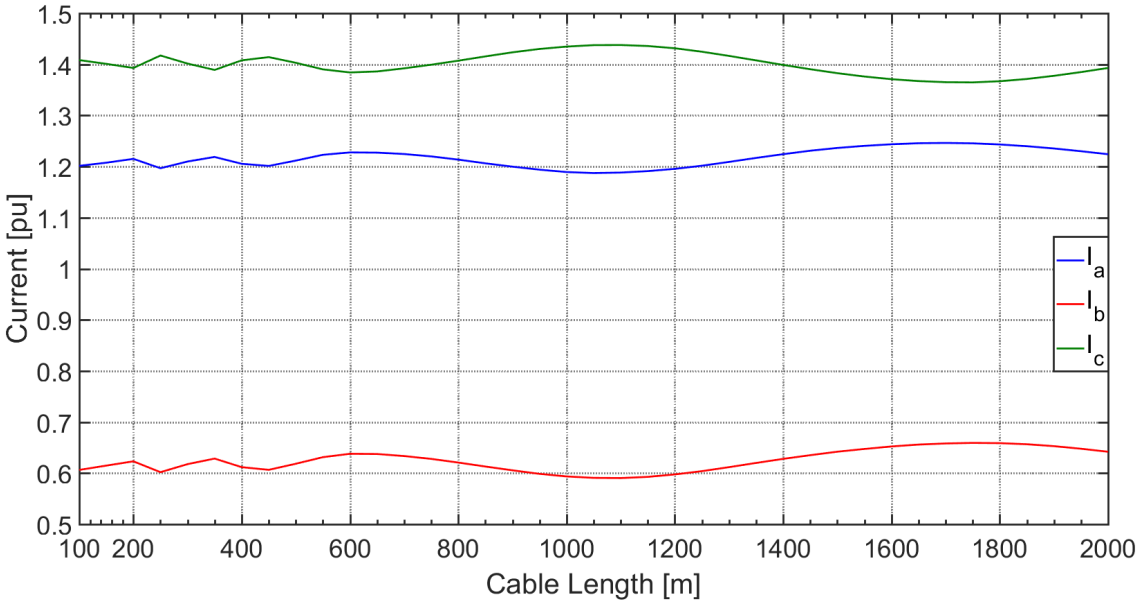


Figure 4.14: Effect of cable length on maximum current in phase A, B and C, with $T_a = 5.5$ and $Delay = 4.5$.

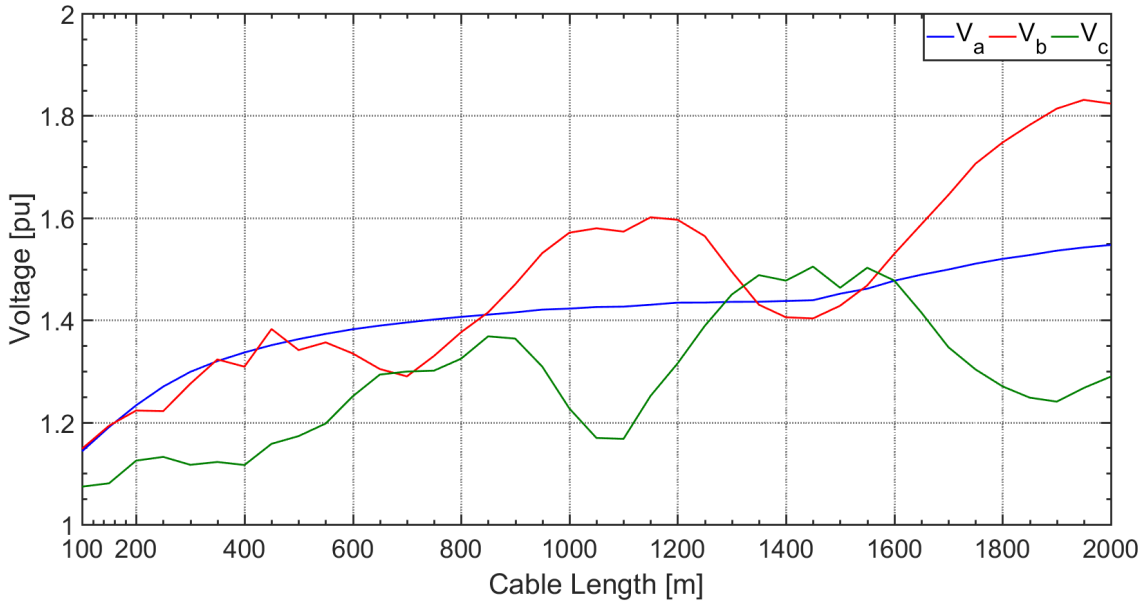


Figure 4.15: Effect of cable length on maximum current in phase A, B and C, with $T_a = 9.0$ and $Delay = 7.0$.

### 4.1.3 The Effect of CVT and its Burden

The effect from the CVTs and their burden is tested with the energizing times found to give maximum current ($T_a = 5.5$ and $Delay = 4.5$) and maximum voltage ($T_a = 9.0$ and $Delay = 7.0$). Simulations are performed without the CVTs, and for variable resistances representing the burden as explained in section 3.2. The resistance is varied from 1 Ω to 1000 Ω, and the currents and voltages are measured at the transformer terminals.

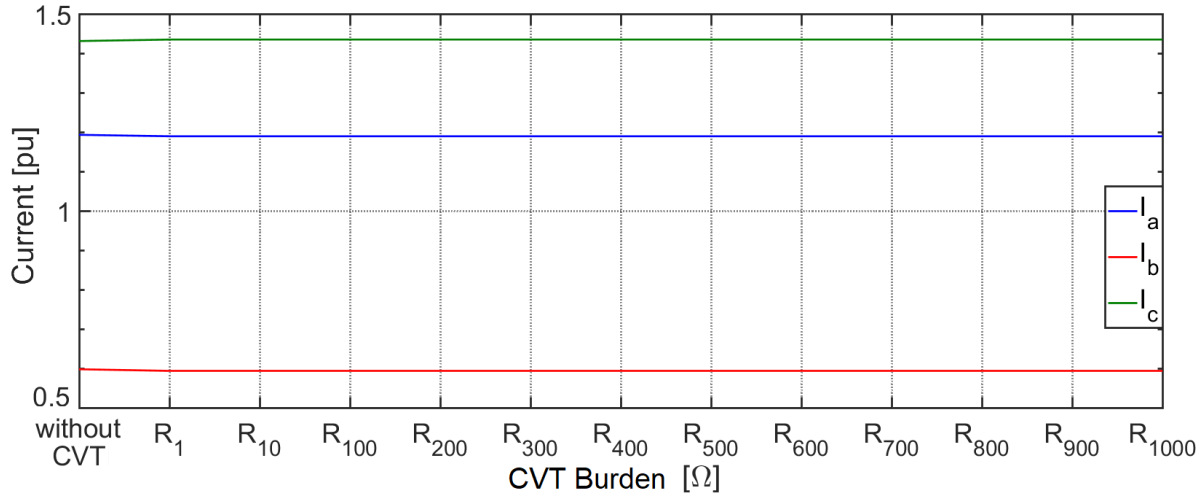


Figure 4.16: Effect from CVT burden on the maximum current in phase A, B and C, with $T_a = 5.5$ and $Delay = 4.5$.

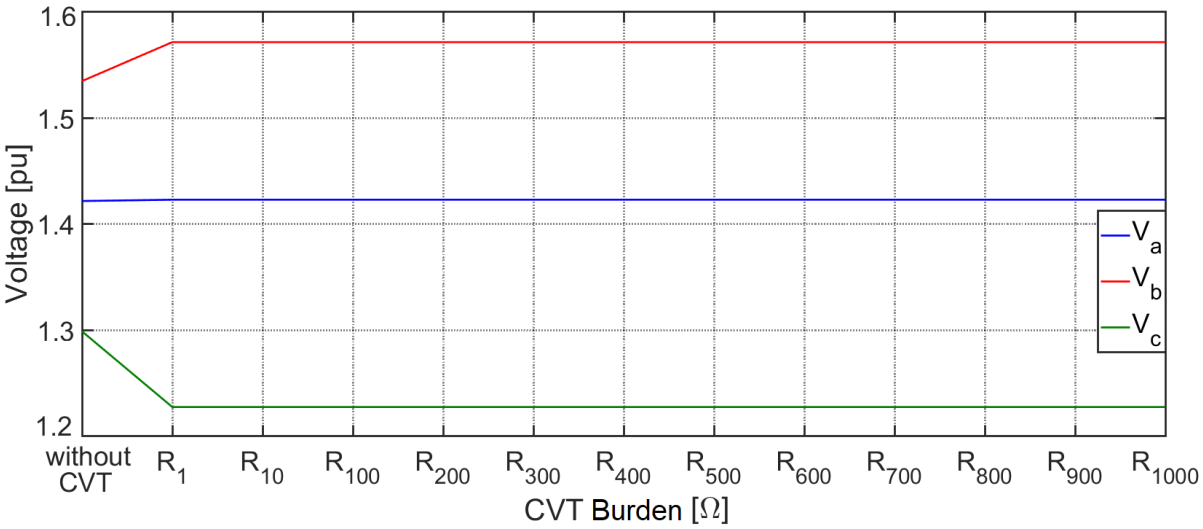


Figure 4.17: Effect from CVT burden on the maximum current in phase A, B and C, with $T_a = 9.0$ and $Delay = 7.0$.

### 4.1.4 Residual Flux and its Effect on Closing Strategies

Now, the generator step-up transformer is initiated with the residual flux to test the closing strategies from section 2.2.3. The residual flux pattern for phase A, B and C is respectively $0.546, -0.523$, and $-0.021$ pu. For the rapid and delayed closing strategies, phase A is energized first, at a time when prospective and residual flux are equal. Phase B and C are energized simultaneously when prospective flux is equal to residual flux in both phases.

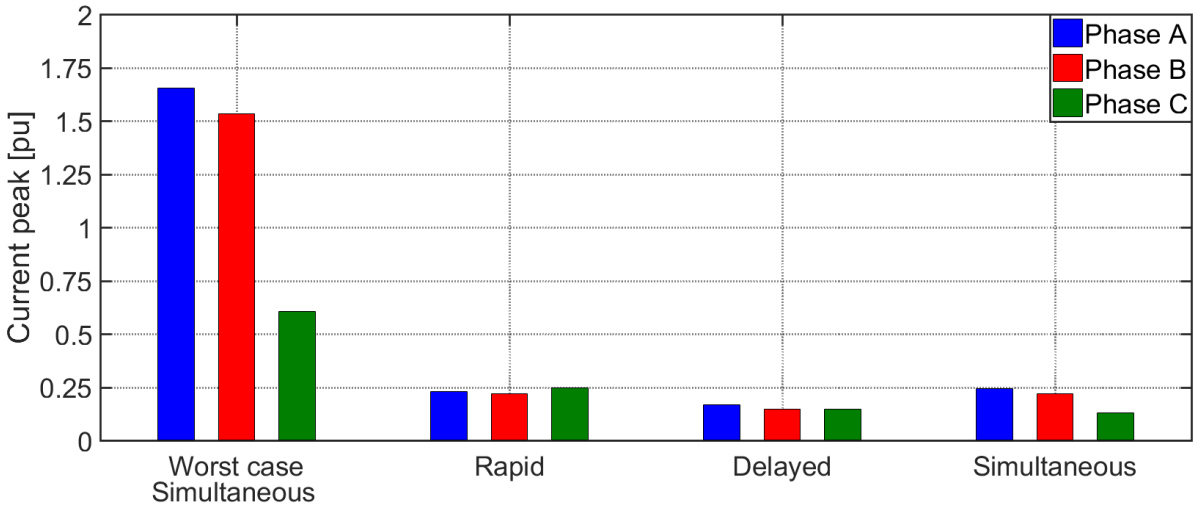


Figure 4.18: Maximum current peak in each phase for different energizing strategies with residual flux.

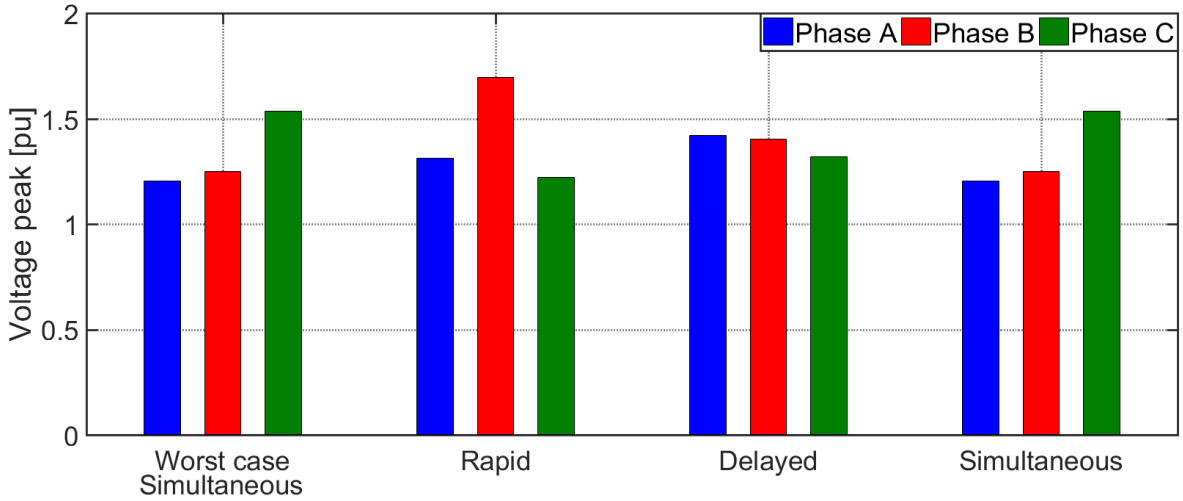


Figure 4.19: Maximum voltage peak in each phase for different energizing strategies with residual flux.

## 4.2 Simulations Compared to Measurements at Site

In this section, simulations are compared to energizing measurements from Nedre Røssåga. Two energizing evens are simulated and compared to a different energizing measurement for both current and voltage. Because of space restrictions in the power station Nedre Røssåga, measurements are performed outdoors, at the supply network end of the feeding cable. The current is measured through current transformers and the voltage is measured via capacitive voltage transformers, both placed between the cable and the switchyard. For that reason the simulation measurement are taken at the point between the circuit breaker and the three phase CVT connection, as indicated by a read circle in Figure 4.20.

At the time of energization, both feeder lines were connected to the switchyard, representing the full grid. Because the residual flux level in the transformer core was unknown at the time of energization, the residual flux is set to zero for both simulations. The time reference for voltage is the same as in Figure 4.1, where negative voltage peak of phase A occurs at time = 10 ms.

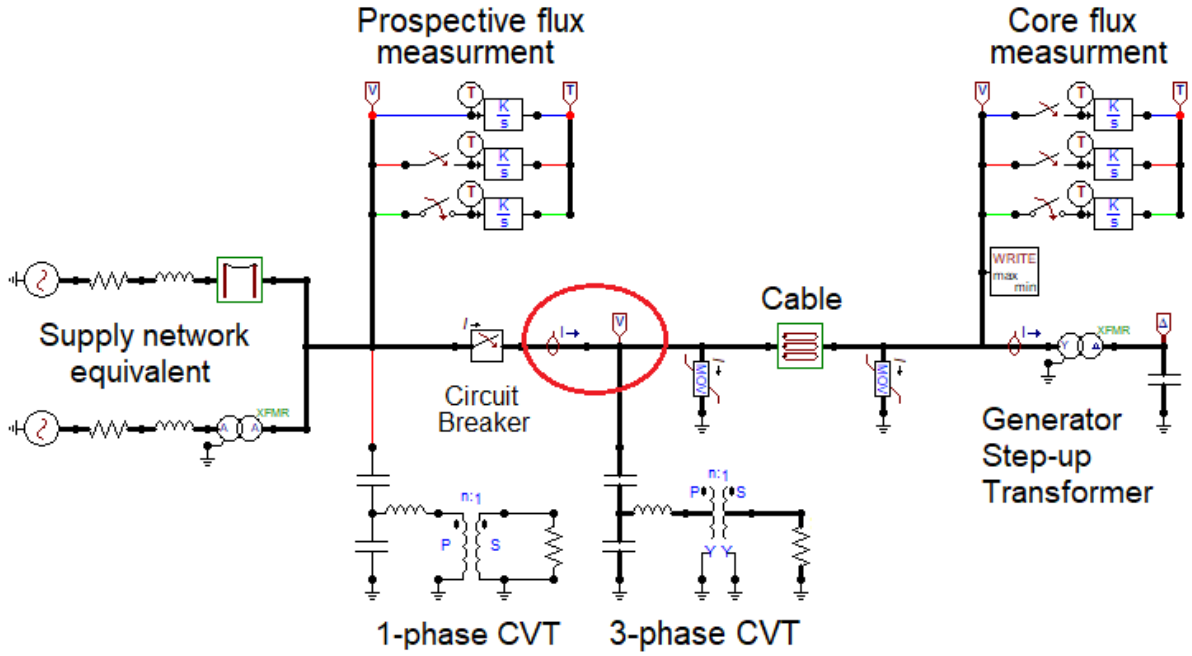


Figure 4.20: The circuit as seen in ATPDraw, point of measurement indicated by red circle.

### 4.2.1 First Energizing Event

Phase A is energized at time = 10 ms, phase B and C is energized at time = 15 ms.

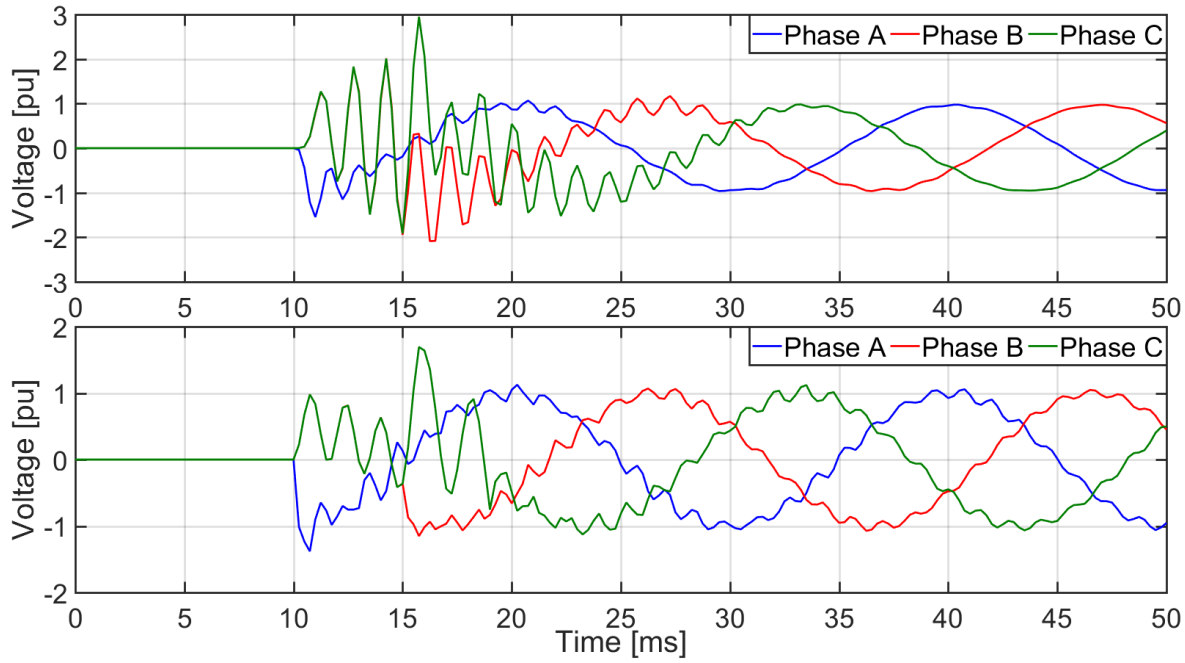


Figure 4.21: Voltage comparison of measurements from Nedre Røssåga (top) and simulations (bottom).

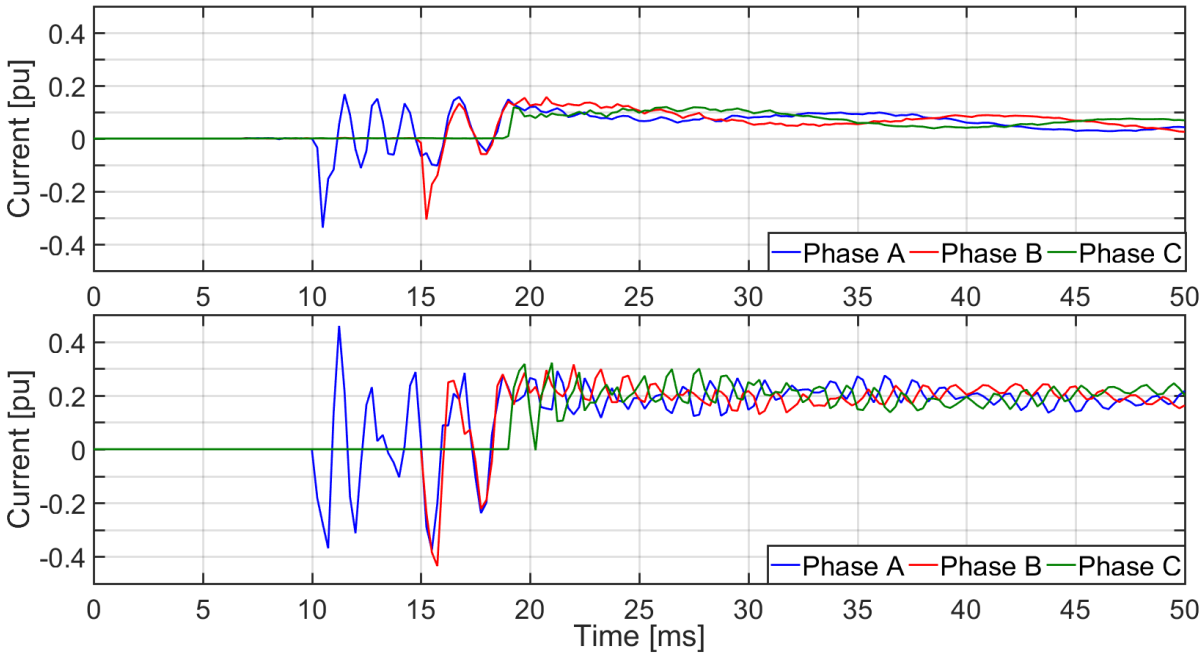


Figure 4.22: Current comparison of measurements from Nedre Røssåga (top) and simulations (bottom).

### 4.2.2 Second Energizing Event

Phase A is energized at time = 10 ms, phase B is energized at = 15 ms, and phase C is energized at time = 19 ms.

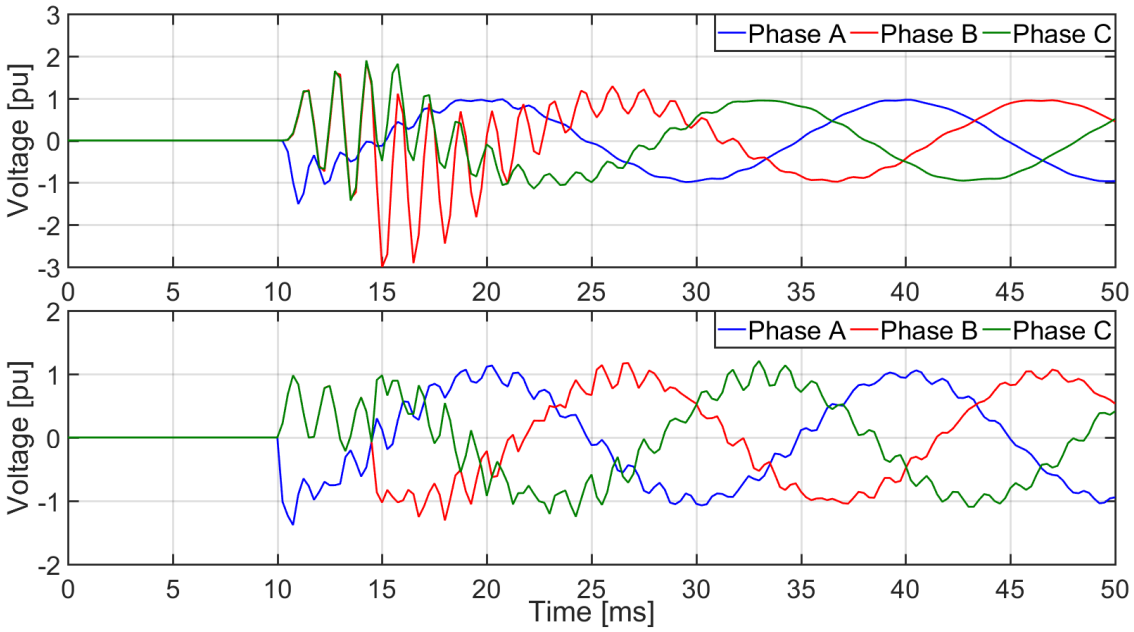


Figure 4.23: Voltage comparison of measurements from Nedre Røssåga (top) and simulations (bottom).

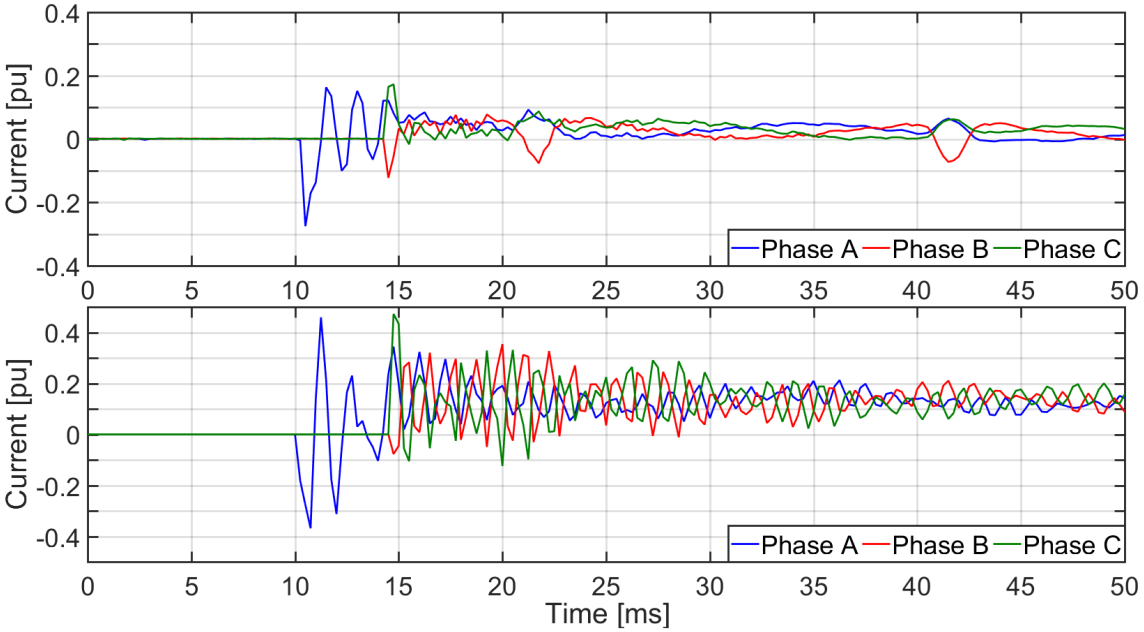


Figure 4.24: Current comparison of measurements from Nedre Røssåga (top) and simulations (bottom).

# Chapter 5

# Analysis and Discussion

The following chapter discuss the results presented in chapter 4, with emphasis on understanding the results based on the theory introduced in chapter 2. This chapter is split in three main parts, where the results from the general transformer energizing studies are analyzed first. In the second part of this chapter the simulations are compared to their corresponding measurements from Nedre Røssåga, with the focus of explaining the deviations rooted in the model from chapter 3. The final section evaluates the strengths and weaknesses of the EMTP model from chapter 3, based on how data was obtained and utilized in ATPDraw, and which options were available.

## 5.1 Analysis of General Energizing Simulations

Figure 4.2 to 4.7 illustrates the core problem of energizing a generator step-up transformer via a feeder cable. As explained in section 2.2, the inrush current magnitude is kept at its minimum by energizing each phase when its voltage is at a peak value. As the residual flux of the transformer core is zero, it is indifferent for the current amplitude if energizing occurs at positive or negative voltage peak, because the total flux over one half period will be zero. For a cable on the other hand, the optimum time of energization is at voltage zero. As explained in section 2.3, energizing a cable at zero voltage ensures that the voltage is kept low when the reflected wave is superimposed on the initial wave. For three phase transformer cores with star-delta winding, the phases have both electrical connection and magnetically coupling. An induced voltage in one phase will therefore influence the currents and voltages in the remaining phases.

By comparing the current to the voltage for each phase in section 4.1.1, it it seen that the current has high values where the voltage has low values. This is especially clear for phase A, were the current acquire high values for $T_a$ around 4 ms to 7 ms, seen in Figure 4.2, which is where the voltage has its lowest values, seen in Figure 4.3. This pattern is also seen for phase B and C, where certain combinations of $Ta$ and $Delay$ gives high current values, but low voltage values. Figure 4.1 unveiled that at time $T_a = 0.0$ ms, the voltage in phase A has its negative peak, and for $T_a = 5$ ms the voltage cross zero. Energizing phase A at $T_a = 5$ ms is therefore the worst case scenario for the inrush current, as it was outlined in Equation (2.5) of section 2.2.1.

Since $Delay$ is specified as the time delay between the energization of phase A and the simultaneous energization of phase B and C, the pattern of high currents and low voltages in phase B and C are dependent on both $T_a$ and $Delay$. Figure 5.1 shows the reference time $T_a$ and the voltage at the grid in all three phases. Table 5.1 shows the $Delay$ time that represents energization at zero voltage for phase B and C, for increasing $T_a$. Phase B has its zero crossing at 11.66 ms and 21.66 ms, while phase C has its zero crossing at 18.33 ms and 27.33 ms, seen from Figure 5.1. This explains why highest currents and lowest voltages are found for different combinations of $T_a$ and $Delay$ in phase B and C, while phase A is almost independent of the $Delay$.

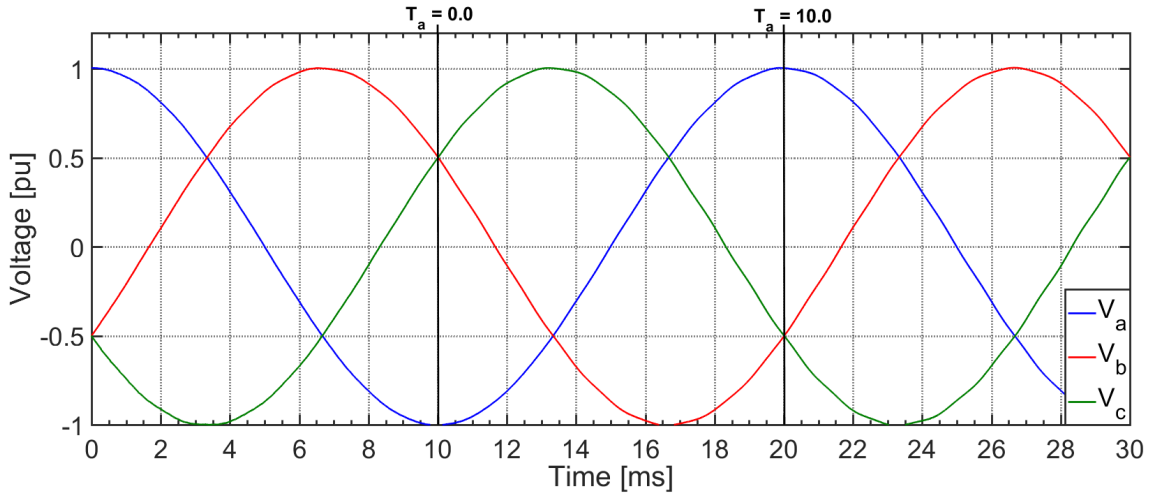


Figure 5.1: Reference time $T_a$ and the voltage in phase A, B, and C.

| $T_a$ [ms] | 0.0 | 1.0 | 2.0 | 3.0 | 4.0 | 5.0 | 6.0 | 7.0 | 8.0 | 9.0 | 10.0 |
|---|---|---|---|---|---|---|---|---|---|---|---|
| $Delay_B$ [ms] | 1.7 | 0.7 | 9.7 | 8.7 | 7.7 | 6.7 | 5.7 | 4.7 | 3.7 | 2.7 | 1.7 |
| $Delay_C$ [ms] | 8.3 | 7.3 | 6.3 | 5.3 | 4.3 | 3.3 | 2.3 | 1.3 | 0.3 | 8.3 | 7.3 |

Table 5.1: Delay times resulting in energization around zero voltage for phase B and C.

The values of Figure 4.2 to 4.7 are displayed in Table C.1 to C.6 in Appendix C. The overall maximum current peak occurring is 1.4348 pu, and the overall maximum voltage peak is 1.5710 pu. Regarding the maximum current and voltage peaks obtained with residual flux in the core, displayed as bar plot in Figure 4.18, it appears that the transformer core does not reach really deep saturation for simulations without residual core flux. Table 5.2 displays the maximum current and voltages occurring for simulations with and without residual flux in the core. The residual flux pattern is the same as in section 4.1.4, that is $0.546, -0.523$, and $-0.021$ pu, for phase A, B and C respectively. It should be noted that the maximum values with residual flux are limited to simultaneous closing strategy, while the values without residual flux are the maximum values found in Table 4.2.

| Max value | Without residual flux | With residual flux | Increase |
|---|---|---|---|
| Current [pu] | 1.4348 | 1.6526 | 15.18 % |
| Voltage [pu] | 1.5710 | 1.6959 | 7.95 % |

Table 5.2: Maximum voltage and current values with and without residual core flux.

The three transformer energizing strategies introduced in section 2.2, named rapid, delayed, and simultaneous closing, were tested with residual flux in section 4.1.4. Figure 4.18 shows that the all three closing strategies are able to limit the amplitude of the inrush current to under 0.25 pu. Table 5.3 summarize the highest occurring amplitudes for each closing strategy, extracted from Figure 4.18. From the table, delayed closing strategy is seen to be the strategy resulting in smallest inrush current. It is also noteworthy that the best case of simultaneous closing perform almost just as good as the delayed and rapid closing strategies. The resulting voltages, seen in Figure 4.19, are more stochastic and not distinctively affected by the closing strategy. They are therefore not further analyzed.

| Closing strategy | Phase A | Phase B | Phase C |
|---|---|---|---|
| Worst simultaneous closing | **1.6526** | 1.5341 | 0.6058 |
| Rapid closing | 0.2304 | 0.2203 | **0.2480** |
| Delayed closing | **0.1670** | 0.1481 | 0.1480 |
| Best simultaneous closing | **0.2447** | 0.2200 | 0.1301 |

Table 5.3: Maximum current peak in each phase for different energizing strategies with residual core flux.

## 5.2 Simulations Compared to Measurements

This section is limited to deal with the results from section 4.2, were simulations and measurements where compared for two energizing events. The terminology *measurement* is used for the actual measurements from Nedre Røssåga, while the term *simulation* is used for the results obtained by simulation of the energizing events.

### 5.2.1 Measured and Simulated Inrush Currents

For both energizing events, the measured current is seen to have a small DC component about 0.1 pu. The DC component is recreated in the simulations, but with twice the magnitude. Furthermore the oscillations seen in the simulations are stronger than those found in the measurements. This indicate that the damping of the simulation model is lower than the damping at Nedre Røssåga. Regarding the model, the following explanations are offered as reasons why the simulated currents deviates from the measured currents.

- The power grid modelled is not a true replica of the real power grid at which Nedre Røssåga is connected. As mentioned in section 3.1.3, the upstream network modelled is purely theoretical, because the factual details about the transmission grid is classified information. As the constructed grid is expected to deviate from the actual grid, so are the simulated inrush currents.

- Statkraft does not perform measurements of the residual core flux when disconnecting the generator step-up transformer. Because the residual flux of the transformer is unknown for the measurements, it was set to zero for the simulations. As explained in section 2.2, and demonstrated in section 5.1, the transformer inrush current depends heavily on the residual flux of the transformer core. Still, the simulated currents are in the same order of magnitude as the measurements, but the pattern is different, clearly seen for phase B in Figure 4.24.

- The Bergeron cable model used to model the feeder cable into the transformer is only completely accurate for the initial frequency of 50 Hz. For higher frequencies, as the oscillations observed for the simulated current, the resistance is too low and the oscillations will not be damped as fast as in the measurements.

Still the simulated currents share some of the characteristics of the measurements. For instance, until phase B and C are energized, the simulated current in Phase A oscillates with the same frequency as the measured current in phase A. The simulations recreate the existing DC component and the convergency of phase A and B, seen particularly well in Figure 4.22.

### 5.2.2 Measured and Simulated Voltages

What is mentioned about the inaccuracies of the model regarding the inrush current is also true for the energizing voltages. However, there is a major difference in the measuring equipment for voltage and current. Measurements of the voltage are performed via the capacitive voltage transformer located between the cable and the circuit breaker. The capacitive voltage divider scale the voltage down to a medium level, and then a transformer is used to transfer the voltage down to a measurable level. The simulated voltages are recorded at the same place as where the three place capacitive voltage transformer is connected, but the simulation metering is done directly.

The voltages in both energizing events are seen to oscillate more for the simulations than for the measurements. For the first 20 ms, the simulated voltage of phase A is seen to coincide well with the measured voltage. The measured voltage for phase B and C are in Figure 4.21 and 4.23 seen to oscillate with an increasing amplitude for the first five milliseconds after the energization of phase A. The amplitudes are seen to reach as high as 3.0 pu before decaying. Oscillations are also present in the simulations for phase B and C, but not with increasing amplitude. The voltages of phase B and C separates when all phases are energized, both in the simulations and in the measurements.

As described in section 3.2, the modelled capacitive voltage transformers are simplified to include only the main components. The simulated voltages are found not to be affected by the capacitive voltage transformer, but the *measurements* may have. The increasing amplitude of the oscillations in phase B and C indicates that there *may* be a resonance between the inductances and capacitances of the CVTs that are not represented in the simplified CVT model from section 3.2.

As a final comment on the two energizing events, it should be mentioned that the sampling frequency of the measurements are 4000 Hz. As the feeder cable resonance frequency is about 49 kHz, the reflected waves are not seen in the measurements. For the sake of comparison, the simulations were also plotted at 4000 Hz in section 4.2.

## 5.3 Discussion of EMTP Model

The EMTP model generated in chapter 3 is based on data from Nedre Røssåga, and where necessary supplemented with standard data from similar components. The relative core dimensions of the generator step-up transformer, and its air core inductance are examples where estimation and other sources than the data-sheets from Nedre Røssåga are used. The modelled capacitive voltage transformers are simplified to a great extend, and supplemented with design criteria from NEK IEC 61869-5 [62], in order to obtain a value for the compensating reactor.

As mention in the previous section where measurements and simulations are compared, the modelled power grid is not an accurate reconstruction of the actual upstream network. As information about the transmission system is classified information, the upstream network of this thesis is modelled as an example network based on data from Statkraft. This will reduce the model's ability to recreate the measurements from Nedre Røssåga. Still, as the results of the general energizing simulations in section 4.1 are of a more general character, their reliability is not affected by the modelled network.

In chapter 3 it was experimented with using frequency a dependent distributed parameter model called JMarti to create the feeder cable model. ATPDraw was not able to generate the ATP file needed for the solver of ATP to run he simulations. The Bergeron model were seen to be more resilient for cables, although not completely accurate for other frequencies than the power system frequency.

The final comment on the EMTP model used in this thesis is dedicated to the circuit breaker. The component is actuating the transients by causing a sudden change in the circuit conditions. In this thesis, the switchyard is simplified to a three phase independently operated circuit breaker, modelled as a three phase ideal switch. As a result, the phenomena electrical pre-arching and mechanical timing deviation are not included in the circuit breaker model. Instead, the closing times for the three phases were in Figure 4.2 to 4.7 changed in steps of 0.5 ms. The figures mentioned are therefore portraying the impact from closing time deviation. The same is to be said about the inaccuracies expected when energizing at falling voltage, as explained in 2.4. Various closing times are accounted for, but their chances of occurring are disregarded .

# Chapter 6

# Conclusion and Future Work

This chapter aims at concluding the work by summing up the main findings of this report, and set fourth some general advise on transformer energization studies. As a final note, recommendations for further work are proposed.

## 6.1 Concluding Remarks

After staring with explaining the basics of general switching transient, chapter 2 deepened in the phenomena of inrush current and resonant overvoltages occurring when energizing a generator step-up transformer via a feeding cable. Three energizing strategies for mitigating inrush currents were described together with the importance of residual core flux and air core inductance. The focus of chapter 2 then shifted to overvoltages from cable-transformer energization. The final section treated the more practical aspects of actuation circuit breakers in high voltage systems.

The EMTP model of the hydro power station Nedre Røssåga were generated with the purpose of simulating various energizing events. In chapter 3, the model was created based on available data from Nedre Røssåga and supplemented with standard data where necessary. General modelling advise stated by CIGRE were used throughout the chapter to include the most important aspects of all the components. Simulations were then performed for different energizing times, energizing strategies, power grid configurations, feeder cable lengths and CVT burdens.

Based on the results presented in chapter 4, and the discussion of the previous chapter, the following findings are highlighted as the most important, when energization a generator step-up transformer via its feeder cable.

- The optimal time to energize a transformer is at voltage peak. The optimal energizing time of a cable is at zero voltage. High inrush currents can therefore be avoided, but at the cost of high energizing voltages at the transformer terminals. There is a clear pattern showing that energizing times resulting in high voltages are the same energizing times giving the lowest currents, and the decision-maker is therefore left with a trade off.

- Uncontrolled energization are found to generate high inrush currents which are increased with residual flux of the transformer. If the residual flux pattern of the transformer is known, the inrush current can be kept low without the voltages exceeding acceptable levels.

- Simulating a great number transformer energizing events may reveal the undesirable outcomes related to high inrush current or high energizing voltages. For the model to be as accurately as possible, standard tests and data-sheets ought to be supplied with design information, especially for the transformer under study.

## 6.2 Proposals for Future Work

- To further investigate the possible resonances seen in the voltage measured by the capacitive voltage transformer, it is recommended to model the both the capacitive voltage transformers and its measuring circuit with a greater level of detail.

- Implementation of a new cable model called Universal Line Model [67] is being planned for ATPDraw. As discussed, the Bergeron cable model does not give a very good fit for frequencies other than its initial frequency. With the new cable model being implemented it will be possible to obtain correct cable impedance over a wide frequency range, causing greater accuracy for the simulated voltages and currents.

- For a more precise analysis of the inrush current occurring during deep saturation of the transformer, its air core inductance should be obtained from the transformer manufacturer. Additionally, more components should be added on the generator step-up transformer low voltage side, in order to further analyze how it affects the inrush current.

# Bibliography


[1] L. Lia, Å. Killingtveit, and M. N. Aas, "Increased generation from upgrading and extension projects," *International Journal on Hydropower and Dams*, vol. 24, 01 2017.

[2] B. Gustavsen, A. P. Brede, and J. O. Tande, "Multivariate analysis of transformer resonant overvoltages in power stations," *IEEE Transactions on Power Delivery*, vol. 26, pp. 2563–2572, Oct 2011.

[3] R. A. Turner and K. S. Smith, "Transformer inrush currents," *IEEE Industry Applications Magazine*, vol. 16, pp. 14–19, 9 2010.

[4] M. Steurer and K. Frohlich, "The impact of inrush currents on the mechanical stress of high voltage power transformer coils," *IEEE Transactions on Power Delivery*, vol. 17, no. 1, pp. 155–160, 2002.

[5] N. Chiesa, A. Avendano, H. K. Høidalen, B. A. Mork, D. Ishchenko, and A. P. Kunze, "On the ringdown transient of transformers," *Energy [J]*, vol. 400, p. 800, 2007.

[6] B. Gustavsen, "Study of transformer resonant overvoltages caused by cable-transformer high-frequency interaction," in *2011 IEEE Power and Energy Society General Meeting*, pp. 1–1, 7 2011.

[7] G. C. Paap, A. A. Alkema, and L. V. der Sluis, "Overvoltages in power transformers caused by no-load switching," *IEEE Transactions on Power Delivery*, vol. 10, pp. 301–307, Jan 1995.

[8] R. Yacamini and A. Abu-Nasser, "Numerical calculation of inrush current in single-phase transformers," *IEE Proceedings B - Electric Power Applications*, vol. 128, pp. 327–334, November 1981.

[9] M. Kizilcay, S. Gröninger, and M. Lösing, "Energization of 380-kv partial networks for the purpose of fast blackstart after system collapse," in *Proceedings International Conference on Power System Transients (IPST 1999), Budapest, Hungary*, 1999.

[10] M. Rioual and J. Reveret, "Energization of step-up transformers for wind-farms: Modeling and its validation by tests performed on a 10 mw site," in *2009 IEEE Power Energy Society General Meeting*, pp. 1–7, July 2009.

[11] CIGRE WG C4.307, "Transformer Energization in Power Systems: A Study Guide," *CIGRE Technical Brochure 568*, 2014.

[12] T. Liu and W. Scott, *Electro magnetic transients program (EMTP) Theory book*. Portland: Bonneville power administration, 1994.

[13] E. Haginomori, T. Koshiduka, J. Arai, and H. Ikeda, *Power system transient analysis: theory and practice using simulation programs (ATP-EMTP)*. John Wiley & Sons, 2016.

[14] A. Greenwood, *Electrical transients in power systems, 2nd edition*. Wiley, 1 1991.

[15] L. V. d. Sluis, *Transients in power systems*. Chichester: Wiley, 2001.

[16] W. Ge, Y. Wang, Z. Zhao, X. Yang, and Y. Li, "Residual flux in the closed magnetic core of a power transformer," *IEEE Transactions on Applied Superconductivity*, vol. 24, pp. 1–4, June 2014.

[17] W. K. Sonnemann, C. L. Wagner, and G. D. Rockefeller, "Magnetizing inrush phenomena in transformer banks," *Transactions of the American Institute of Electrical Engineers. Part III: Power Apparatus and Systems*, vol. 77, pp. 884–892, 4 1958.

[18] R. Cano-González, A. Bachiller-Soler, J. A. Rosendo-Macías, and G. Álvarez Cordero, "Controlled switching strategies for transformer inrush current reduction: A comparative study," *Electric Power Systems Research*, vol. 145, pp. 12–18, 2016.

[19] A. Norouzi, "Open phase conditions in transformers analysis and protection algorithm," in *2013 66th Annual Conference for Protective Relay Engineers*, pp. 112–125, April 2013.

[20] J. Wang and R. Lascu, "Zero sequence circuit of three-legged core type transformers," in *2009 62nd Annual Conference for Protective Relay Engineers*, pp. 188–213, March 2009.

[21] J. J. Winders, *Power transformers : principles and applications*, vol. 17 of *Power engineering*. New York: Marcel Dekker, 2002.

[22] J. H. Brunke, *Elimination of transient inrush currents when energizing unloaded power transformers*. PhD thesis, Swiss Federal Institute of Technology Zurich, 1998.

[23] S. V. Kulkarni, *Transformer Engineering: Design and Practice*. New York: Marcel Dekker, 1 ed., 2004.

[24] J. H. Brunke and K. J. Frohlich, "Elimination of Transformer Inrush Currents by Controlled Switching - Part I Theoretical Considerations," *IEEE Transactions on Power Delivery*, vol. 16, pp. 276–280, 4 2001.

[25] E. Colombo and G. Santagostino, "Results of the inquiries on actual network conditions when switching magnetizing and small inductive currents and on transformer and shunt reactor saturation characteristics," *Electra*, vol. 94, pp. 35–53, 1984.

[26] J. H. Brunke and K. J. Frohlich, "Elimination of Transformer Inrush Currents by Controlled Switching - Part II Application and Performance Considerations," *IEEE Transactions on Power Delivery*, vol. 16, pp. 281–285, 4 2001.

[27] CIGRE WG A3.07, "Controlled switching of unloaded power transformers," *Electra*, vol. 212, pp. 38–47, 2004.

[28] L. Prikler, G. Bánfai, G. Bán, and P. Becker, "Reducing the magnetizing inrush current by means of controlled energization and de-energization of large power transformers," *Electric Power Systems Research*, vol. 76, no. 8, pp. 642–649, 2006.

[29] M. Boyra, "Transient overvoltages in cable systems part 2 – experiments on fast transients in cable systems," Master's thesis, Chalmers tekniska högskola, 2007.

[30] H. K. Høidalen, *Overspenninger og overspenningsvern*. NTNU, Faculty of Information Technology and Electrical Engineering, 2017.

[31] T. Hasman, "Reflection and transmission of traveling waves on power transformers," *IEEE Transactions on Power Delivery*, vol. 12, pp. 1684–1689, Oct 1997.

[32] F. F. Da Silva and C. Leth Bak, *Electromagnetic Transients in Power Cables*, vol. 72 of *Power Systems*. London: Springer London, 2013 ed., 2013.

[33] CIGRE JWG A2/C4.39, "Electrical Transient Interaction Between Transformers and the Power System: Part 1 Expertise," *CIGRE Technical Brochure 577A*, 2014.

[34] D. Durbak, "Temporary overvoltages following transformer energizing," *Siemens PTI Newsletter*, vol. 99, pp. 1–3, Sept 2006.

[35] CIGRE WG C4.307, "Resonance and Ferroresonance in Power Networks," *CIGRE Technical Brochure 569*, 2014.

[36] C. Charalambous, Z. Wang, P. Jarman, and M. Osborne, "Core Structure and its Association with Transformer Susceptibility towards Ferroresonance," in *International Conference on Power Systems Transients (IPST2009)*, 01 2009.

[37] J. A. Martinez-Velasco, *Transient analysis of power systems: solution techniques, tools and applications*. John Wiley & Sons, 2014.

[38] K. Niayesh and M. Runde, *Power Switching Components: Theory, Applications and Future Trends*. Power Systems, Cham: Springer International Publishing, 2017.

[39] Norsk Eletronisk Koimite, "NEK IEC TR 62271-302:2010 High voltage switchgear and controllgear," techreport, IEC, 2011.

[40] H. Hamada, A. Eto, T. Maekawa, T. Koshizuka, S. Nishiwaki, N. Miyake, K. Arai, and M. Kosakada, "RDDS (rate of decrease of dielectric strength) measurement for gas circuit breaker," in *IEEE/PES Transmission and Distribution Conference and Exhibition*, vol. 3, pp. 1755–1759 vol.3, Oct 2002.

[41] J. C. Oliveira, C. E. Tavares, R. Apolonio, A. B. Vasconcellos, and H. S. Bronzeado, "Transformer Controlled Switching to Eliminate Inrush Current - Part I: Theory and Laboratory Validation," in *2006 IEEE/PES Transmission Distribution Conference and Exposition: Latin America*, pp. 1–5, Aug 2006.

[42] H. S. Bronzeado, S. O. Pinto, P. Jonsson, J. C. De Oliveira, and M. L. R. Chaves, "Transformer Controlled Switching to Eliminate Inrush Current - Part II: Field Tests on a 100MVA Three-phase Transformer," in *2006 IEEE/PES Transmission Distribution Conference and Exposition: Latin America*, pp. 1–7, Aug 2006.

[43] T. Liu, M. Petit, H. Siguerdidjane, and T. Jung, "Statistical study of power transformer controlled switching with circuit breaker characteristics considerations," in *2010 IEEE International Conference on Control Applications*, pp. 202–205, Sep. 2010.

[44] J. A. Martinez, "Parameter determination for power systems transients," in *2007 IEEE Power Engineering Society General Meeting*, pp. 1–6, June 2007.

[45] J. Lopez-Roldan, G. Campos, H. De Herdt, J. Min, R. Van Velthoven, T. Sels, J. Karas, and M. Popov, "Fast transients overvoltages produced by switching distribution transformers with a vacuum circuit breaker: simulation and testing," in *Power Quality Conference, EA Technology*, 2002.

[46] CIGRE WG 33.02, "Guidelines for Representation of Network Elements when Calculating Transients," *CIGRE Technical Brochure 39*, 1990.

[47] H. K. Høidalen, B. A. Mork, F. Gonzalez, D. Ishchenko, and N. Chiesa, "Implementation and verification of the hybrid transformer model in atpdraw," *Electric Power Systems Research*, vol. 79, no. 3, pp. 454–459, 2009.

[48] B. A. Mork, F. Gonzalez, D. Ishchenko, D. L. Stuehm, and J. Mitra, "Hybrid transformer model for transient simulation - part i: Development and parameters," *IEEE Transactions on Power Delivery*, vol. 22, pp. 248–255, Jan 2007.

[49] H. K. Høidalen, N. Chiesa, A. Avendaño, and B. A. Mork, "Developments in the hybrid transformer model – Core modeling and optimization," in *International Conference on Power Systems Transients (IPST2011)*, 2011.

[50] H. K. Høidalen, N. Chiesa, A. Avendano, and B. Mork, "Developments in the hybrid transformer model–core modeling and optimization," *IPST'2011*, 2011.

[51] N. Chiesa, "Power transformer modelling: Advanced core model," Master's thesis, Politecnico di Milano, Italy, 2005.

[52] L. Prikler and H. K. Høidalen, *ATPDraw version 5.6 for Windows 9x/NT/2000/XP Users' Manual*, 2009.

[53] B. A. Mork, F. Gonzalez-Molina, and J. Mitra, "Parameter estimation and advancement in transformer models for EMTP simulations. task/activity MTU-4: Develop library of model topologies," tech. rep., Bonneville Power Administration, Portland USA, 2003.

[54] B. A. Mork, D. Ishchenko, F. Gonzalez, and S. D. Cho, "Parameter Estimation Methods for Five-Limb Magnetic Core Model," *IEEE Transactions on Power Delivery*, vol. 23, pp. 2025–2032, Oct 2008.

[55] J. R. Marti, L. Marti, and H. W. Dommel, "Transmission line models for steady-state and transients analysis," in *Proceedings. Joint International Power Conference Athens Power Tech,*, vol. 2, pp. 744–750, Sep. 1993.

[56] P. Jinsheng, *Assessment of transformer energisation transients and their impacts on power systems*. PhD thesis, University of Manchester, 2013.

[57] H. K. Høidalen and A. H. Soloot, "Cable Modelling in ATP – from NODA to TYPE94," in *Proc. EMTP Users Group meeting, Helsinki, Finland*, 08 2010.

[58] R. Iravani, A. K. S. Chandhury, I. D. Hassan, J. A. Martinez, A. S. Morched, B. A. Mork, M. Parniani, D. Shirmohammadi, and R. A. Walling, "Modeling guidelines for low frequenct transients," *Modeling and Analysis of System Transients using Digital Systems*, 1998.

[59] NEK EN 50182:2001, "Conductors for overhead lines - round wire concentric lay stranded conductors," 2011.

[60] S. Zubić and P. Balcerek, "Impedance surfing method for CVT transient mitigation," in *2016 10th International Conference on Compatibility, Power Electronics and Power Engineering*, pp. 64–69, June 2016.

[61] V. P. Mahadanaarachchi and R. Ramakumar, "Analysis of capacitive voltage transformer transients with wind farm integration," in *2009 Power Systems Conference*, pp. 1–8, March 2009.

[62] NEK IEC 61869-5:2011, "Instrument transformers - part 5: Additional requirements of capacitor voltage transformers," 2011.

[63] J. A. Martinez, J. Mahseredjian, and B. Khodabakhchian, "Parameter determination for modeling system transients-part vi: Circuit breakers," *IEEE Transactions on Power Delivery*, vol. 20, pp. 2079–2085, July 2005.

[64] N. S. Lazarev, A. R. Shul'ga, and R. N. Shul'ga, "Controlled switching of transformers," *Russian Electrical Engineering*, vol. 82, p. 365, Sep 2011.

[65] A. Ebner, M. Bosch, and R. Cortesi, "Controlled switching of transformers - effects of closing time scatter and residual flux uncertainty," in *2008 43rd International Universities Power Engineering Conference*, pp. 1–5, Sep. 2008.

[66] M. H. Hashem, A. M. Elmorshedy, and A. M. Emam, "Attenuation of Transformer Inrush Current Using Controlled Switching System on Delta-Star Transformer," in *2018 Twentieth International Middle East Power Systems Conference (MEPCON)*, pp. 882–886, Dec 2018.

[67] A. Morched, B. Gustavsen, and M. Tartibi, "A universal model for accurate calculation of electromagnetic transients on overhead lines and underground cables," *IEEE Transactions on Power Delivery*, vol. 14, pp. 1032–1038, July 1999.

# Appendix A

**Derivation of the wave equation describing steady state wave propagation.**

With reference to Figure 2.13, Kirchhoff's voltage law and current law are stated as follows:

$$u - i \cdot R\partial x - L \cdot \frac{\partial i}{\partial t} \cdot \partial x - u - \frac{\partial u}{\partial x} \cdot \partial x = 0 \tag{A.1}$$

$$-\frac{\partial u}{\partial x} = L \cdot \frac{\partial i}{\partial t} + R \cdot i \tag{A.2}$$

and

$$i - u \cdot G\partial x - C \cdot \frac{\partial u}{\partial t} \cdot \partial x - i - \frac{\partial i}{\partial x} \cdot \partial x = 0 \tag{A.3}$$

$$-\frac{\partial i}{\partial x} = C \cdot \frac{\partial u}{\partial t} + G \cdot u \tag{A.4}$$

For a loss-less line we set $R = G = 0$ and take the derivative with respect to $x$ and $t$ for Equation (A.2) and (A.4) respectively:

$$-\frac{\partial^2 u}{\partial x^2} = L \cdot \frac{\partial i}{\partial x}\frac{\partial i}{\partial t} \tag{A.5}$$

$$-\frac{\partial i}{\partial x}\frac{\partial i}{\partial t} = C \cdot \frac{\partial^2 u}{\partial t^2} \tag{A.6}$$

Inserting Equation (A.6) into Equation (A.5) results in the loss-less wave equation for the voltage propagating in the line:

$$\frac{\partial^2 u}{\partial x^2} - LC \cdot \frac{\partial^2 u}{\partial t^2} = 0 \tag{A.7}$$

Equation (A.7) has the general solution:

$$u = u_1(x - vt) + u_2(x + vt) \tag{A.8}$$

$$v = \frac{1}{\sqrt{LC}} = \textit{wave velocity}$$

The two arbitrary functions $u_1(x - vt)$ and $u_2(x + vt)$ describe two waves going in each direction with velocity $v$, and it is seen that the voltage is the *sum* of them both. Replacing $u$ with $u_1$ in Equation (A.6) results in the current propagating in positive x direction:

$$i_1 = Cvu_1 = C\frac{1}{\sqrt{LC}}u_1 = \frac{u_1}{\sqrt{\frac{L}{C}}} \tag{A.9}$$

$$Z_b = \frac{u_1}{i_1} = \sqrt{\frac{L}{C}} \tag{A.10}$$

$Z_b$ is the wave impedance for the loss-less line. Skriv litt mer om den. By the same means as of Equation (A.9), replacing $u$ with $u_2$ in Equation (A.5) results in the current propagating in the negative x-direction.

$$i_2 = -Cu_2v = -C\frac{1}{\sqrt{LC}}u_2 = -\frac{u_2}{\sqrt{\frac{L}{C}}} = -\frac{u_2}{Z_b} \tag{A.11}$$

It is now seen that the current in the line is the *difference* of two travelling waves travelling in opposite direction:

$$i = i_1(x - vt) + i_2(x + vt) = \frac{1}{Z_b}u_1(x - vt) - \frac{1}{Z_b}u_2(x + vt) \tag{A.12}$$

For a loss-less line in air, the wave propagation speed is equal to the speed of light:

$$v = \frac{1}{\sqrt{LC}} = \frac{1}{\sqrt{\mu_0\varepsilon_0}} \approx c \approx 300\text{m}/\mu\text{sec}$$

# Appendix B

The 420 kV feeding cable installed at Nedre Røssåga [1].

Silec Cable
a General Cable company

## CABLE STRUCTURE
## 630 mm² ALUMINIUM XLPE 420 kV CABLE

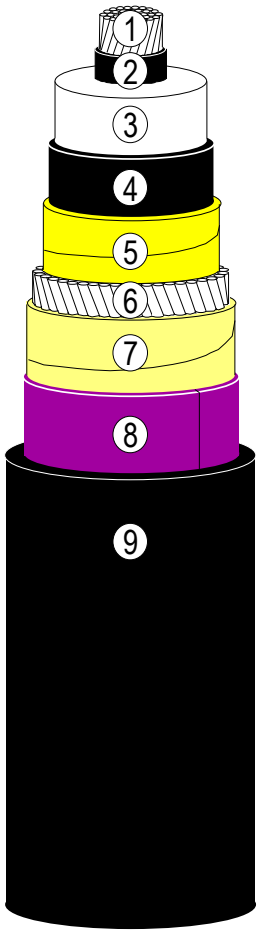


**1 - CONDUCTOR**
Cross-section : 630 mm²
Material : aluminium
Indicative diameter : 30,5 mm

**2 - INNER SEMI-CONDUCTIVE LAYER**
Indicative thickness : 2,4 mm

**3 - INSULATION**
Material : PEX (XLPE)
Minimum average thickness : 27 mm *

**4 - OUTER SEMI-CONDUCTIVE LAYER**
Indicative thickness : 1,5 mm

**5 - SWELLING TAPE**

**6 - WIRE SCREEN**
Material : aluminum
Indicative diameter : 1,715 mm each
Cross-section : 189 mm²

**7 - SWELLING TAPE**

**8 - ALUMINIUM FOIL LONGITUDINALLY APPLIED**
Stuck onto the outer sheath
Indicative thickness : 0.5 mm

**9 - EXTRUDED OUTER SHEATH AND SEMI-CONDUCTIVE LAYER**
Material : high density polyethylene
Indicative thickness : 4 mm **

**INDICATIVE EXTERNAL DIAMETER :** 111 mm

**INDICATIVE WEIGHT :** 10,2 kg/m

**MINIMUM BENDING RADIUS**
- in permanent : 2,25 m
- during installation : 3,35 m

**MAXIMUM PULLING TENSION :** 3150 daN

**MAXIMUM SIDEWALL PRESSURE :** 1000 daN/m

* The measured thickness at any point may be smaller within the tolerances defined in the standard IEC 62067.

** The measured thickness at any point may be smaller within the tolerances defined in the standard IEC 62067.
The thickness of the extruded semi-conductive layer is considered an integral part of the total sheath thickness.

[1] Cable data provided by and used by permission of, Ronny Goin, Statkraft.

# Appendix C

| $T_a[ms]$ | Delay [ms] | | | | | | | | | |
|---|---|---|---|---|---|---|---|---|---|---|
| | 0.0 | 0.5 | 1.0 | 1.5 | 2.0 | 2.5 | 3.0 | 3.5 | 4.0 | 4.5 |
| 0.0 | 0.370 | 0.497 | 0.472 | 0.345 | 0.426 | 0.348 | 0.285 | 0.282 | 0.190 | 0.191 |
| 0.5 | 0.412 | 0.434 | 0.505 | 0.361 | 0.341 | 0.336 | 0.259 | 0.187 | 0.187 | 0.187 |
| 1.0 | 0.443 | 0.350 | 0.499 | 0.355 | 0.248 | 0.318 | 0.277 | 0.178 | 0.262 | 0.307 |
| 1.5 | 0.560 | 0.438 | 0.599 | 0.469 | 0.321 | 0.432 | 0.405 | 0.266 | 0.408 | 0.441 |
| 2.0 | 0.678 | 0.556 | 0.688 | 0.562 | 0.423 | 0.562 | 0.541 | 0.410 | 0.561 | 0.642 |
| 2.5 | 0.777 | 0.663 | 0.785 | 0.654 | 0.536 | 0.674 | 0.654 | 0.569 | 0.741 | 0.812 |
| 3.0 | 0.862 | 0.759 | 0.841 | 0.721 | 0.646 | 0.767 | 0.804 | 0.756 | 0.904 | 0.961 |
| 3.5 | 0.904 | 0.813 | 0.859 | 0.796 | 0.767 | 0.909 | 0.946 | 0.908 | 1.034 | 1.076 |
| 4.0 | 0.921 | 0.851 | 0.897 | 0.872 | 0.904 | 1.018 | 1.040 | 1.038 | 1.129 | 1.158 |
| 4.5 | 0.911 | 0.877 | 0.944 | 0.974 | 1.021 | 1.096 | 1.122 | 1.134 | 1.197 | 1.210 |
| 5.0 | 0.892 | 0.941 | 1.002 | 1.041 | 1.092 | 1.143 | 1.161 | 1.193 | 1.225 | 1.215 |
| 5.5 | 0.912 | 1.006 | 1.025 | 1.063 | 1.140 | 1.151 | 1.162 | 1.218 | 1.208 | 1.189 |
| 6.0 | 0.928 | 1.033 | 1.002 | 1.060 | 1.144 | 1.118 | 1.131 | 1.202 | 1.165 | 1.130 |
| 6.5 | 0.909 | 1.021 | 0.965 | 1.027 | 1.123 | 1.069 | 1.071 | 1.160 | 1.090 | 1.057 |
| 7.0 | 0.865 | 0.990 | 0.889 | 0.958 | 1.061 | 0.966 | 0.962 | 1.066 | 0.965 | 0.951 |
| 7.5 | 0.783 | 0.907 | 0.780 | 0.857 | 0.967 | 0.845 | 0.841 | 0.959 | 0.827 | 0.841 |
| 8.0 | 0.689 | 0.817 | 0.660 | 0.746 | 0.857 | 0.703 | 0.694 | 0.812 | 0.662 | 0.669 |
| 8.5 | 0.559 | 0.692 | 0.505 | 0.584 | 0.690 | 0.514 | 0.499 | 0.628 | 0.451 | 0.433 |
| 9.0 | 0.438 | 0.585 | 0.374 | 0.432 | 0.559 | 0.331 | 0.317 | 0.459 | 0.245 | 0.203 |
| 9.5 | 0.413 | 0.544 | 0.426 | 0.371 | 0.496 | 0.339 | 0.285 | 0.375 | 0.191 | 0.191 |
| 10.0 | 0.370 | 0.497 | 0.472 | 0.346 | 0.426 | 0.347 | 0.286 | 0.282 | 0.191 | 0.191 |

| $T_a[ms]$ | Delay [ms] *continued* | | | | | | | | | | |
|---|---|---|---|---|---|---|---|---|---|---|---|
| | 5.0 | 5.5 | 6.0 | 6.5 | 7.0 | 7.5 | 8.0 | 8.5 | 9.0 | 9.5 | 10.0 |
| 0.0 | 0.191 | 0.191 | 0.206 | 0.247 | 0.213 | 0.374 | 0.371 | 0.371 | 0.480 | 0.429 | 0.432 |
| 0.5 | 0.187 | 0.187 | 0.302 | 0.269 | 0.297 | 0.451 | 0.358 | 0.351 | 0.541 | 0.384 | 0.376 |
| 1.0 | 0.178 | 0.275 | 0.394 | 0.271 | 0.377 | 0.527 | 0.360 | 0.408 | 0.581 | 0.377 | 0.371 |
| 1.5 | 0.303 | 0.489 | 0.589 | 0.451 | 0.565 | 0.675 | 0.532 | 0.564 | 0.694 | 0.515 | 0.498 |
| 2.0 | 0.514 | 0.680 | 0.756 | 0.624 | 0.729 | 0.821 | 0.684 | 0.715 | 0.830 | 0.650 | 0.662 |
| 2.5 | 0.710 | 0.857 | 0.922 | 0.808 | 0.894 | 0.965 | 0.833 | 0.852 | 0.931 | 0.827 | 0.914 |
| 3.0 | 0.873 | 0.998 | 1.045 | 0.942 | 1.011 | 1.057 | 0.936 | 0.996 | 1.130 | 0.982 | 1.041 |
| 3.5 | 1.006 | 1.105 | 1.129 | 1.048 | 1.095 | 1.130 | 1.112 | 1.193 | 1.200 | 1.138 | 1.199 |
| 4.0 | 1.120 | 1.188 | 1.198 | 1.133 | 1.209 | 1.292 | 1.229 | 1.273 | 1.314 | 1.222 | 1.234 |
| 4.5 | 1.188 | 1.226 | 1.216 | 1.240 | 1.335 | 1.314 | 1.307 | 1.356 | 1.309 | 1.259 | 1.281 |
| 5.0 | 1.224 | 1.231 | 1.275 | 1.341 | 1.329 | 1.342 | 1.363 | 1.327 | 1.294 | 1.284 | 1.253 |
| 5.5 | 1.222 | 1.258 | 1.304 | 1.321 | 1.323 | 1.329 | 1.316 | 1.277 | 1.252 | 1.232 | 1.230 |
| 6.0 | 1.232 | 1.261 | 1.234 | 1.297 | 1.283 | 1.236 | 1.247 | 1.205 | 1.176 | 1.177 | 1.197 |
| 6.5 | 1.216 | 1.172 | 1.127 | 1.233 | 1.158 | 1.085 | 1.157 | 1.146 | 1.146 | 1.159 | 1.146 |
| 7.0 | 1.145 | 1.020 | 1.003 | 1.136 | 0.973 | 0.931 | 1.066 | 1.060 | 1.060 | 1.081 | 1.060 |
| 7.5 | 1.018 | 0.843 | 0.853 | 0.960 | 0.867 | 0.867 | 0.914 | 0.910 | 0.910 | 0.955 | 0.910 |
| 8.0 | 0.831 | 0.635 | 0.638 | 0.790 | 0.758 | 0.758 | 0.758 | 0.758 | 0.758 | 0.796 | 0.758 |
| 8.5 | 0.623 | 0.465 | 0.465 | 0.604 | 0.597 | 0.597 | 0.597 | 0.597 | 0.597 | 0.598 | 0.597 |
| 9.0 | 0.412 | 0.351 | 0.351 | 0.389 | 0.384 | 0.384 | 0.394 | 0.384 | 0.384 | 0.544 | 0.384 |
| 9.5 | 0.214 | 0.191 | 0.191 | 0.239 | 0.191 | 0.260 | 0.392 | 0.331 | 0.400 | 0.496 | 0.423 |
| 10.0 | 0.191 | 0.191 | 0.206 | 0.246 | 0.212 | 0.374 | 0.371 | 0.372 | 0.480 | 0.428 | 0.432 |

Table C.1: Maximum current peaks at phase A as a function of the energizing times $T_a$ and *Delay*. Complementary to Figure 4.2.

| $T_a[ms]$ | Delay [ms] | | | | | | | | | |
|---|---|---|---|---|---|---|---|---|---|---|
| | 0.0 | 0.5 | 1.0 | 1.5 | 2.0 | 2.5 | 3.0 | 3.5 | 4.0 | 4.5 |
| 0.0 | 1.545 | 1.420 | 1.419 | 1.419 | 1.419 | 1.419 | 1.419 | 1.419 | 1.419 | 1.419 |
| 0.5 | 1.502 | 1.365 | 1.364 | 1.364 | 1.364 | 1.364 | 1.364 | 1.364 | 1.364 | 1.364 |
| 1.0 | 1.420 | 1.278 | 1.278 | 1.278 | 1.282 | 1.278 | 1.278 | 1.290 | 1.278 | 1.278 |
| 1.5 | 1.304 | 1.244 | 1.229 | 1.254 | 1.291 | 1.219 | 1.191 | 1.287 | 1.192 | 1.211 |
| 2.0 | 1.268 | 1.216 | 1.282 | 1.236 | 1.239 | 1.204 | 1.168 | 1.251 | 1.176 | 1.175 |
| 2.5 | 1.246 | 1.166 | 1.235 | 1.200 | 1.229 | 1.150 | 1.147 | 1.232 | 1.177 | 1.167 |
| 3.0 | 1.253 | 1.146 | 1.198 | 1.203 | 1.216 | 1.133 | 1.138 | 1.199 | 1.148 | 1.136 |
| 3.5 | 1.221 | 1.109 | 1.149 | 1.147 | 1.166 | 1.094 | 1.096 | 1.129 | 1.127 | 1.109 |
| 4.0 | 1.145 | 1.082 | 1.096 | 1.108 | 1.118 | 1.087 | 1.092 | 1.112 | 1.098 | 1.092 |
| 4.5 | 1.089 | 1.133 | 1.073 | 1.112 | 1.150 | 1.076 | 1.105 | 1.117 | 1.068 | 1.089 |
| 5.0 | 1.147 | 1.078 | 1.114 | 1.155 | 1.054 | 1.087 | 1.102 | 1.078 | 1.097 | 1.062 |
| 5.5 | 1.081 | 1.100 | 1.149 | 1.067 | 1.068 | 1.092 | 1.066 | 1.080 | 1.046 | 1.045 |
| 6.0 | 1.116 | 1.106 | 1.110 | 1.149 | 1.107 | 1.121 | 1.131 | 1.114 | 1.113 | 1.113 |
| 6.5 | 1.188 | 1.151 | 1.173 | 1.229 | 1.174 | 1.190 | 1.181 | 1.172 | 1.172 | 1.172 |
| 7.0 | 1.232 | 1.172 | 1.241 | 1.339 | 1.284 | 1.284 | 1.284 | 1.284 | 1.284 | 1.284 |
| 7.5 | 1.314 | 1.217 | 1.316 | 1.431 | 1.367 | 1.367 | 1.367 | 1.367 | 1.367 | 1.367 |
| 8.0 | 1.368 | 1.290 | 1.351 | 1.485 | 1.411 | 1.410 | 1.410 | 1.410 | 1.410 | 1.410 |
| 8.5 | 1.453 | 1.372 | 1.393 | 1.505 | 1.427 | 1.426 | 1.426 | 1.426 | 1.426 | 1.426 |
| 9.0 | 1.520 | 1.424 | 1.423 | 1.486 | 1.422 | 1.422 | 1.422 | 1.422 | 1.422 | 1.422 |
| 9.5 | 1.552 | 1.437 | 1.435 | 1.436 | 1.435 | 1.435 | 1.435 | 1.435 | 1.435 | 1.435 |
| 10.0 | 1.543 | 1.420 | 1.419 | 1.419 | 1.419 | 1.419 | 1.419 | 1.419 | 1.419 | 1.419 |

| $T_a[ms]$ | Delay [ms] *continued* | | | | | | | | | | |
|---|---|---|---|---|---|---|---|---|---|---|---|
| | 5.0 | 5.5 | 6.0 | 6.5 | 7.0 | 7.5 | 8.0 | 8.5 | 9.0 | 9.5 | 10.0 |
| 0.0 | 1.419 | 1.419 | 1.419 | 1.419 | 1.419 | 1.419 | 1.419 | 1.419 | 1.419 | 1.419 | 1.419 |
| 0.5 | 1.364 | 1.364 | 1.364 | 1.364 | 1.364 | 1.364 | 1.364 | 1.364 | 1.364 | 1.364 | 1.364 |
| 1.0 | 1.278 | 1.304 | 1.287 | 1.278 | 1.352 | 1.278 | 1.278 | 1.326 | 1.278 | 1.278 | 1.278 |
| 1.5 | 1.258 | 1.284 | 1.265 | 1.219 | 1.313 | 1.236 | 1.230 | 1.293 | 1.218 | 1.218 | 1.218 |
| 2.0 | 1.226 | 1.256 | 1.234 | 1.226 | 1.312 | 1.226 | 1.216 | 1.228 | 1.216 | 1.216 | 1.216 |
| 2.5 | 1.209 | 1.235 | 1.214 | 1.211 | 1.287 | 1.194 | 1.183 | 1.183 | 1.183 | 1.183 | 1.193 |
| 3.0 | 1.156 | 1.181 | 1.187 | 1.160 | 1.227 | 1.158 | 1.158 | 1.209 | 1.203 | 1.158 | 1.242 |
| 3.5 | 1.124 | 1.130 | 1.162 | 1.141 | 1.141 | 1.141 | 1.141 | 1.141 | 1.141 | 1.141 | 1.144 |
| 4.0 | 1.100 | 1.095 | 1.108 | 1.092 | 1.114 | 1.092 | 1.092 | 1.111 | 1.115 | 1.092 | 1.141 |
| 4.5 | 1.056 | 1.038 | 1.050 | 1.081 | 1.062 | 1.050 | 1.086 | 1.129 | 1.101 | 1.090 | 1.132 |
| 5.0 | 1.056 | 1.065 | 1.094 | 1.067 | 1.050 | 1.085 | 1.108 | 1.104 | 1.096 | 1.103 | 1.096 |
| 5.5 | 1.055 | 1.079 | 1.057 | 1.066 | 1.082 | 1.106 | 1.113 | 1.104 | 1.108 | 1.120 | 1.064 |
| 6.0 | 1.113 | 1.113 | 1.113 | 1.113 | 1.113 | 1.113 | 1.113 | 1.113 | 1.113 | 1.113 | 1.113 |
| 6.5 | 1.174 | 1.172 | 1.172 | 1.186 | 1.172 | 1.172 | 1.222 | 1.192 | 1.172 | 1.223 | 1.196 |
| 7.0 | 1.284 | 1.284 | 1.284 | 1.284 | 1.284 | 1.284 | 1.284 | 1.284 | 1.284 | 1.284 | 1.284 |
| 7.5 | 1.367 | 1.367 | 1.367 | 1.367 | 1.367 | 1.367 | 1.367 | 1.367 | 1.367 | 1.367 | 1.367 |
| 8.0 | 1.410 | 1.410 | 1.410 | 1.410 | 1.410 | 1.410 | 1.410 | 1.410 | 1.410 | 1.410 | 1.410 |
| 8.5 | 1.426 | 1.426 | 1.426 | 1.426 | 1.426 | 1.426 | 1.426 | 1.426 | 1.426 | 1.426 | 1.426 |
| 9.0 | 1.422 | 1.422 | 1.422 | 1.422 | 1.422 | 1.422 | 1.422 | 1.422 | 1.422 | 1.422 | 1.422 |
| 9.5 | 1.435 | 1.435 | 1.435 | 1.435 | 1.435 | 1.435 | 1.435 | 1.435 | 1.435 | 1.435 | 1.435 |
| 10.0 | 1.419 | 1.419 | 1.419 | 1.419 | 1.419 | 1.419 | 1.419 | 1.419 | 1.419 | 1.419 | 1.419 |

Table C.2: Maximum voltage peaks at phase A as a function of the energizing times $T_a$ and *Delay*. Complementary to Figure 4.3.

| $T_a[ms]$ | Delay [ms] | | | | | | | | | |
|---|---|---|---|---|---|---|---|---|---|---|
| | 0.0 | 0.5 | 1.0 | 1.5 | 2.0 | 2.5 | 3.0 | 3.5 | 4.0 | 4.5 |
| 0.0 | 0.891 | 1.016 | 0.696 | 0.741 | 0.799 | 0.455 | 0.335 | 0.441 | 0.172 | 0.213 |
| 0.5 | 0.919 | 1.014 | 0.678 | 0.692 | 0.724 | 0.389 | 0.291 | 0.395 | 0.169 | 0.212 |
| 1.0 | 0.912 | 0.986 | 0.625 | 0.638 | 0.688 | 0.357 | 0.250 | 0.327 | 0.167 | 0.208 |
| 1.5 | 0.887 | 0.942 | 0.610 | 0.615 | 0.643 | 0.310 | 0.193 | 0.306 | 0.202 | 0.305 |
| 2.0 | 0.899 | 0.937 | 0.597 | 0.592 | 0.601 | 0.281 | 0.190 | 0.362 | 0.295 | 0.385 |
| 2.5 | 0.923 | 0.922 | 0.611 | 0.587 | 0.574 | 0.269 | 0.250 | 0.404 | 0.379 | 0.453 |
| 3.0 | 0.919 | 0.896 | 0.595 | 0.551 | 0.518 | 0.281 | 0.317 | 0.425 | 0.445 | 0.510 |
| 3.5 | 0.884 | 0.815 | 0.558 | 0.497 | 0.449 | 0.343 | 0.389 | 0.429 | 0.501 | 0.558 |
| 4.0 | 0.814 | 0.726 | 0.502 | 0.420 | 0.456 | 0.404 | 0.442 | 0.432 | 0.543 | 0.578 |
| 4.5 | 0.726 | 0.604 | 0.414 | 0.439 | 0.437 | 0.456 | 0.479 | 0.502 | 0.574 | 0.585 |
| 5.0 | 0.610 | 0.451 | 0.427 | 0.434 | 0.433 | 0.488 | 0.517 | 0.555 | 0.591 | 0.595 |
| 5.5 | 0.462 | 0.402 | 0.429 | 0.420 | 0.501 | 0.519 | 0.536 | 0.599 | 0.609 | 0.594 |
| 6.0 | 0.428 | 0.415 | 0.418 | 0.462 | 0.560 | 0.537 | 0.547 | 0.659 | 0.622 | 0.570 |
| 6.5 | 0.388 | 0.484 | 0.420 | 0.498 | 0.604 | 0.558 | 0.593 | 0.710 | 0.618 | 0.541 |
| 7.0 | 0.398 | 0.541 | 0.434 | 0.528 | 0.691 | 0.605 | 0.618 | 0.735 | 0.581 | 0.528 |
| 7.5 | 0.436 | 0.590 | 0.489 | 0.621 | 0.784 | 0.641 | 0.624 | 0.737 | 0.546 | 0.489 |
| 8.0 | 0.513 | 0.728 | 0.573 | 0.694 | 0.839 | 0.646 | 0.602 | 0.718 | 0.479 | 0.412 |
| 8.5 | 0.642 | 0.836 | 0.633 | 0.740 | 0.867 | 0.624 | 0.569 | 0.665 | 0.374 | 0.314 |
| 9.0 | 0.743 | 0.932 | 0.685 | 0.768 | 0.877 | 0.599 | 0.506 | 0.598 | 0.278 | 0.215 |
| 9.5 | 0.838 | 0.991 | 0.706 | 0.767 | 0.851 | 0.535 | 0.425 | 0.510 | 0.171 | 0.219 |
| 10.0 | 0.891 | 1.016 | 0.696 | 0.740 | 0.799 | 0.456 | 0.335 | 0.441 | 0.171 | 0.214 |

| $T_a[ms]$ | Delay [ms] *continued* | | | | | | | | | | |
|---|---|---|---|---|---|---|---|---|---|---|---|
| | 5.0 | 5.5 | 6.0 | 6.5 | 7.0 | 7.5 | 8.0 | 8.5 | 9.0 | 9.5 | 10.0 |
| 0.0 | 0.236 | 0.172 | 0.289 | 0.195 | 0.418 | 0.672 | 0.581 | 0.719 | 0.973 | 0.797 | 0.819 |
| 0.5 | 0.234 | 0.171 | 0.342 | 0.263 | 0.501 | 0.748 | 0.638 | 0.738 | 0.976 | 0.774 | 0.761 |
| 1.0 | 0.250 | 0.274 | 0.444 | 0.355 | 0.593 | 0.800 | 0.666 | 0.746 | 0.943 | 0.716 | 0.676 |
| 1.5 | 0.317 | 0.366 | 0.528 | 0.438 | 0.644 | 0.812 | 0.664 | 0.718 | 0.871 | 0.628 | 0.575 |
| 2.0 | 0.352 | 0.447 | 0.598 | 0.511 | 0.674 | 0.813 | 0.653 | 0.675 | 0.785 | 0.537 | 0.469 |
| 2.5 | 0.382 | 0.521 | 0.654 | 0.554 | 0.686 | 0.784 | 0.613 | 0.602 | 0.673 | 0.484 | 0.571 |
| 3.0 | 0.414 | 0.575 | 0.671 | 0.576 | 0.670 | 0.720 | 0.543 | 0.578 | 0.712 | 0.552 | 0.605 |
| 3.5 | 0.478 | 0.614 | 0.674 | 0.585 | 0.631 | 0.643 | 0.603 | 0.684 | 0.695 | 0.624 | 0.677 |
| 4.0 | 0.527 | 0.636 | 0.659 | 0.570 | 0.623 | 0.728 | 0.654 | 0.698 | 0.758 | 0.631 | 0.644 |
| 4.5 | 0.579 | 0.636 | 0.614 | 0.618 | 0.738 | 0.704 | 0.693 | 0.762 | 0.692 | 0.633 | 0.666 |
| 5.0 | 0.614 | 0.612 | 0.645 | 0.730 | 0.710 | 0.718 | 0.754 | 0.697 | 0.657 | 0.652 | 0.543 |
| 5.5 | 0.623 | 0.644 | 0.704 | 0.715 | 0.717 | 0.731 | 0.700 | 0.660 | 0.631 | 0.547 | 0.477 |
| 6.0 | 0.656 | 0.695 | 0.660 | 0.724 | 0.720 | 0.643 | 0.663 | 0.616 | 0.492 | 0.487 | 0.444 |
| 6.5 | 0.718 | 0.660 | 0.611 | 0.739 | 0.643 | 0.559 | 0.628 | 0.499 | 0.369 | 0.426 | 0.589 |
| 7.0 | 0.724 | 0.584 | 0.555 | 0.703 | 0.522 | 0.457 | 0.554 | 0.339 | 0.451 | 0.432 | 0.735 |
| 7.5 | 0.690 | 0.503 | 0.493 | 0.614 | 0.391 | 0.355 | 0.426 | 0.418 | 0.535 | 0.529 | 0.872 |
| 8.0 | 0.612 | 0.384 | 0.368 | 0.505 | 0.244 | 0.199 | 0.335 | 0.524 | 0.623 | 0.609 | 0.973 |
| 8.5 | 0.514 | 0.259 | 0.234 | 0.362 | 0.203 | 0.309 | 0.309 | 0.648 | 0.753 | 0.704 | 0.977 |
| 9.0 | 0.384 | 0.202 | 0.190 | 0.268 | 0.332 | 0.470 | 0.430 | 0.753 | 0.838 | 0.702 | 0.976 |
| 9.5 | 0.250 | 0.175 | 0.189 | 0.237 | 0.441 | 0.582 | 0.481 | 0.727 | 0.938 | 0.759 | 0.901 |
| 10.0 | 0.235 | 0.171 | 0.289 | 0.194 | 0.416 | 0.672 | 0.581 | 0.718 | 0.973 | 0.798 | 0.818 |

Table C.3: Maximum current peaks at phase B as a function of the energizing times $T_a$ and *Delay*. Complementary to Figure 4.4.

| $T_a[ms]$ | Delay [ms] | | | | | | | | | |
|---|---|---|---|---|---|---|---|---|---|---|
| | 0.0 | 0.5 | 1.0 | 1.5 | 2.0 | 2.5 | 3.0 | 3.5 | 4.0 | 4.5 |
| 0.0 | 1.214 | 1.196 | 1.228 | 1.130 | 1.331 | 1.374 | 1.226 | 1.380 | 1.471 | 1.386 |
| 0.5 | 1.147 | 1.231 | 1.305 | 1.154 | 1.337 | 1.367 | 1.281 | 1.441 | 1.501 | 1.406 |
| 1.0 | 1.088 | 1.250 | 1.365 | 1.148 | 1.400 | 1.410 | 1.344 | 1.471 | 1.516 | 1.440 |
| 1.5 | 1.095 | 1.286 | 1.395 | 1.161 | 1.440 | 1.452 | 1.379 | 1.496 | 1.542 | 1.444 |
| 2.0 | 1.085 | 1.352 | 1.418 | 1.208 | 1.481 | 1.469 | 1.377 | 1.511 | 1.537 | 1.410 |
| 2.5 | 1.096 | 1.398 | 1.436 | 1.268 | 1.501 | 1.514 | 1.412 | 1.486 | 1.491 | 1.342 |
| 3.0 | 1.184 | 1.416 | 1.414 | 1.322 | 1.485 | 1.532 | 1.424 | 1.426 | 1.412 | 1.240 |
| 3.5 | 1.249 | 1.438 | 1.438 | 1.376 | 1.490 | 1.520 | 1.397 | 1.358 | 1.297 | 1.108 |
| 4.0 | 1.320 | 1.456 | 1.465 | 1.426 | 1.486 | 1.467 | 1.337 | 1.259 | 1.153 | 1.091 |
| 4.5 | 1.388 | 1.447 | 1.482 | 1.449 | 1.446 | 1.379 | 1.245 | 1.157 | 1.121 | 1.067 |
| 5.0 | 1.436 | 1.476 | 1.471 | 1.431 | 1.372 | 1.260 | 1.144 | 1.117 | 1.071 | 1.058 |
| 5.5 | 1.512 | 1.477 | 1.418 | 1.381 | 1.267 | 1.136 | 1.110 | 1.093 | 1.055 | 1.048 |
| 6.0 | 1.558 | 1.435 | 1.333 | 1.298 | 1.130 | 1.097 | 1.105 | 1.054 | 1.037 | 1.040 |
| 6.5 | 1.562 | 1.362 | 1.216 | 1.180 | 1.104 | 1.071 | 1.052 | 1.066 | 1.078 | 1.080 |
| 7.0 | 1.530 | 1.255 | 1.126 | 1.151 | 1.113 | 1.093 | 1.097 | 1.113 | 1.176 | 1.102 |
| 7.5 | 1.462 | 1.116 | 1.068 | 1.143 | 1.078 | 1.070 | 1.078 | 1.175 | 1.244 | 1.140 |
| 8.0 | 1.354 | 1.148 | 1.102 | 1.143 | 1.097 | 1.116 | 1.099 | 1.241 | 1.311 | 1.166 |
| 8.5 | 1.260 | 1.082 | 1.092 | 1.112 | 1.137 | 1.155 | 1.107 | 1.284 | 1.355 | 1.221 |
| 9.0 | 1.226 | 1.105 | 1.115 | 1.111 | 1.194 | 1.258 | 1.136 | 1.316 | 1.401 | 1.271 |
| 9.5 | 1.245 | 1.148 | 1.188 | 1.129 | 1.282 | 1.331 | 1.184 | 1.364 | 1.446 | 1.341 |
| 10.0 | 1.215 | 1.196 | 1.226 | 1.129 | 1.330 | 1.373 | 1.228 | 1.378 | 1.473 | 1.385 |

| $T_a[ms]$ | Delay [ms] *continued* | | | | | | | | | | |
|---|---|---|---|---|---|---|---|---|---|---|---|
| | 5.0 | 5.5 | 6.0 | 6.5 | 7.0 | 7.5 | 8.0 | 8.5 | 9.0 | 9.5 | 10.0 |
| 0.0 | 1.427 | 1.546 | 1.461 | 1.359 | 1.461 | 1.238 | 1.106 | 1.205 | 1.147 | 1.070 | 1.101 |
| 0.5 | 1.451 | 1.548 | 1.423 | 1.289 | 1.358 | 1.165 | 1.105 | 1.141 | 1.094 | 1.110 | 1.097 |
| 1.0 | 1.435 | 1.508 | 1.354 | 1.189 | 1.237 | 1.116 | 1.092 | 1.141 | 1.102 | 1.147 | 1.082 |
| 1.5 | 1.385 | 1.434 | 1.249 | 1.116 | 1.211 | 1.093 | 1.087 | 1.102 | 1.100 | 1.161 | 1.087 |
| 2.0 | 1.316 | 1.325 | 1.113 | 1.112 | 1.137 | 1.071 | 1.066 | 1.036 | 1.143 | 1.238 | 1.138 |
| 2.5 | 1.219 | 1.232 | 1.119 | 1.096 | 1.131 | 1.085 | 1.109 | 1.090 | 1.213 | 1.217 | 1.151 |
| 3.0 | 1.137 | 1.155 | 1.085 | 1.082 | 1.109 | 1.133 | 1.156 | 1.063 | 1.236 | 1.273 | 1.200 |
| 3.5 | 1.111 | 1.143 | 1.053 | 1.045 | 1.055 | 1.120 | 1.124 | 1.156 | 1.275 | 1.252 | 1.317 |
| 4.0 | 1.092 | 1.065 | 1.032 | 1.062 | 1.069 | 1.156 | 1.213 | 1.157 | 1.321 | 1.338 | 1.347 |
| 4.5 | 1.055 | 1.038 | 1.067 | 1.073 | 1.118 | 1.228 | 1.193 | 1.282 | 1.367 | 1.343 | 1.424 |
| 5.0 | 1.050 | 1.056 | 1.081 | 1.122 | 1.202 | 1.205 | 1.295 | 1.345 | 1.359 | 1.420 | 1.453 |
| 5.5 | 1.056 | 1.097 | 1.121 | 1.184 | 1.225 | 1.279 | 1.340 | 1.374 | 1.409 | 1.445 | 1.464 |
| 6.0 | 1.088 | 1.159 | 1.187 | 1.181 | 1.322 | 1.310 | 1.372 | 1.442 | 1.431 | 1.447 | 1.488 |
| 6.5 | 1.119 | 1.265 | 1.187 | 1.248 | 1.401 | 1.301 | 1.422 | 1.505 | 1.427 | 1.443 | 1.486 |
| 7.0 | 1.189 | 1.324 | 1.205 | 1.327 | 1.446 | 1.300 | 1.469 | 1.550 | 1.391 | 1.428 | 1.420 |
| 7.5 | 1.216 | 1.346 | 1.229 | 1.396 | 1.465 | 1.354 | 1.501 | 1.552 | 1.338 | 1.364 | 1.321 |
| 8.0 | 1.278 | 1.390 | 1.244 | 1.431 | 1.525 | 1.374 | 1.498 | 1.523 | 1.251 | 1.267 | 1.220 |
| 8.5 | 1.319 | 1.421 | 1.305 | 1.473 | 1.563 | 1.367 | 1.450 | 1.455 | 1.156 | 1.191 | 1.200 |
| 9.0 | 1.386 | 1.486 | 1.381 | 1.485 | **1.571** | 1.333 | 1.384 | 1.379 | 1.091 | 1.134 | 1.155 |
| 9.5 | 1.416 | 1.510 | 1.428 | 1.451 | 1.539 | 1.301 | 1.214 | 1.238 | 1.139 | 1.068 | 1.116 |
| 10.0 | 1.427 | 1.547 | 1.460 | 1.360 | 1.460 | 1.238 | 1.105 | 1.206 | 1.148 | 1.071 | 1.101 |

Table C.4: Maximum voltage peaks at phase B as a function of the energizing times $T_a$ and *Delay*. Complementary to Figure 4.5.

| $T_a[ms]$ | Delay [ms] | | | | | | | | | |
|---|---|---|---|---|---|---|---|---|---|---|
| | 0.0 | 0.5 | 1.0 | 1.5 | 2.0 | 2.5 | 3.0 | 3.5 | 4.0 | 4.5 |
| 0.0 | 0.900 | 0.745 | 0.973 | 0.800 | 0.543 | 0.656 | 0.509 | 0.220 | 0.243 | 0.230 |
| 0.5 | 0.843 | 0.661 | 0.869 | 0.658 | 0.382 | 0.476 | 0.314 | 0.223 | 0.168 | 0.228 |
| 1.0 | 0.755 | 0.559 | 0.723 | 0.492 | 0.229 | 0.319 | 0.241 | 0.249 | 0.161 | 0.223 |
| 1.5 | 0.651 | 0.426 | 0.564 | 0.343 | 0.299 | 0.295 | 0.204 | 0.308 | 0.198 | 0.292 |
| 2.0 | 0.512 | 0.325 | 0.466 | 0.313 | 0.349 | 0.250 | 0.191 | 0.480 | 0.427 | 0.517 |
| 2.5 | 0.432 | 0.375 | 0.424 | 0.295 | 0.401 | 0.252 | 0.403 | 0.696 | 0.654 | 0.739 |
| 3.0 | 0.399 | 0.420 | 0.365 | 0.351 | 0.502 | 0.475 | 0.640 | 0.891 | 0.862 | 0.951 |
| 3.5 | 0.385 | 0.442 | 0.325 | 0.497 | 0.676 | 0.695 | 0.849 | 1.049 | 1.040 | 1.122 |
| 4.0 | 0.428 | 0.465 | 0.491 | 0.669 | 0.838 | 0.882 | 1.014 | 1.180 | 1.189 | 1.254 |
| 4.5 | 0.459 | 0.594 | 0.663 | 0.841 | 0.972 | 1.035 | 1.166 | 1.277 | 1.298 | 1.361 |
| 5.0 | 0.602 | 0.698 | 0.834 | 0.975 | 1.068 | 1.167 | 1.273 | 1.329 | 1.368 | 1.420 |
| 5.5 | 0.708 | 0.801 | 0.968 | 1.074 | 1.139 | 1.258 | 1.339 | 1.344 | 1.397 | **1.435** |
| 6.0 | 0.809 | 0.869 | 1.061 | 1.147 | 1.169 | 1.301 | 1.368 | 1.318 | 1.383 | 1.420 |
| 6.5 | 0.878 | 0.901 | 1.138 | 1.183 | 1.162 | 1.320 | 1.361 | 1.255 | 1.335 | 1.343 |
| 7.0 | 0.914 | 0.911 | 1.176 | 1.183 | 1.128 | 1.296 | 1.310 | 1.152 | 1.247 | 1.191 |
| 7.5 | 0.923 | 0.885 | 1.158 | 1.139 | 1.043 | 1.222 | 1.219 | 1.018 | 1.111 | 1.012 |
| 8.0 | 0.904 | 0.837 | 1.136 | 1.079 | 0.944 | 1.134 | 1.104 | 0.854 | 0.951 | 0.830 |
| 8.5 | 0.893 | 0.832 | 1.119 | 1.044 | 0.886 | 1.044 | 0.973 | 0.703 | 0.783 | 0.664 |
| 9.0 | 0.923 | 0.831 | 1.103 | 0.997 | 0.793 | 0.944 | 0.846 | 0.537 | 0.631 | 0.534 |
| 9.5 | 0.930 | 0.803 | 1.056 | 0.902 | 0.680 | 0.802 | 0.680 | 0.364 | 0.445 | 0.388 |
| 10.0 | 0.900 | 0.746 | 0.972 | 0.801 | 0.541 | 0.654 | 0.510 | 0.220 | 0.243 | 0.231 |

| $T_a[ms]$ | Delay [ms] *continued* | | | | | | | | | | |
|---|---|---|---|---|---|---|---|---|---|---|---|
| | 5.0 | 5.5 | 6.0 | 6.5 | 7.0 | 7.5 | 8.0 | 8.5 | 9.0 | 9.5 | 10.0 |
| 0.0 | 0.245 | 0.172 | 0.226 | 0.407 | 0.412 | 0.428 | 0.758 | 0.814 | 0.693 | 0.961 | 0.967 |
| 0.5 | 0.262 | 0.205 | 0.255 | 0.610 | 0.587 | 0.597 | 0.897 | 0.928 | 0.790 | 1.021 | 1.009 |
| 1.0 | 0.466 | 0.401 | 0.456 | 0.784 | 0.755 | 0.740 | 1.007 | 1.016 | 0.848 | 1.048 | 0.994 |
| 1.5 | 0.646 | 0.588 | 0.632 | 0.930 | 0.890 | 0.852 | 1.092 | 1.065 | 0.885 | 1.044 | 0.971 |
| 2.0 | 0.849 | 0.775 | 0.806 | 1.074 | 1.015 | 0.948 | 1.140 | 1.096 | 0.898 | 1.055 | 0.961 |
| 2.5 | 1.038 | 0.966 | 0.988 | 1.224 | 1.156 | 1.076 | 1.241 | 1.175 | 0.977 | 1.011 | 0.783 |
| 3.0 | 1.197 | 1.133 | 1.152 | 1.333 | 1.253 | 1.171 | 1.290 | 1.137 | 0.854 | 0.906 | 0.690 |
| 3.5 | 1.307 | 1.255 | 1.263 | 1.385 | 1.313 | 1.223 | 1.169 | 0.964 | 0.829 | 0.752 | 0.547 |
| 4.0 | 1.392 | 1.345 | 1.345 | 1.421 | 1.287 | 1.087 | 1.067 | 0.886 | 0.688 | 0.644 | 0.456 |
| 4.5 | 1.431 | 1.392 | 1.391 | 1.326 | 1.114 | 1.039 | 0.923 | 0.714 | 0.623 | 0.499 | 0.483 |
| 5.0 | 1.421 | 1.399 | 1.306 | 1.135 | 1.046 | 0.909 | 0.735 | 0.631 | 0.487 | 0.474 | 0.510 |
| 5.5 | 1.379 | 1.294 | 1.151 | 1.027 | 0.899 | 0.743 | 0.615 | 0.476 | 0.451 | 0.515 | 0.575 |
| 6.0 | 1.249 | 1.124 | 1.059 | 0.857 | 0.721 | 0.631 | 0.438 | 0.440 | 0.463 | 0.579 | 0.631 |
| 6.5 | 1.046 | 0.997 | 0.931 | 0.647 | 0.581 | 0.481 | 0.455 | 0.456 | 0.470 | 0.649 | 0.602 |
| 7.0 | 0.839 | 0.864 | 0.742 | 0.439 | 0.429 | 0.302 | 0.506 | 0.436 | 0.485 | 0.668 | 0.540 |
| 7.5 | 0.658 | 0.711 | 0.561 | 0.367 | 0.274 | 0.322 | 0.514 | 0.416 | 0.472 | 0.638 | 0.474 |
| 8.0 | 0.461 | 0.523 | 0.354 | 0.346 | 0.218 | 0.312 | 0.504 | 0.366 | 0.426 | 0.587 | 0.446 |
| 8.5 | 0.289 | 0.352 | 0.198 | 0.322 | 0.188 | 0.274 | 0.460 | 0.299 | 0.395 | 0.661 | 0.555 |
| 9.0 | 0.251 | 0.198 | 0.200 | 0.289 | 0.190 | 0.202 | 0.456 | 0.369 | 0.507 | 0.834 | 0.691 |
| 9.5 | 0.250 | 0.175 | 0.209 | 0.241 | 0.179 | 0.274 | 0.612 | 0.621 | 0.599 | 0.905 | 0.856 |
| 10.0 | 0.245 | 0.171 | 0.226 | 0.406 | 0.413 | 0.428 | 0.756 | 0.815 | 0.692 | 0.960 | 0.967 |

Table C.5: Maximum current peaks at phase C as a function of the energizing times $T_a$ and *Delay*. Complementary to Figure 4.6.

| $T_a[ms]$ | Delay [ms] | | | | | | | | | |
|---|---|---|---|---|---|---|---|---|---|---|
| | 0.0 | 0.5 | 1.0 | 1.5 | 2.0 | 2.5 | 3.0 | 3.5 | 4.0 | 4.5 |
| 0.0 | 1.226 | 1.160 | 1.189 | 1.361 | 1.243 | 1.352 | 1.468 | 1.440 | 1.320 | 1.365 |
| 0.5 | 1.280 | 1.152 | 1.230 | 1.394 | 1.329 | 1.379 | 1.486 | 1.423 | 1.266 | 1.363 |
| 1.0 | 1.356 | 1.185 | 1.277 | 1.468 | 1.377 | 1.376 | 1.470 | 1.364 | 1.209 | 1.360 |
| 1.5 | 1.395 | 1.237 | 1.337 | 1.510 | 1.393 | 1.334 | 1.411 | 1.283 | 1.227 | 1.345 |
| 2.0 | 1.483 | 1.325 | 1.363 | 1.516 | 1.378 | 1.267 | 1.326 | 1.304 | 1.237 | 1.358 |
| 2.5 | 1.541 | 1.375 | 1.360 | 1.489 | 1.322 | 1.230 | 1.318 | 1.344 | 1.239 | 1.319 |
| 3.0 | 1.556 | 1.392 | 1.342 | 1.419 | 1.242 | 1.274 | 1.350 | 1.314 | 1.248 | 1.288 |
| 3.5 | 1.535 | 1.379 | 1.298 | 1.321 | 1.259 | 1.273 | 1.345 | 1.280 | 1.217 | 1.273 |
| 4.0 | 1.480 | 1.325 | 1.259 | 1.313 | 1.271 | 1.308 | 1.290 | 1.246 | 1.203 | 1.188 |
| 4.5 | 1.382 | 1.247 | 1.250 | 1.319 | 1.302 | 1.257 | 1.286 | 1.187 | 1.152 | 1.132 |
| 5.0 | 1.259 | 1.254 | 1.303 | 1.323 | 1.249 | 1.277 | 1.202 | 1.151 | 1.117 | 0.999 |
| 5.5 | 1.229 | 1.300 | 1.344 | 1.243 | 1.273 | 1.215 | 1.150 | 1.105 | 1.022 | 0.975 |
| 6.0 | 1.223 | 1.343 | 1.306 | 1.216 | 1.246 | 1.164 | 1.111 | 1.000 | 1.025 | 1.060 |
| 6.5 | 1.216 | 1.315 | 1.305 | 1.171 | 1.210 | 1.134 | 1.053 | 1.023 | 1.051 | 1.172 |
| 7.0 | 1.162 | 1.300 | 1.302 | 1.098 | 1.195 | 1.063 | 1.032 | 1.071 | 1.116 | 1.271 |
| 7.5 | 1.101 | 1.278 | 1.206 | 1.080 | 1.143 | 1.100 | 1.098 | 1.156 | 1.166 | 1.378 |
| 8.0 | 1.096 | 1.273 | 1.187 | 1.109 | 1.137 | 1.157 | 1.201 | 1.228 | 1.260 | 1.458 |
| 8.5 | 1.119 | 1.245 | 1.192 | 1.193 | 1.143 | 1.215 | 1.273 | 1.277 | 1.326 | 1.489 |
| 9.0 | 1.104 | 1.244 | 1.136 | 1.216 | 1.158 | 1.220 | 1.338 | 1.374 | 1.343 | 1.491 |
| 9.5 | 1.153 | 1.210 | 1.148 | 1.303 | 1.217 | 1.291 | 1.415 | 1.427 | 1.338 | 1.426 |
| 10.0 | 1.225 | 1.160 | 1.192 | 1.362 | 1.244 | 1.353 | 1.469 | 1.439 | 1.321 | 1.364 |

| $T_a[ms]$ | Delay [ms] *continued* | | | | | | | | | | |
|---|---|---|---|---|---|---|---|---|---|---|---|
| | 5.0 | 5.5 | 6.0 | 6.5 | 7.0 | 7.5 | 8.0 | 8.5 | 9.0 | 9.5 | 10.0 |
| 0.0 | 1.326 | 1.156 | 1.411 | 1.404 | 1.159 | 1.337 | 1.311 | 1.101 | 1.167 | 1.168 | 1.107 |
| 0.5 | 1.368 | 1.194 | 1.396 | 1.371 | 1.112 | 1.301 | 1.242 | 1.095 | 1.108 | 1.104 | 1.159 |
| 1.0 | 1.400 | 1.191 | 1.362 | 1.348 | 1.094 | 1.276 | 1.177 | 1.082 | 1.093 | 1.110 | 1.236 |
| 1.5 | 1.377 | 1.171 | 1.329 | 1.303 | 1.098 | 1.210 | 1.124 | 1.113 | 1.111 | 1.151 | 1.304 |
| 2.0 | 1.321 | 1.140 | 1.308 | 1.201 | 1.054 | 1.113 | 1.052 | 1.107 | 1.102 | 1.147 | 1.356 |
| 2.5 | 1.296 | 1.110 | 1.284 | 1.158 | 1.076 | 1.086 | 1.090 | 1.191 | 1.144 | 1.263 | 1.388 |
| 3.0 | 1.260 | 1.061 | 1.199 | 1.073 | 1.039 | 1.036 | 1.118 | 1.269 | 1.222 | 1.317 | 1.441 |
| 3.5 | 1.167 | 1.074 | 1.092 | 0.996 | 1.067 | 1.061 | 1.177 | 1.279 | 1.292 | 1.387 | 1.423 |
| 4.0 | 1.123 | 1.000 | 1.020 | 1.037 | 1.166 | 1.134 | 1.244 | 1.372 | 1.370 | 1.370 | 1.428 |
| 4.5 | 1.017 | 0.981 | 1.015 | 1.140 | 1.153 | 1.211 | 1.344 | 1.405 | 1.361 | 1.410 | 1.345 |
| 5.0 | 0.980 | 1.021 | 1.119 | 1.138 | 1.228 | 1.339 | 1.390 | 1.380 | 1.404 | 1.337 | 1.294 |
| 5.5 | 1.029 | 1.104 | 1.146 | 1.235 | 1.327 | 1.392 | 1.389 | 1.389 | 1.344 | 1.298 | 1.294 |
| 6.0 | 1.141 | 1.118 | 1.264 | 1.356 | 1.363 | 1.396 | 1.412 | 1.308 | 1.314 | 1.313 | 1.313 |
| 6.5 | 1.212 | 1.193 | 1.377 | 1.427 | 1.333 | 1.419 | 1.365 | 1.239 | 1.360 | 1.366 | 1.246 |
| 7.0 | 1.282 | 1.263 | 1.457 | 1.431 | 1.306 | 1.398 | 1.267 | 1.241 | 1.398 | 1.317 | 1.226 |
| 7.5 | 1.364 | 1.314 | 1.489 | 1.410 | 1.247 | 1.360 | 1.270 | 1.276 | 1.414 | 1.272 | 1.211 |
| 8.0 | 1.415 | 1.326 | 1.472 | 1.349 | 1.198 | 1.418 | 1.311 | 1.251 | 1.368 | 1.235 | 1.157 |
| 8.5 | 1.434 | 1.314 | 1.421 | 1.282 | 1.238 | 1.450 | 1.304 | 1.229 | 1.374 | 1.194 | 1.143 |
| 9.0 | 1.436 | 1.251 | 1.405 | 1.308 | 1.227 | 1.445 | 1.290 | 1.202 | 1.345 | 1.193 | 1.102 |
| 9.5 | 1.387 | 1.182 | 1.400 | 1.369 | 1.184 | 1.388 | 1.305 | 1.121 | 1.261 | 1.189 | 1.077 |
| 10.0 | 1.326 | 1.156 | 1.413 | 1.405 | 1.159 | 1.338 | 1.310 | 1.100 | 1.165 | 1.168 | 1.106 |

Table C.6: Maximum voltage peaks at phase C as a function of the energizing times $T_a$ and *Delay*. Complementary to Figure 4.7.